TECTONIC FIBROUS VEINS: INITIATION AND EVOLUTION.

OUACHITA OROGEN, ARKANSAS

A Dissertation

by

PABLO CERVANTES

Submitted to the Office of Graduate Studies of
Texas A&M University
in partial fulfillment of the requirements for the degree of

DOCTOR OF PHILOSOPHY

August 2007

Major Subject: Geology

TECTONIC FIBROUS VEINS: INITIATION AND EVOLUTION.

OUACHITA OROGEN, ARKANSAS

A Dissertation

by

PABLO CERVANTES

Submitted to the Office of Graduate Studies of
Texas A&M University
in partial fulfillment of the requirements for the degree of

DOCTOR OF PHILOSOPHY

Approved by:

Chair of Committee,	David V. Wiltschko
Committee Members,	Andreas Kronenberg
	Ethan Grossman
	William Lamb
	John W. Morse
Head of Department,	John Spang

August 2007

Major Subject: Geology

ABSTRACT

Tectonic Fibrous Veins: Initiation and Evolution.

Ouachita Orogen, Arkansas. (August 2007)

Pablo Cervantes, B.S., Universidad Nacional Autónoma de México;

M.S., Texas A&M University

Chair of Advisory Committee: Dr. David V. Wiltschko

Veins are ubiquitous features in deformed rocks. Despite observations on syntectonic veins spanning two centuries, fundamental questions remain unanswered. Their origin as fractures is largely established but it is still not known why these fractures initiate where they do and how the vein evolves once started. We studied veins from the Lower Ordovician Mazarn Formation in the Arkansas' Ouachitas combining textural observations, stable isotopes, fluid inclusions, SEM-based cathodoluminescence and electron back-scattered diffraction to understand the initial stage of vein formation, its later evolution, the role of fluids and their environment of formation.

The veins are located at boudin necks and are synchronous with cleavage formation. Texturally, veins are characterized by veinlets (thin veins between 5 and 25 μm thick) that parallel the vein-host interface and fibers (columns of quartz or calcite) perpendicular to the vein-host interface between 30 and 350 μm wide. Veinlets are localized fractures filled with quartz. The crystallographic orientation of the precipitated material in veinlets is inherited from host grains at the micron scale and

replicated as fibers' lengths grow to centimeters. The vein-forming fluid was cyclically supersaturated yet never very far from saturation.

$\delta^{18}O$ values of vein quartz and host are within 2‰ of each other suggesting that the fluid was rock-buffered. Nevertheless, $\delta^{18}O$ and $\delta^{13}C$ define a 'J' shaped trend. Although it is not possible to date any portion of this curve, the simplest explanation is that the fluid evolved from rock-buffered in a closed system to fluid-dominated in an open system. The range of pressure-temperature conditions of vein formation is between 275 and 385 °C and 1100 and 3400 bars, from fluid inclusions and quartz-calcite oxygen isotopes thermometry.

By examining a vein from tip to middle, we have established a sequence of events from inception to maturity in vein growth. Vein formation starts with folding followed by flattening of resistant sandstone layers which in turn gives rise to boudinage. Boudinage formation allowed for fracture localization along boudin-necks. The vein grew by the repeated addition of veinlets in the neck region. Recrystallization later modified the fibers by obliterating some evidence of the veinlets and moving fiber walls.

TABLE OF CONTENTS

Page

LIST OF FIGURES

1. INTRODUCTION

Veins are common features in deformed rocks. Their study over two centuries has resulted in a wealth of observations from a variety of tectonic regimes. However, lacking from these studies is a consensus as to their mechanism of formation (e.g., Ramsay, 1980; Cox, 1987; Fisher and Brantely, 1992; Bons, 2000; and Hilgers and Urai, 2002). Their initiation as fractures is well established but the dilation mechanism is at the center of the debate. Two mechanisms have been proposed: (1) continuous fracturing or the crack-seal mechanism (Ramsay, 1980; Cox and Etheridge, 1983; Fisher and Brantley, 1992; Fisher et al., 1995; and Laubach et al., 2004) and (2) force of crystallization (Taber, 1916, 1918 and 1920; Misik, 1971; Li, 2000; Means and Li, 2001; Wiltschko and Morse, 2001). Fabrics resulting from these mechanisms will be different. On the one hand veins formed by the crack-seal mechanism will propagate as cracks followed by complete healing along the length of the crack (e.g. Cox and Etheridge, 1983). On the other[1] hand, veins formed by force of crystallization should grow as vein minerals grow and prop the host walls apart.

Tied to the debate of mechanism of formation of veins is the discussion over the mechanism of transport of the vein material. Force of crystallization requires diffusion as the transport mechanism from source to the vein. Veins need not to be part of a fracture network. The crack-seal mechanism as originally proposed (Ramsay, 1980) requires advection of fluid in and out of fractures to allow precipitation of the material

---

This dissertation follows the style and format of Journal of Structural Geology.

in the veins. Fisher and Brantley (1992) and Fisher et al. (1995) show that the amount of fluid required to precipitate quartz veins by advection is far larger than the volume of a fracture and suggest instead that diffusion is the most likely mechanism of material transport. Their vein model is a form of the “crack-seal” model but the material transport is by diffusion where a fluid film of 10’s of m length (depth) and μm’s wide drive the fracturing process and allows for diffusion through the host to fill the fracture. For their model, fracture connectivity is required.

To address these problems we sampled veins from the Ouachita Mountains in Arkansas. These veins are typical in that they are fibrous and show ‘crack-seal’ textures or banding parallel to the vein wall. In addition, the veins show several new features not found elsewhere which help to better illustrate the processes that formed them.

In Section 2 we study the fabrics of an entire to understand its evolution from initiation through propagation. The approach taken is to trade space for time by examining the vein’s tip as representing the early stage of formation and its middle as a mature stage. The assumption made is that vein growth is self-similar.

In section 3 we combine structural data and microtextural descriptions of the veins with stable isotopes, fluid inclusions and mineralogical data to constrain the environment of formation of this set of fibrous, banded veins.

In Section 4 we isolate an individual veinlet and study it using SEM-based cathodoluminescence and SEM-based electron-backscattered diffraction. The idea is that the vein starts as one veinlet. The understanding of a veinlet will yield information into the intial stage of vein formation.

2. SYNTECTONIC VEIN FABRIC DEVELOPMENT, OUACHITA OROGEN, ARKANSAS: TRADING SPACE FOR TIME

2.1 Précis

By examining a vein from its tip to middle, we have established a sequence of events from inception to maturity in vein growth. Veins from the Lower Ordovician Mazarn Formation in the Arkansas' Ouachitas are composed of veinlets and fibers. Veinlets are quartz filled narrow (5-25 μm) features parallel to the main body of the vein. Fibers are columns of quartz and calcite whose long axis is oriented perpendicular to the vein-host interface. These features are formed by two processes. Veinlets are formed by localized fractures that filled with quartz. Recrystallization later modified the fibers by obliterating some evidence of the veinlets and moving fiber walls. Evidence for recrystallization includes, 1) wide fibers (> 150 μm) with fluid inclusion trails parallel to fiber long axis that span the entire fiber length, 2) change in cathodoluminescence color between quartz in fibers (pink) and quartz in veinlets (blue), and 3) remnants of veinlet blue cathodoluminescence inside fibers.

We propose a model of vein formation that starts with folding followed by flattening of resistant sandstone layers that gave rise to boudinage. Boudinage formation allowed for fracture localization along boudin-necks. The vein grows by the repeated addition of veinlets in the neck region. Recrystallization altered the shape of previously formed fibers.

2.2 Introduction

Despite a wealth of observations on syntectonic veins from a variety of tectonic regimes, there is no consensus as to the mechanism of formation (e.g., Ramsay, 1980; Cox, 1987; Fisher and Brantely, 1992; Bons, 2000; and Hilgers and Urai, 2002). At the center of the debate is the dilation mechanism. Two mechanisms have been proposed: (1) force of crystallization (Taber, 1916, 1918 and 1920; Misik, 1971; Li, 2000; Means and Li, 2001; Wiltschko and Morse, 2001) and (2) continuous fracturing or the crack-seal mechanism (Ramsay, 1980; Cox and Etheridge, 1983; Fisher and Brantley, 1992; Fisher et al., 1995; and Laubach et al., 2004).

Fabrics resulting from these mechanisms will be different. On the one hand veins formed by the crack-seal mechanism will propagate as cracks followed by complete healing along the length of the crack (e.g. Cox and Etheridge, 1983). On the other hand veins formed by force of crystallization should grow as vein minerals grow and prop the host walls apart.

To date, fabric observations have nearly exclusively been confined to small portions of veins due to the problem of scale (although see Laubach et al., 2004). Veins that are meters long may be made up of grains that are microns in size, a range of 6 orders of magnitude. This approach has not yielded the observations necessary to separate between mechanisms.

The study of an entire vein provides an opportunity to trace the formation of a vein from initiation through propagation. The approach we have taken is to trade space for

time by examining a vein tip as representing the early stage of formation and the middle as a mature stage. The assumption made is that vein growth is self-similar.

The vein sampled for this study came from the Ouachita Mountains in Arkansas. This vein is typical in that it is fibrous and shows ‘crack-seal’ textures or banding parallel to the vein wall. In addition, the vein shows several new features not found elsewhere which help to better illustrate the processes that formed it.

2.3 Geological Setting

The veins of interest are found in the Benton Uplift of the Ouachita fold and thrust belt. The latter orogenic belt trends east-west and extends from central Arkansas to southeastern Oklahoma (Figure 1A). To the east, the Ouachita system plunges beneath Mesozoic and Tertiary sediments of the Mississippi embayment. To the southwest the fold and thrust belt is covered by Cretaceous and Tertiary sediments of the Gulf coastal plain and reemerges in the Marathon and Solitario uplifts in western Texas. (Blythe et al., 1988; Arbenz, 1989). Based on COCORP reflection profiles, Lillie et al. (1983) and Nelson et al. (1982) proposed that during the lower Paleozoic the area was a south facing passive continental margin followed in the Mississippian by collision with a southern, unknown continent with North-America. A thick Carboniferous marine shale facies at least 12 km thick (e.g., Houseknecht and Matthews, 1985) was emplaced on coeval shelf carbonates. During the final stages of the collision, reverse faults cut crystalline basement, resulting in the northward and vertical movement of a portion of the continental margin producing the Benton and Broken Bow uplifts (Figure 1A).

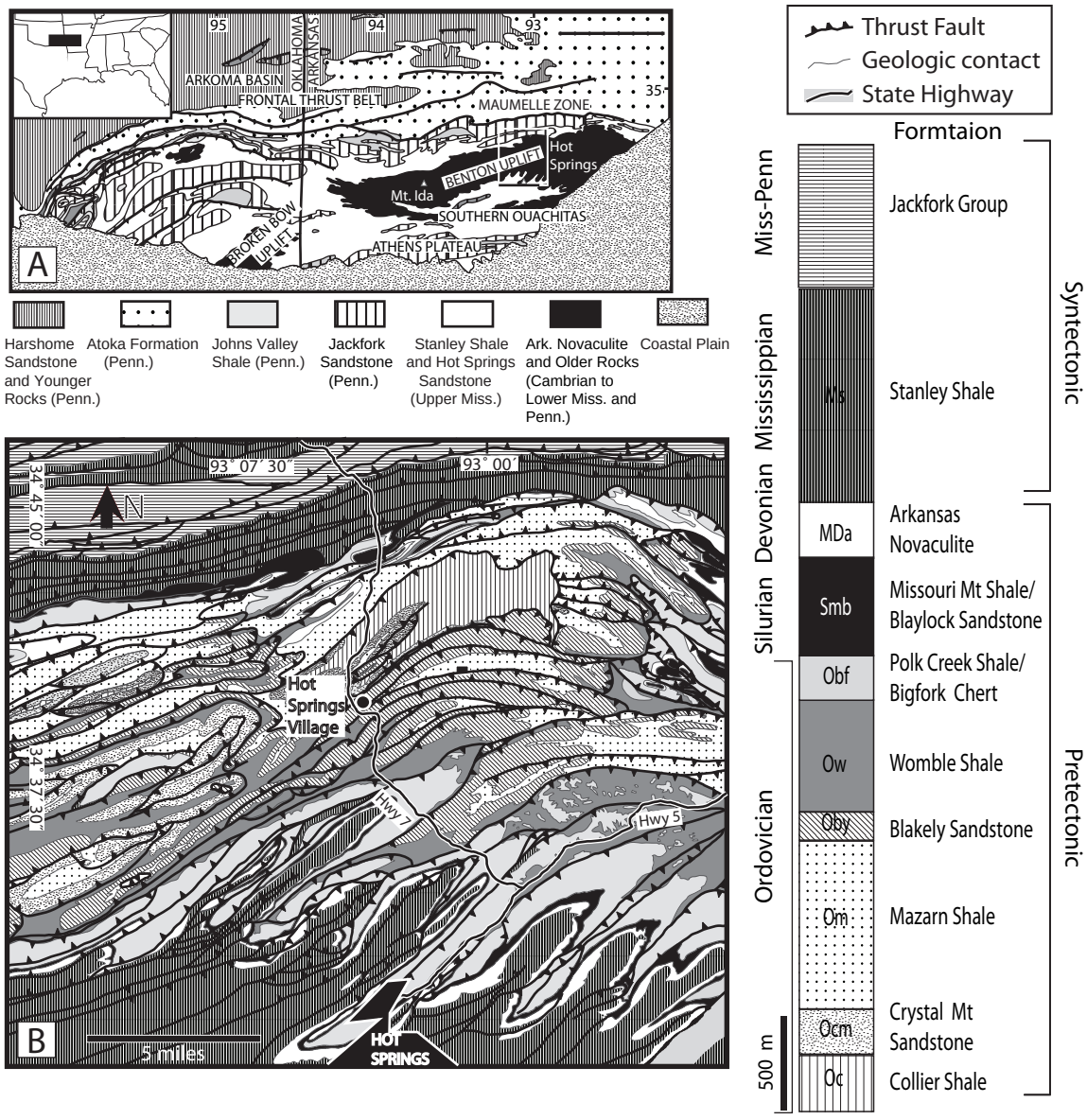

Fig. 1. Geologic map of the Ouachitas. A) Geologic map of the Ouachitas after Miser (1959). The white outlined square shows the location of the Hot Springs area. B) Regional Geology of the Hot Springs, AR area with the location of the Lake Pineda Outcrop (solid black square) after Haley and Stone (1996)

The frontal portion of the Ouachitas consist of north to northwest verging folds and thrusts faults, although the most exterior structure in places is a triangle zone (e.g., Arbenz, 1989). Uplift of the core of the orogen (Broken Bow and Benton uplifts) has resulted in south-vergent folds and north-dipping cleavage on the south flank of the core. The deeper structures causing the core uplift displace margin sediments and/or continental crust on thrusts that most likely crop out at the thrust front. This deep thrusting was a late event because sediments are continuous both north and south of the uplifts until late Pennsylvanian or earliest Permian. Paleo-thermal gradients, while cut by thrust faults, are more shallow than would be predicted from burial of each thrusted sequence suggesting that thrusting was synchronous with peak metamorphism (Underwood et al., 1988). Vitrinite reflectance values increase to the southeast, leading Houseknecht and Matthews (1985) to suggest that postorogenic Cretaceous plutons influenced the thermal maturation of the core of the orogen. However, apatite fission track analysis results show that regional cooling of the Ouachitas took place in Late Paleozoic, before emplacement of postectonic Cretaceous plutons within the Mississippi Embayment (Arne, 1992).

Most of the rocks exposed in the Benton uplift are sedimentary and consists of thinly bedded (<4 km thick) series of Cambrian to lower Mississippian deep-water shales, chert, submarine debris flow and turbidite sandstone (Arkansas Novaculite and Arbuckle facies), overlain by a thick (>13 km) sequence of Mississippian to Permian flysch represented by Stanley shale through lower Atoka Formation; (e.g. Lowe, 1989; Morris, 1989). Rock ages within the Benton Uplift range from Ordovician (Collier

Shale) to Lower Mississippian (Arkansas Novaculite); see Figure (1). The Upper Mississippian syntectonic Stanley Shale unconformably overlies the Arkansas Novaculite (Figure 1A). As pointed out by Arbenz (1989), the most competent units (Carboniferous) collectively overlie less competent units (lower Paleozoic), opposite to the mechanical stratigraphy found in the Appalachians to the east. Considering regional transport direction as the perpendicular to regional fold axes and thrust fault traces, it was from the SE in the Ouachitas.

The highest concentration of quartz veins in the Ouachitas are found in a region 50 to 65 km wide at the center of the Benton-Broken Bow Uplifts (Miser, 1959). The rocks containing veins are also the rocks with highest metamorphic grade. The central part of the Benton Uplift is characterized by both north dipping thrust faults and south-verging overturned folds (Figure 1B). Miser (1959) observed that the veins in this region follow faults, bedding planes and fractures, the latter cutting across folds. The structural setting of the veins in the Ouachitas suggest that the veins are synorogenic (Nielsen et al., 1989; Viele and Thomas, 1989). Radiometric dating of adularia in commercial quartz veins yield Late Pennsylvanian to Early Permian ages (Bass and Ferrara, 1969; Denison et al., 1977; Shelton et al., 1986).

2.4 Outcrop Geology

All samples come from an outcrop located at Hot Springs Village, 13 miles north of Hot Springs, AK. The outcrop functions as the spillway for the Lake Pineda Dam briefly described in Stone et al. (1994). The rocks exposed at the outcrop are from the

Lower Ordovician Mazarn Shale, a interbedded banded green and black shale, laminated fine-grained gray siltstone, and minor lenses of fine-grained brownish-gray quartzitic sandstone. This formation has been interpreted to have been deposited as density and marine currents from sources in the north or northeast (Stone and McFarland, 1981; Lowe, 1989).

These rocks were deformed and metamorphosed up to greenschist facies as part of the Benton uplift. The outcrop is crossed by two thrust faults oriented N60E (Figure 2). Fold wavelengths varying from cm to m. Small (cm to dm) folded sandstone layers are contained within shale beds whereas larger wavelength folds involve thicker (dm to m) sandstone beds. All shale units display cleavage in outcrop.

Bedding (Figure 3A) strikes NE-SW with dips tending toward subhorizontal. Cleavage (Figure 3C) is subhorizontal and at a low angle to bedding, indicating subvertical flattening. Fold axes (Figure 3B) are consistent with those observed in other areas of the Benton uplift, namely NE-SW trending axes as reported by Viele (1989). Fold axes and bedding orientations are consistent with NW-SE contraction. Fractures (Figure 3E) show two orthogonal conjugate sets. Fractures cut across all features in the outcrop. Thrust faults both cut through folds and parallel fold axial planes.

Veins (Figure 3D) are either subvertical or subhorizontal. The veins described come from the vertical sets. Based on shapes in hand sample, two main types of veins were observed in the outcrop: 1) low and 2) high aspect ratio. The low aspect ratio veins are thin and elongated in shape and range between 0.1 and 1 m long and between 1 mm and 4 mm wide. The high aspect ratio veins are lensatic in shape and range between 30 cm

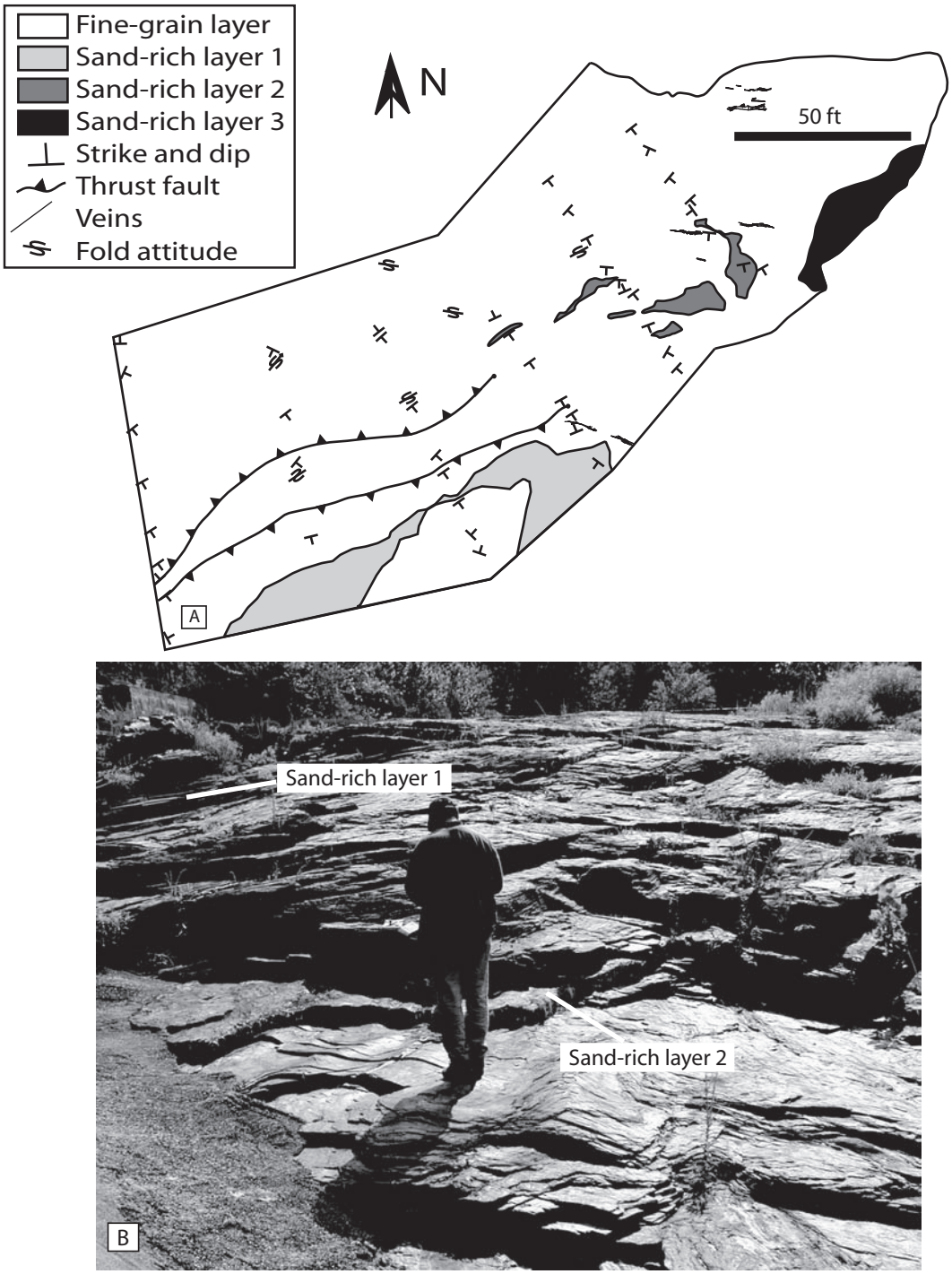

Fig. 2. Lake Pineda dam outcrop geology. A) Map of the oucrop. B) Photo of the outcrop.

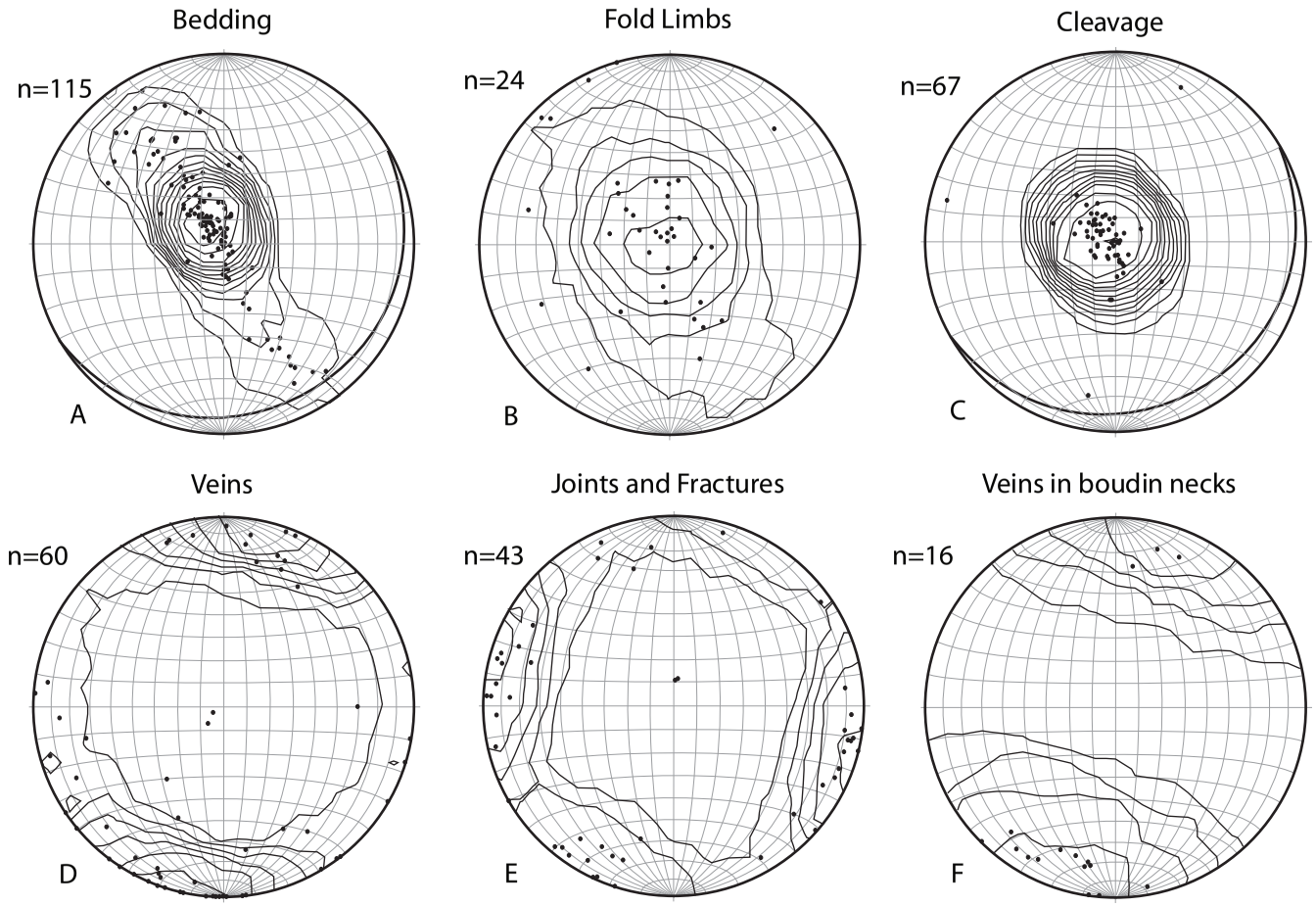

Fig. 3. Structural data from Pineda Dam outcrop. All figures are lower hemisphere, equal area projections. All contours are Kamb contours with σ=2.0. A) Poles to bedding planes from the entire outcrop. The bold great circle represents the orientation of the main thrust fault in the outcrop. B) Poles to bedding (fold limbs) from small folds in the outcrop. C) Poles to cleavage planes of the entire outcrop. Great circle represents the orientation of the main thrust fault. D) Poles to vein orientations. E) Poles to fracture orientations. F) Poles to orientations of veins in boudin necks.

and 5 m long and between 5 cm and 40 cm wide. All veins are both fibered and bi-mineralic with quartz and calcite fibers. In hand sample, cross-cutting relationships show that veins are earlier than faults and, synchronous with cleavage formation because cleavage and veins cross-cut each other.

Sandstone beds in the outcrop are boudinaged (Figures 4A and B). High aspect ratio veins are located at the boudin necks. The relationship between low aspect ratio veins and boudinage is not clear from the outcrop exposure. The linear correlation between bed thickness and separation between boudin necks where the veins are located supports the mechanical link between boudinage and veins (Figure 4C). The orientation of boudin necks (boudin axes) correspond to the largest concentration of vein orientations NW-SE (Figure 3F). This supports the observation that high aspect ratio veins are located at boudin necks.

2.5 Vein Textures

The vein we studied in detail is 62 cm long and up to 5 mm wide. Its midline is oriented N75W and the vein walls are vertical. The depth of the vein into the outcrop is unknown but from the sample obtained is at least 1 cm. The vein is fibrous throughout its length with quartz and calcite fibers and rare apatite grains (Figure 5). To understand the differences in texture across the vein, we describe the host, veinlets, fibers and vein-host interface.

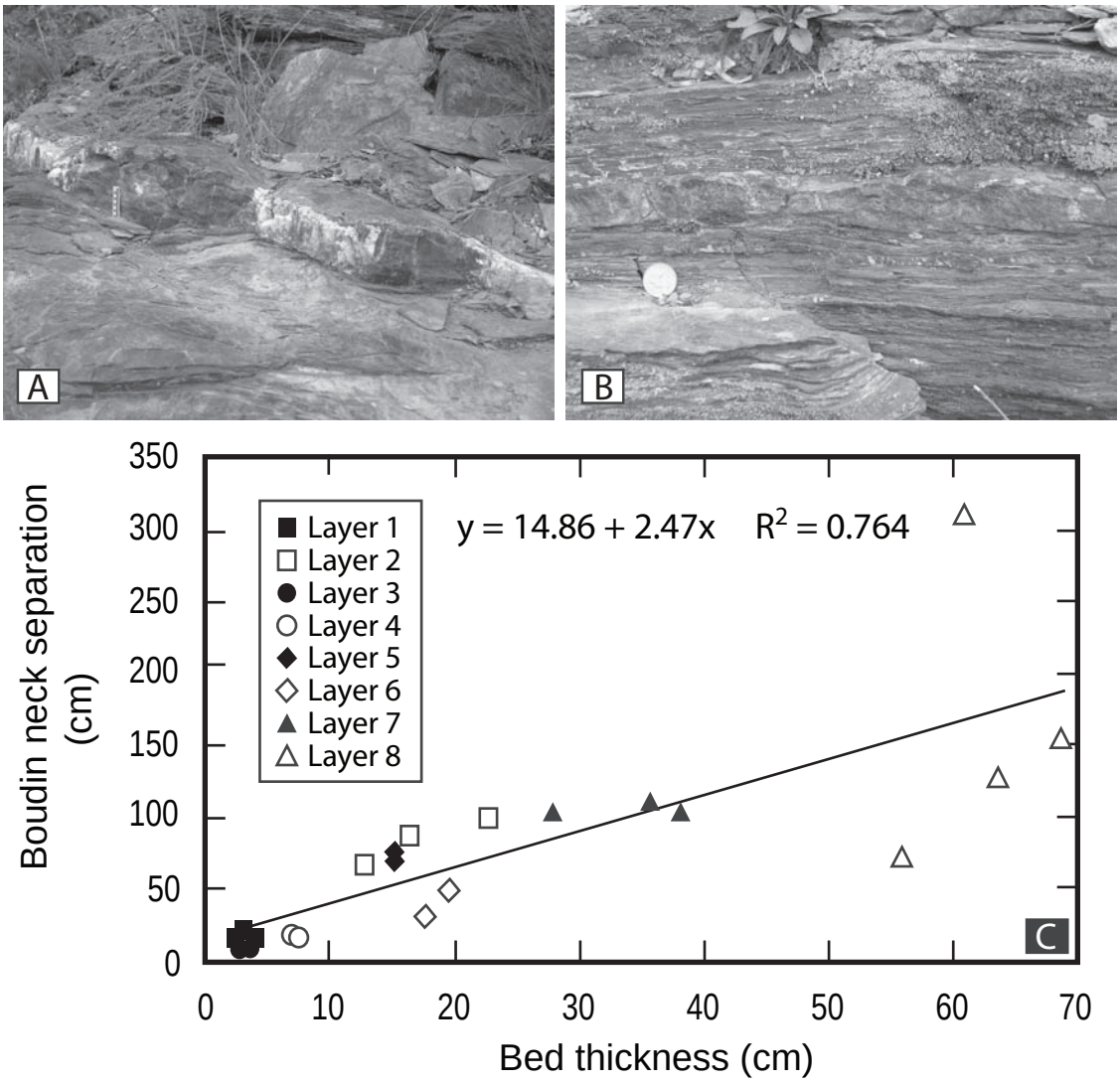

Fig. 4: Boudinage at Pineda Dam Outcrop. A) boudinage in a thick sandstone layer (30.5 cm). Marked scale in the photo represents 10 cm. B) boudinage in a thin sandstone layer (3.81 cm). A quarter dollar is shown for scale. C) Plot of bed thickness vs. separation of boudin necks in the Pineda outcrop. These feature show a linear correlation described by the line shown with R2 = 0.76.

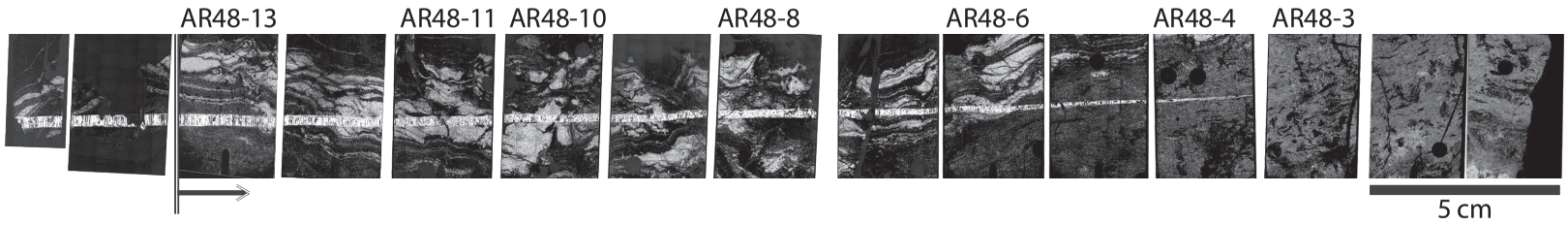

Fig. 5. Elongate vein AR-48. Crossed-polar photomicrographs of the thin sections comprising sample AR-48.

2.5.1 Host

The host consists of interbedded layers cm to m thick and laminations mm to cm thick of both fine-grained (silt to clay size) and coarse-grained (medium sand to silt size) material. Veins in the outcrop are best exposed along, and are normal to, slip surfaces. These slip surfaces are observed on bedding planes of the thicker (dm to m thick) layers of sandstone. The veins described here are contained in two different slip surfaces, vertically separated by approximately 0.5 m in the same stratigraphic unit.

Electron-microprobe X-ray maps obtained from different areas of various thin sections combined with XRD analyses of both coarse-grain and fine-grain host fractions, were used to determine the mineralogy and abundances of the host material. The mineralogy of the coarse-grained host is mostly quartz (>75% by area on X-ray maps) with varying amounts of clay minerals (illite), chlorite, and traces of other minerals like apatite, calcite and feldspars. The mineralogy of the fine-grained host is similar but clay minerals and chlorite are more abundant than quartz (<45% by area on the X-ray maps).

Composite SEM-CL images combining 3 filters (red, blue, green) show that 1) host quartz luminescence is different from that of the vein quartz and, 2) the difference in luminescence between quartz in the host and the veins shows clear evidence of host grains fractured and displaced by vein mineralization (Figures 6A and C)

Microscopically, host cleavage is delineated by dark linear bands 5 to 30 μm thick where the host rock is devoid of quartz and higher concentrations of phyllosilicates are

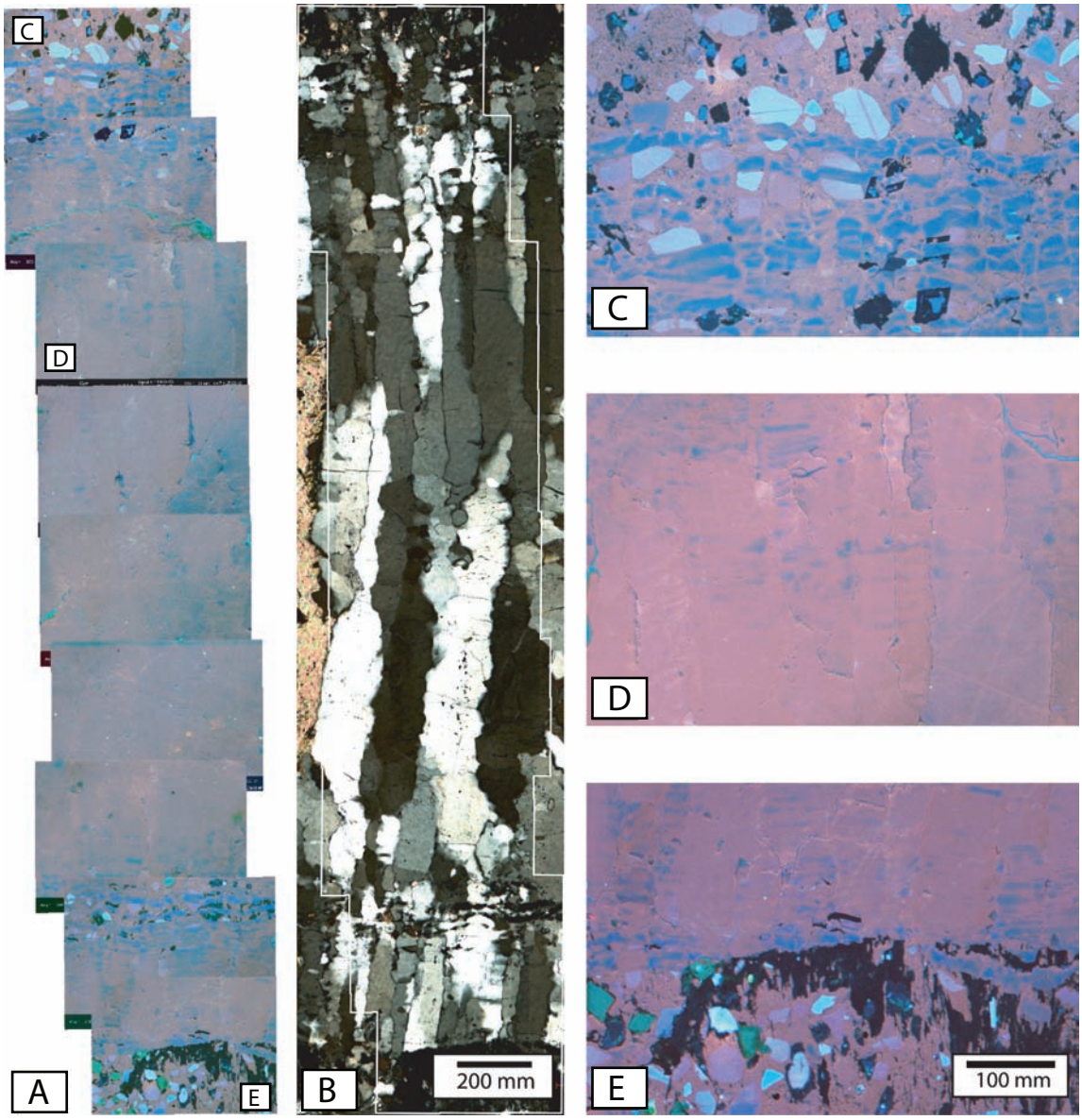

Fig. 6. Polychromatic SEM-CL photomosaic of a section from sample AR-48-13. A) Polychromatic SEM-CL photomosaic of entire vein width. B) Optical photomosaic under crossed-polars showing same area of A. C) Detailed SEM-CL photograph from host-vein interface showing fractured host grains. D) Detailed SEM-CL photograph from main body of vein. E) Detailed SEM-CL photograph of host-vein interface showing sliver of host. See location on Figure 7.

found as compare to the concentration of these minerals in the surrounding host. This suggests that quartz is preferentially dissolved at these features.

2.5.2 Veinlets

A nearly ubiquitous feature of this vein is the preservation of veinlets. Veinlets are defined in this paper as thin (5 - 25 μm) veins parallel or at low angles to the host-vein interface. Veinlets have the same mineralogy as the larger vein. Veinlets can be found next to one another or separated by host segments up to 15 to 30 μm wide. The host segments have the same mineralogy and texture as the host adjacent to the vein (Figures 6A, 6C, 6E and 7C). Their abundance varies with location along the vein. Veinlets are more abundant close to the tip where they represent 100% of the total vein width whereas near the center they represent approximately 5% of the total vein width.

Veinlets are present along the entire length of the vein, regardless of host grain size (Figures 6, 7, 8, and 9). False color SEM-CL images show that there is a difference in luminescence color between: 1) quartz in veinlets, 2) quartz in the main body of the vein, and 3) quartz in the host. Color differences indicate variations in trace element chemistry of the quartz (Hervig and Peacock, 1989; Perny et al., 1992; Watt et al., 1997; Monecke et al., 2002). Quartz in veinlets luminesces blue, quartz in fibers along the main body of the vein luminesces pink, whereas quartz in the host luminesces from light blue to green (Figures 6 and 9). SEM-CL shows sharp boundaries between grains inside some veinlets. We interpret these sharp contacts as being euhedral terminations of the quartz inside the veinlets (Figure 6C).

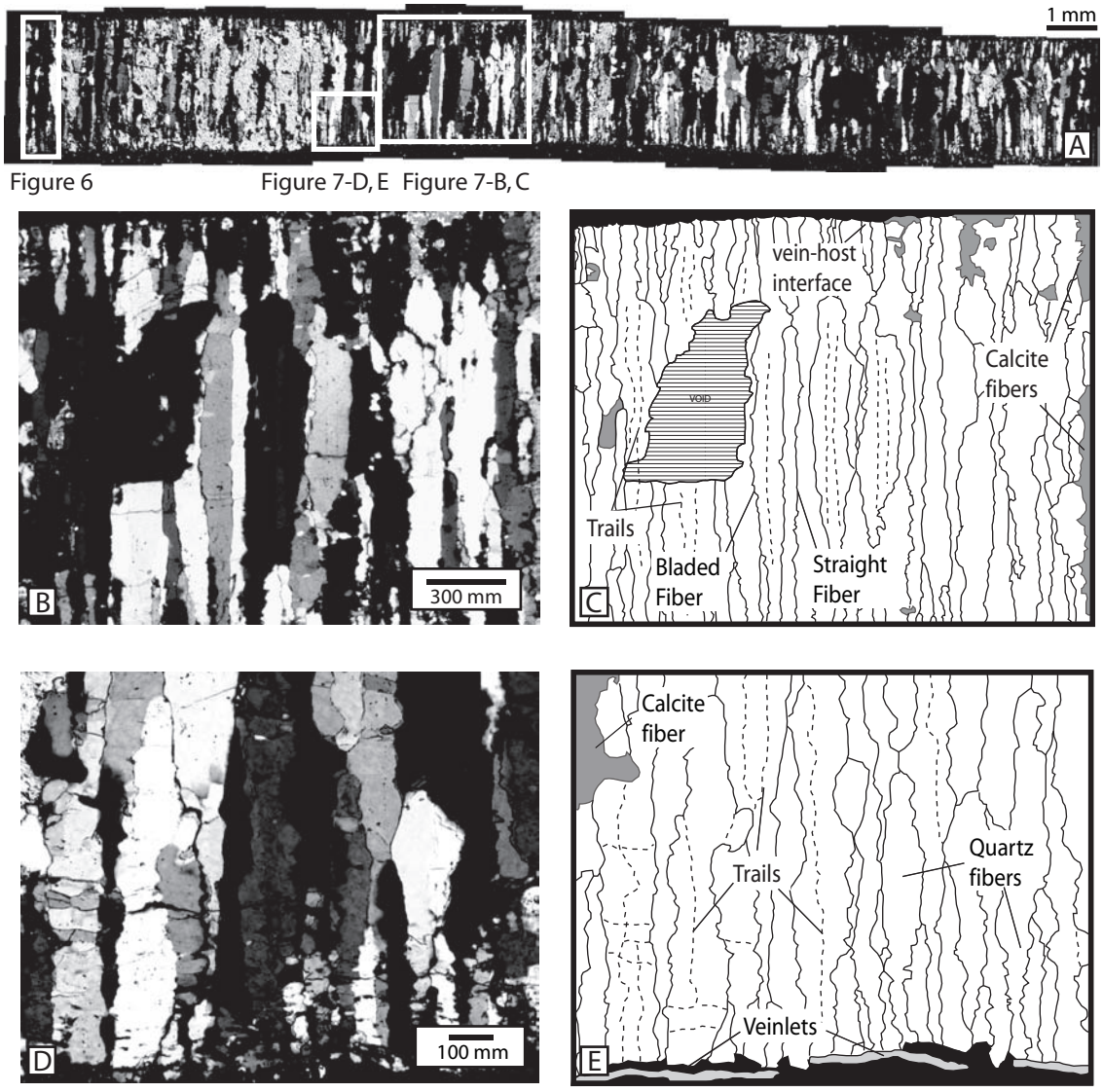

Fig. 7. Photomicrographs showing mid-region vein characteristics. A) Photomicrograph from section AR-48-13 showing the complete vein. B) Photomicrograph of a segment from section AR-48-13. C) Line trace of (B) showing the important features. D) Close up photomicrograph of a segment from section AR-48-13. E) Line trace of (D) showing important features.

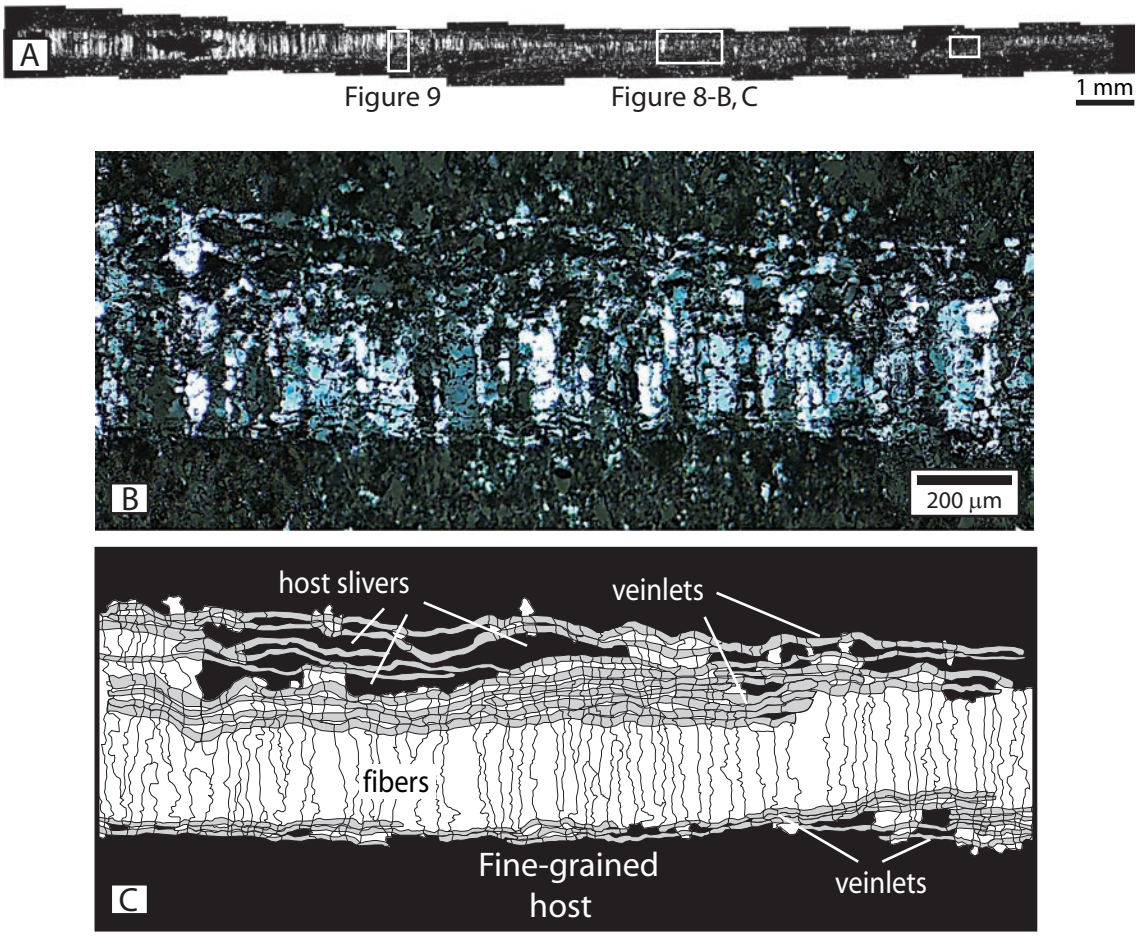

Fig 8. Photomicrographs showing tip-region vein characteristics. A) Photomicrograph from section AR-48-4 showing the complete vein. B) Photomicrograph of a segment from section AR-48-4. C) Line trace of (B) showing the important features. D) Close up photomicrograph of a segment from section AR-48-4. E) Line trace of (D) showing important features.

2.5.3 Fibers

Fibers are elongated strips of quartz and calcite. The fibers are perpendicular to the vein-host interface. Quartz fibers are the most abundant in the vein (>85% of total number of fibers). Quartz fibers aspect ratios (length/width) vary from 0.5 to 25 with a mean at 8. Calcite fiber aspect ratios vary from 0.25 to 11 with mean at 4.5. The calcite in fibers is twinned. Quartz fibers show optical continuity along their length. The optical continuity is interrupted in areas where the fiber is irregular in shape (Figures 7B and C). Fiber shapes in lengthwise section can be straight rectangular (fiber width is constant over the length of the fiber) or lensatic (fiber width increases along the fiber length toward the center of the fiber); (Figures 7A and B). Fibers contain fluid inclusions arrayed both in bands aligned parallel to the host-vein interface and trails aligned parallel to the long axis of the fibers. Inclusion bands are ubiquitous in quartz fibers whereas inclusion trails are exclusive to thick fibers (>100 μm). Thick fibers may show more than one trail spanning the whole length of the fiber (Figures 7A through E).

Contacts between fibers are jagged as has been observed by others (e.g., Ramsay, 1980; Cox and Etheridge, 1983; Cox, 1987; Fisher and Brantley, 1992). The irregularities (steps) along fiber-to-fiber contacts are between 5 to 25 μm or about the same size as veinlet thickness (Figures 6B, 7B and C). SEM-CL shows growth bands parallel to vein-host interface. The width of the growth bands is similar to veinlet thickness. Growth bands disappear towards the center of fibers. Under SEM-CL long

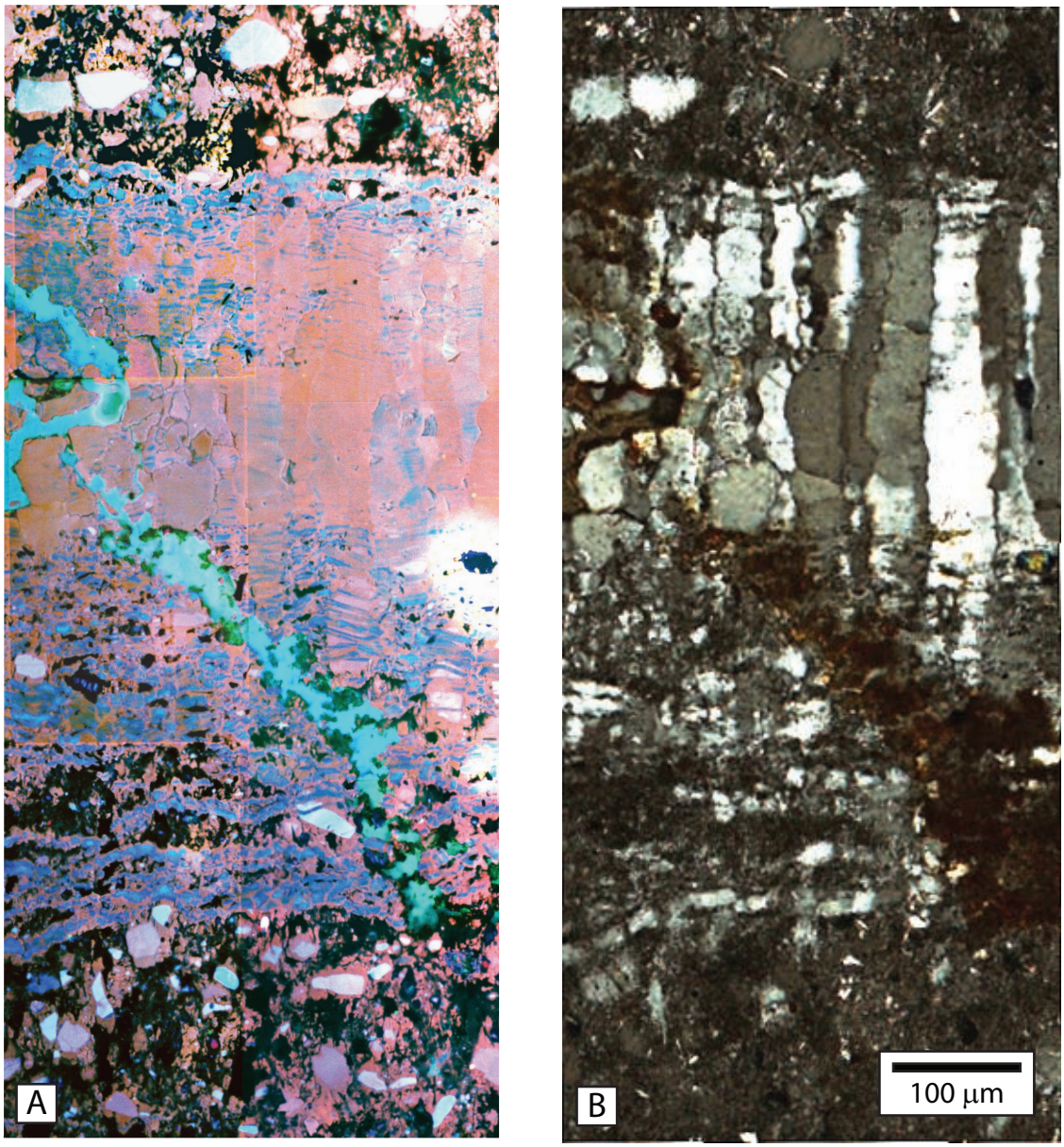

Fig. 9. Polychromatic SEM-CL photomosaic of a section from sample AR-48-4. A) Polychromatic SEM-CL photomosaic of entire vein width. B) Optical photomosaic under crossed-polars showing same area of A. See location in Figure 8.

fibers display ribbons that luminesce in blue parallel to the vein-host interface with shapes and sizes similar to veinlets. These ribbons are commonly enclosed inside the fibers and do not continue across fiber-fiber contacts. We interpret these features as remnants of original veinlets (Figures 6D and 9A).

2.5.4 Host-Fiber Contacts

Measurements of detrital quartz grains in the hosts from several thin sections on both fine and coarse grained host show that the dimensions of the largest grains in the host have dimensions of the same order as the thinnest quartz fibers in the vein (between 20 and 100 μm); (Figure 10). Fiber width in veinlets cutting fine-grained host is thinner than those in veinlets cutting coarse-grained host, less than 20 μm versus less than 50 μm, respectively (Figures 11D and F).

Host mineralogy influences fiber composition. Calcite fibers in the vein are only found adjacent to calcite-rich laminations in the host.

The number of veinlets separated by host segments or slivers in a given vein segment is affected by host grain size. The number of veinlets decreases adjacent to coarse grained host but increases adjacent to fine grained host (Figures 11A and B). This observation is consistent throughout the length of the vein.

2.5.5 Textural Comparison between Vein Center and Vein Tip

The most distinctive differences between tip and middle of the vein are: 1) the host-vein interface in the central part of the vein is smooth and well defined (Figure 7)

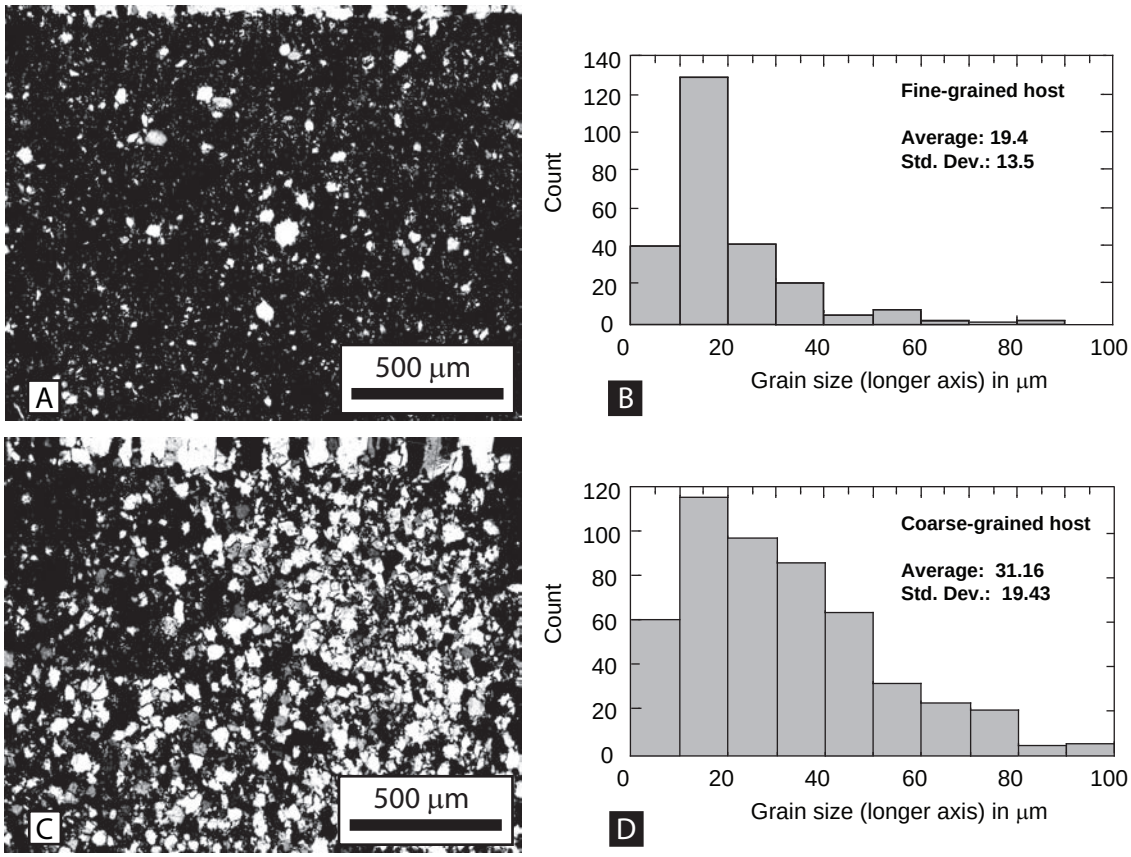

Fig. 10. Comparison between coarse-grained and fine-grained hosts. A) Photomicrograph of a fine-grained section (sample AR-48). B) Histogram of grain size distribution for fine-grained host. C) Photomicrograph of coarse-grained host section (sample AR-48). D) Histogram of grain size distribution for coarse-grained host.

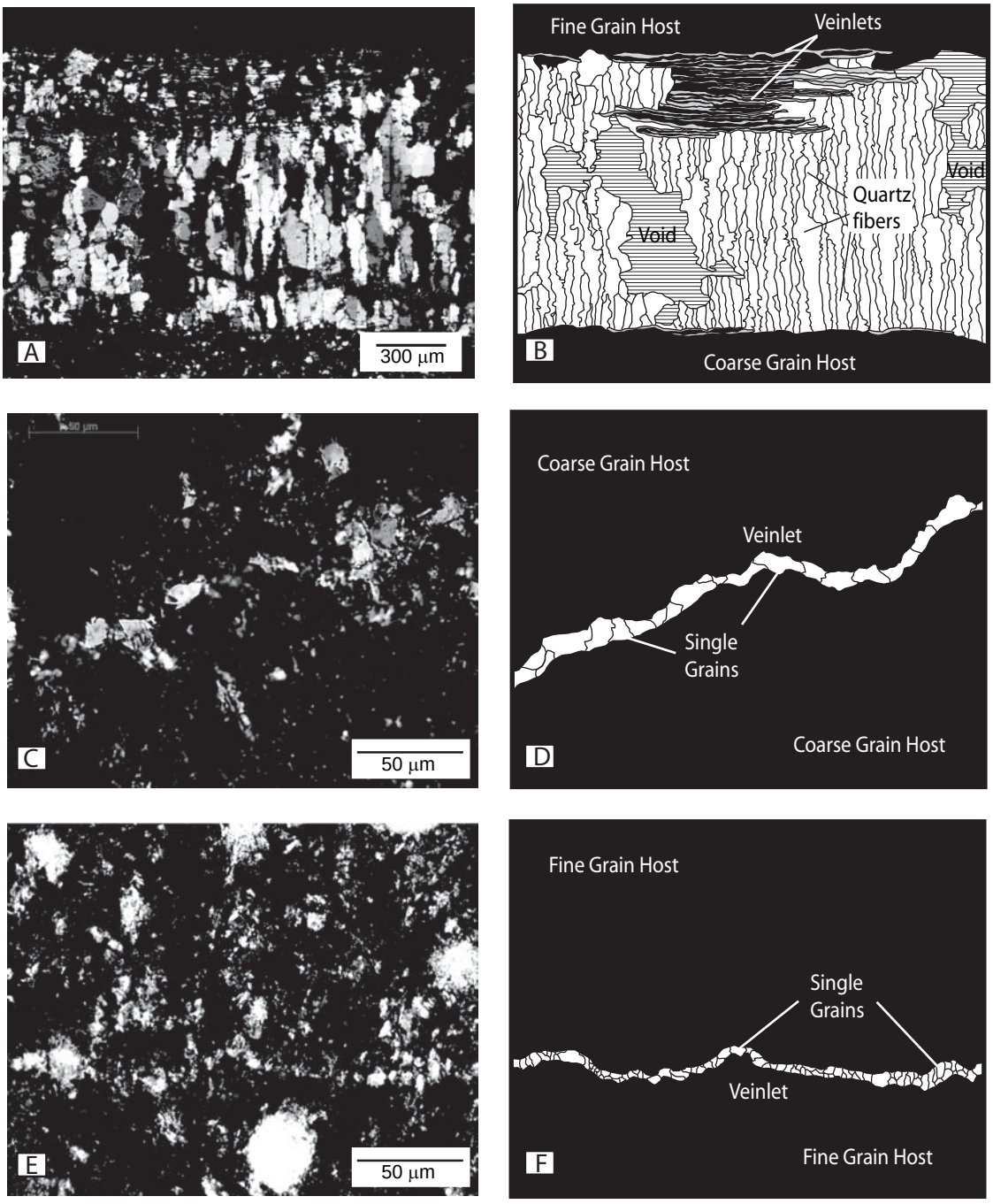

Fig. 11. Photomicrographs showing veinlet characteristics. A) Photomicrograph from section AR-48-6 showing the irregular distribution of veinlets along a vein section. Veinlets start and/or end at fibers. Veinlet width is constant along their length. B) Line trace of (A). C) Photomicrograph of one veinlet cutting across coarse-grained host at section AR-48-13. D) Line trace of (C). E) Photomicrograph of one veinlet cutting across fine-grained host. F) Line trace of (E).

whereas irregular and difficult to define at the tip (Figure 8). 2) Fiber width decreases towards the tip (Figure 12). The average width increases from the tip to the center of the vein (Figure 12). The thinnest fibers in all sections have similar values ranging between 50 and 100 μm (Figure 12A). The thickest fibers are only found in the center of the vein and they range between 150 and 350 μm (Figures 12A and B). Wide fibers (>150 μm) show fluid inclusion trails parallel to fiber long axes (Figure 7). Fibers that span the entire width of the vein are more abundant close to the tip (~ 80% of the fibers) than at the center of the vein (< 15%).

Veinlets are less abundant in the center of the vein than in the tip. Veinlets represent between 5% and 20% of the total volume of the vein at the central region (Figure 7) whereas at the tip they represent between 40 and 100% (Figures 8B, D and 13). Host bands parallel to the vein-host interface are more abundant in the tip region (Figures 8, 9 and 13). The number of veinlets is reduced as the tip is approached up to the point where the tip is formed by only one veinlet (Figure 13). Under cathodoluminescence fibers close to the tip contain more blue luminescent bands than fibers in the central region of the vein (Figures 6 and 9A). Fibers close to the tip retain the original luminescence from incorporated fractured host grains while fibers at the center of the vein do not show this remnant luminescence (Figure 6D).

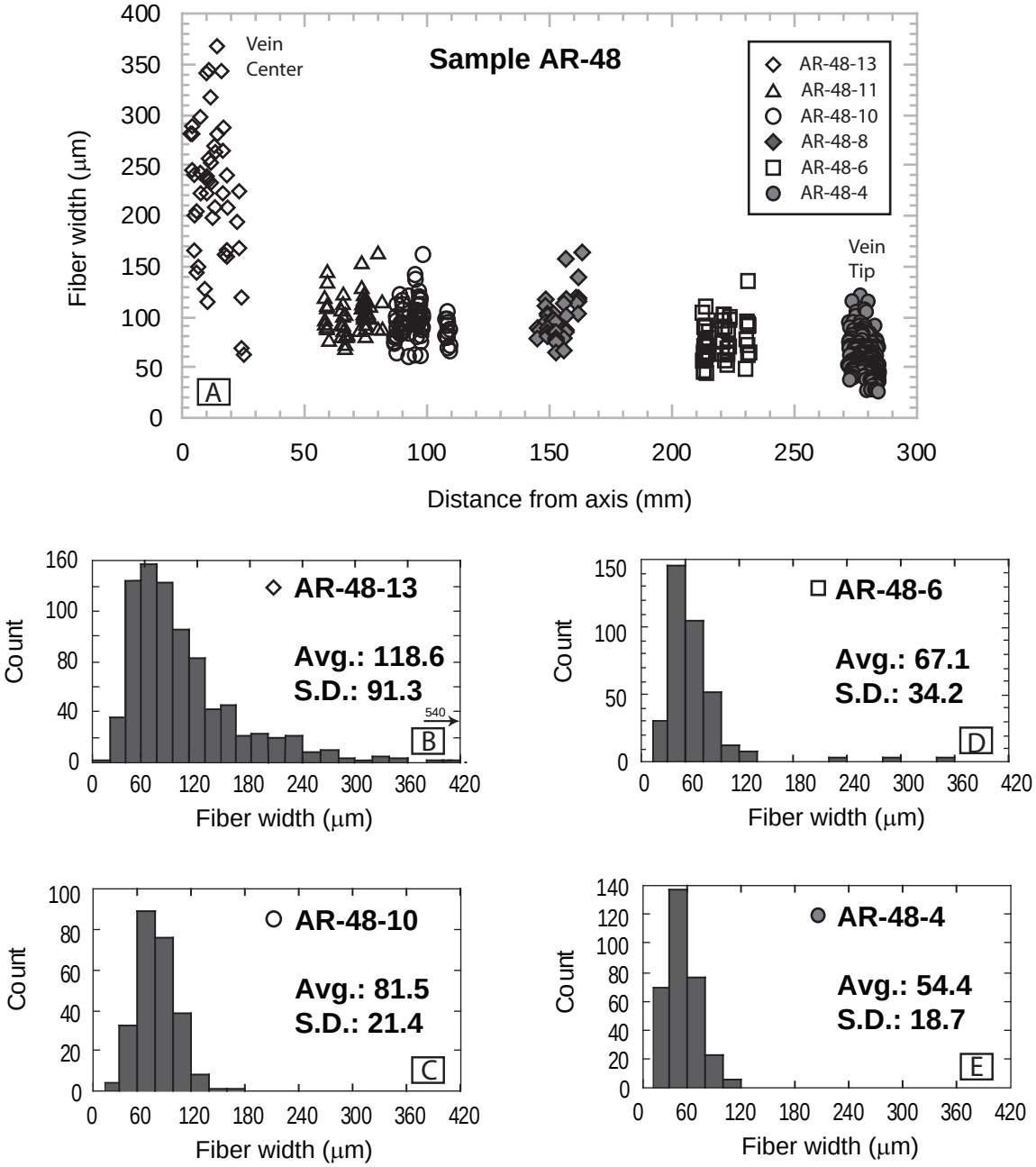

Fig. 12. Plot of fiber width vs. distance from mid-point (x-axis on Figure 5) for sample AR-48. For the plot only fibers spanning the entire width of the vein were considered. A) Plot of all measurements from sample AR-48 (thin sections 4, 6, 8, 10, 11, and 13). B) Histogram of fiber widths from sample AR-48-13. C) Histogram of fiber widths from sample AR-48-10. D) Histogram of fiber widths from sample AR-48-6. E) Histogram of fiber widths from sample AR-48-4.

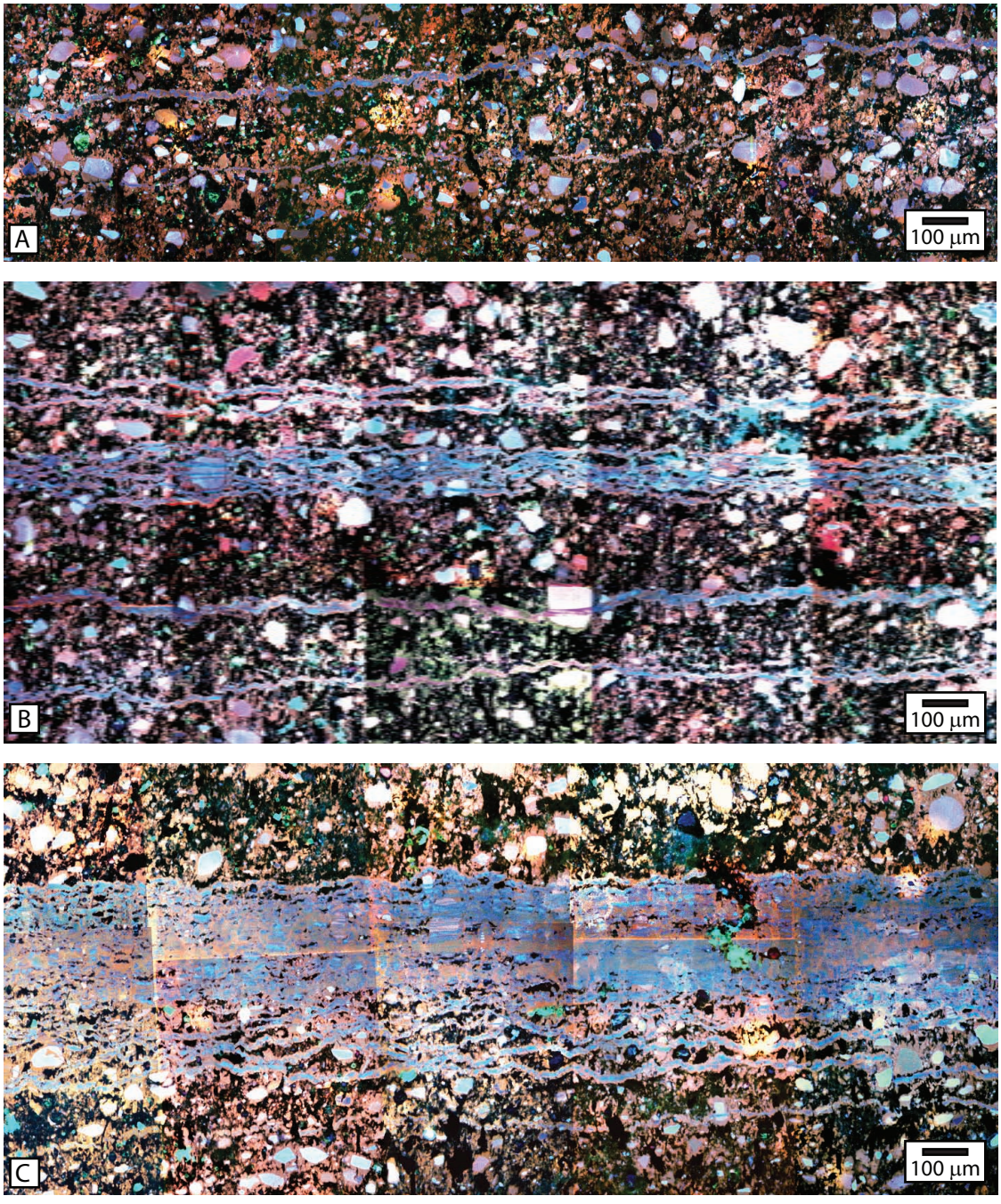

Fig. 13. Veinlet numbers as the vein tip is approached. Polychromatic SEM-CL photomosaic of one segment of section AR-48-4 and two segments of section AR-48-3. A) Polychromatic SEM-CL photomosaic of the segment from section AR-48-3 closest to the tip. B) Polychromatic SEM-CL photomosaic of the segment from section AR-48-3 adjacent to section AR-48-4. C) Polychromatic SEM-CL photomosaic of the segment from section AR-48-4 adjacent to section AR-48-3

2.6 Discussion

2.6.1 Vein Origin

This vein displays many of the textural features described in the literature as evidence for the crack-seal process. Among these observations are: 1) the same minerals are found in both vein and host (Ramsay, 1980; Cox, 1987; Fisher and Brantley, 1992; Hilgers and Urai, 2002), 2) the fibers in the vein maintain the same optical orientation even where the fiber walls change orientation (Ramsay, 1980; Cox and Etheridge, 1983; Fisher and Brantley, 1992; Bons, 2000; and Hilgers and Urai, 2002) and, 3) the fiber width is similar to host grain size (e.g., Cox and Etheridge, 1983).

The Ouachita vein also shows regularly spaced fluid inclusion bands that cross-cut vein fibers and parallel the vein-host interface. This vein does not show solid inclusion bands of different mineralogy than the fiber as described in other studies (e.g., Ramsay, 1980; Cox and Etheridge, 1983; and Fisher and Brantley, 1992).

Although the vein has several characteristics similar those described in veins from other studies, it also displays uncommon features. The most striking are the veinlets. Veinlets are observed throughout the vein's length. They have been described in the literature as: 1) thin filled fractures with no clear localization of the growth surface (Durney and Ramsay, 1973), 2) fracture and precipitation sites responsible for the formation of stretched-crystals (Passchier and Trouw, 1996) and 3) planar segments

separated by short wall segments, inclined or at moderate angles to the vein margin (Cox, 1987).

Fracturing and precipitation result in the formation of veinlets. Each veinlet represents a new filled fracture. We suggest that veinlets coalesce to form the vein. The evidence we have described is that: 1) they are always present at the edge between vein and host, 2) the tip of the vein is a single veinlet, 3) fractured host grains are cut by veinlets and the host fragments are separated by the veinlet mineralization, 4) veinlets are more pronounced at vein walls and become less distinct towards the center of the vein, and 5) fibers show growth bands with similar luminescence signature as veinlets parallel to host-vein interface. These growth bands represent remnants of fracturing events.

Fiber textures suggest that fibers form by a continuous process of recrystallization produced by dissolution-reprecipitation and manifested as grain boundary migration. The observations leading to this suggestion are: 1) increasing fiber width with distance from the vein tip, 2) presence of inclusion trails inside wide fibers (>100 μm) parallel to the long axis of the fiber. These inclusion trails represent previous fiber-fiber contacts that, after grain boundary migration, were incorporated in a larger fiber, 3) fiber widths are larger towards the center of the vein although thin fibers (on the order of host grain sizes) are observed throughout the vein length, 4) the spacing of inclusion trails in thick fibers is similar to the widths of thin fibers without inclusion trails and, 5) the difference in luminescence between the quartz in the veinlets and the quartz in the fibers along the main body of the vein is an effect of grain boundary migration.

Remnants of veinlets are evidenced in fibers showing blue stripes parallel to the vein-host interface.

The best evidence of recrystallization comes from the difference in luminescence between quartz in veinlets and quartz in fibers. Differences in luminescence represent variations in the chemistry and concentration of the impurities in the quartz (Hervig and Peacock, 1989; Perny et al., 1992; Watt et al., 1997; Monecke et al., 2002).

Differences in quartz luminescence have been used to discriminate between episodes of quartz crystal growth. For instance, Goldstein and Rossi (2002) used SEM-CL to describe the textures of quartz overgrowths around detrital grains in sandstones. They observed that the overgrowths followed the crystallographic orientations of the detrital grains and determined that the textures observed (growth banding and growth zoning) could only be explained as recrystallization of silica unstable phases such as opal-CT, cryptocrystalline quartz or microcrystalline quartz into a more stable phase like coarse quartz. Bignall et al. (2004) analyzed euhedral quartz crystals under SEM-CL. They observed textures that revealed generations of crystal growth, dissolution and fracturing under SEM-CL that appeared optically continuous. They were able to tie different growth bands with different fluid conditions using fluid inclusions.

The presence of impurities in quartz has been shown to be directly related to crystal growth rates. Ihinger and Zink, (2000) analyzed the geochemical variations as well as concentration of impurities of three different hydrous species (AlOH, LiOH and HOH) through different cuts across a single Brazilian crystal. Where these impurities are embedded within the crystal they provide a continuous record of the relative growth

rate of the individual crystal faces. Based on the work of Watson and Liang (1995) and Paquette and Reeder (1995) that showed that impurity concentrations will increase with increasing growth rate independent of pressure and temperature of the environment, Ihinger and Zink (2000) proposed that when the crystal grows at a rate too fast to maintain equilibrium, impurity concentrations will increase with increasing growth rate and result in chemically distinguishable zones. Kawasaki (2003) showed that inhomogeneities in the crystal faces caused by the presence of impurities are tied to growth rates. He also showed that these inhomogeneities can affect the luminescence intensity of quartz.

We suggest that the differences in luminescence between the quartz precipitated in the veinlets and the quartz precipitated after recrystallization can be explain by two processes involving different rates, similar to what Ihinger and Zink (2000) observed. For example, if the rate of precipitation of the quartz deposited on the veinlets was fast because the fluid was far from equilibrium (high supersaturation) the precipitating quartz could contain high impurity concentrations whereas if the quartz precipitated at a slower rate from a fluid closer to equilibrium (low supersaturation) after recrystallization the quartz could contains less impurities.

The observation that fibers grow laterally at the expense of previously formed fibers suggests that dissolution-reprecipitation might be controlled by one or both of these two processes: 1) preferential dissolution of particular quartz faces and/or 2) differential dissolution of different quartz faces due to differences in rate of growth. Preferential dissolution of particular quartz faces can be tied to the composition of impurities

preferentially incorporated along particular crystallographic orientations (Ihinger and Zink, 2000). For example, AlOH defects can be preferentially oriented along channels that run parallel to the c-axis. Dove (1999) and Dove et al. (2005) showed that quartz dissolution rates are inhibited by the presence of Al and Fe. These two observations combined would result in the preferential dissolution of quartz faces with less Al impurities. The second process suggests that preferential dissolution of quartz faces can be tied to differences in rate of growth for different crystal faces. Iwasaki et al. (1998) evaluated growth rates for different quartz faces comparing synthetic quartz growth experiments against computer generated geometrical crystal growth experiments. They observed that the rate of crystal growth parallel to c-axis is five times faster than the next fastest crystal face (r-face) and more than 150 times faster than the slowest crystal face (m-face). The same effect of growth rate with orientation was described by Lander et al. (2002) and Laubach, et al. (2004) after studying textural characteristics of natural quartz veins under cathodoluminescence. These studies suggest that dissolution-reprecipitation processes will favor crystallographic orientations with faster growth rates.

Either of these or a combination of both processes could be the driving force for grain boundary migration where dissolution of less stable quartz orientations (for example, faces with less Al impurities and/or faces growing at slower rates) and further precipitation of more stable ones occurs along fiber-fiber contacts.

From the observation of the vein's texture we suggest that vein evolution and growth involves: a) fracturing and precipitation and b) later recrystallization expressed as grain boundary migration.

2.6.2 Association of Veins and Boudinage

The means by which fracturing is localized has been one of the concerns of previous authors. Ramsay (1980) and Cox and Etheridge (1983) suggest that fracturing occurred along areas of strength contrast in the host enhanced by abnormal fluid pressure. Fisher and Brantley (1992) and Fisher et al. (1995) suggest that fracturing occurs at the host vein interface due to lower cohesion between the host rock and the newly precipitated material. Taber (1920), Means and Li (2000) and Wiltschko and Morse (2001) suggest that fracture propagation and subsequent vein widening is caused by pressure due to growing crystals.

Our field observations show that veining and boudinage are mechanically linked. We suggest that boudinage is responsible for the localization of the stress required to form these veins.

In the Lake Pineda outcrop, boudinage is observed at several scales. Large veins (meters long and 10's of cm wide) are associated to boudinage necks formed in sandstone layers 10's of centimeters thick whereas thin and elongated veins (cm long and up to 1 cm wide) are associated with sandstone laminae less than 1 cm thick. The width of the veins is a direct effect of the thickness of the sandstone layer containing the veins. The close relationship between boudinage and veining has been described by

many authors (e.g. De Paor et al., 1991; Swanson, 1992; Sintubin et al., 2000; Bojar et al., 2001; Urai et al., 2001).

Several mechanical models have been proposed to explain the formation of boudinage and to understand the stress conditions necessary to form this structure. All models place the formation of boudinage as a response to viscosity contrast between the layer containing the boudins and the material surrounding it and the distance between boudin necks as a relation between layer thickness and viscosity contrast between layers.

Smith (1977) compared folding and boudinage as geological structures developed after instabilities or perturbation in a layer contained in a matrix with different mechanical properties both with non-Newtonian rheologies. He established that boudinage grow on a competent layer surrounded by a less competent matrix and that the shape of the boudins and the separation between boudin necks is a function of the orientation of stresses. Boudinage formed by layer parallel extension comes from normal compression.

Mandal et al. (2000) modeled boudinage in multilayers of alternate brittle and ductile layers under layer normal-compression. Competent (brittle) layers were modeled as elastic solids whereas incompetent (ductile) layers were modeled as Newtonian viscous solids. Using the Griffith criterion for the dynamic analysis of failure of brittle layers, they established that the layer-thickness ratio and the strength ratio between the tensile strength of the brittle unit and the ductile flow strength of the ductile units are the principal physical factors controlling the type of boudinage

observed. Tensile fracture boudinage (caused by layer parallel extension) develops when the layer thickness ratio (thickness of brittle layer/thickness of ductile layer) is low and when the strength ratio between the brittle layer and the ductile layer is high.

Pollard and Fletcher (2005) proposed that boudinage occurs in an isotropic power-law fluid in contact with a plastic solid. Their model suggests that the distance between boudin necks is related to the thickness of the layer and that boudinage formation is favored in nearly plane deformation. Their stress analysis shows that stress perturbations or deviations from the mean stress are negative where the layer is thinnest. These negative perturbations correspond to tensile stresses in the layer whereas the regions where the layer is thickest are subjected to compressive stresses.

These models show that once pinching of the stronger layer starts, stresses localized at these thin regions originating the formation of boudin necks. Boudinage in the Lake Pineda outcrop always occurs when a layer of sandstone is surrounded by slate. The differences in mechanical properties of these rocks allowed the localization of stresses that originated boudinage. We suggest that the repeated cracking required to form our vein is controlled by these structures forming in the sandstone.

2.7 Integrated Kinematic-Chemical Model

Our kinematic model of vein evolution incorporates the following stages. Stage 1: Folding of the sedimentary sequence (Figure 14A). The wavelengths of the folds are controlled by the thickness of the competent layers (sandstone). Continued deformation resulted in the formation of recumbent folds and thrust faults (Figure 14B). Stage 2:

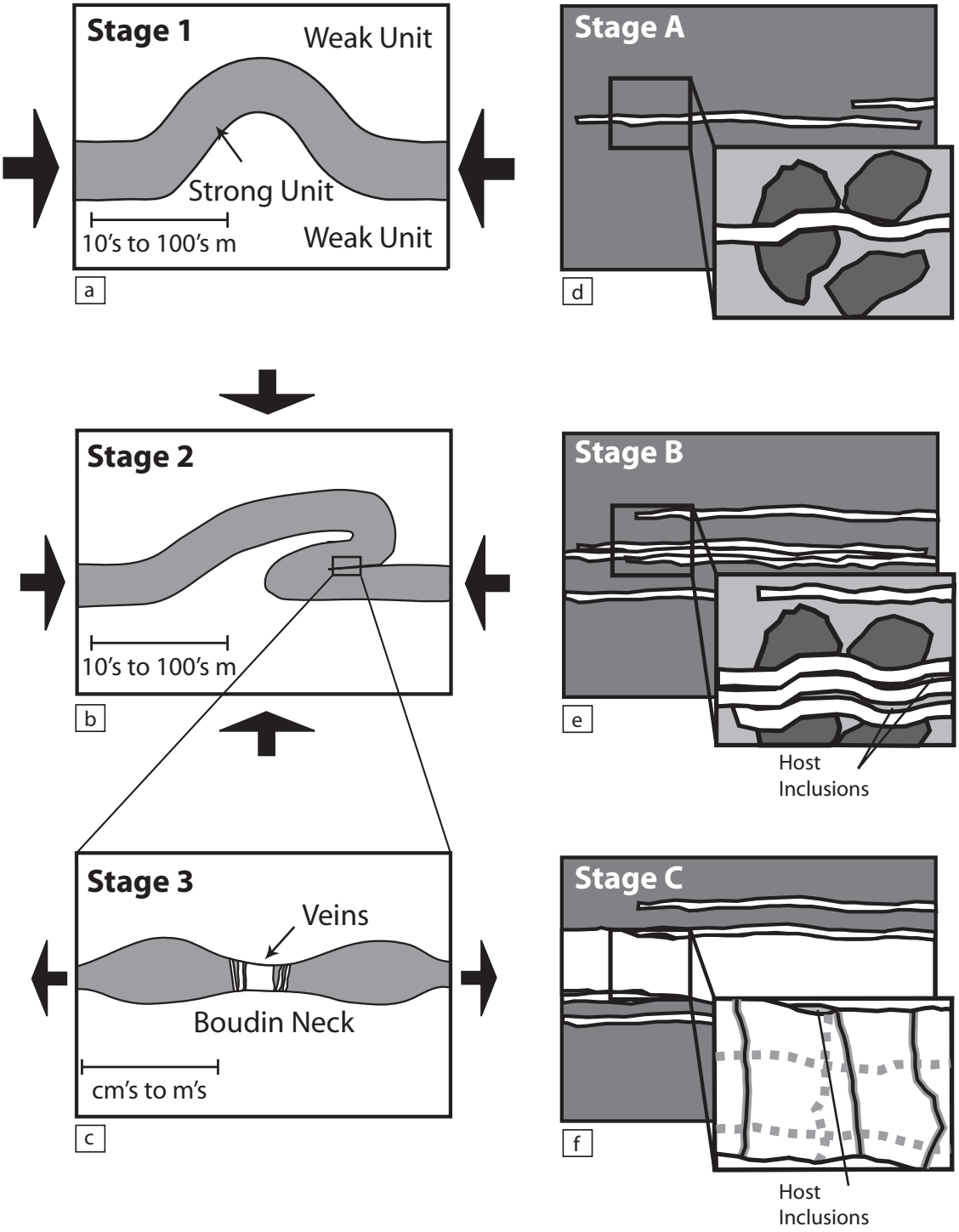

Fig. 14. Schematic diagram showing vein growth model. See explanation of stages in text. a) Stage 1 of deoformation. b) Stage 2 of deformation. c) Stage 3 of deformation. d) Stage A of vein formation. e) Stage B of vein formation. f) Stage C of vein formation.

The emplacement of duplexes at depth changed the orientation of the far-field stress rotating the maximum principal stress from horizontal to vertical. This rotation caused the flattening of the deformed sedimentary sequence (Figure 14B). Stage 3: Flattening of the overturned and fractured fold limbs resulted in dissolution giving rise to cleavage and layer parallel extension of the more resistant layers resulting in the formation of boudinage of the sandstone layers (Figure 14C).

The stages involved in the formation of the vein follow the evolution of the encasing boudin. Stage A: Individual fractures originated at the necks of boudins. Fracturing along necks generated chemical potential gradients allowing vein forming material to diffuse towards the neck and precipitate. Coarse-grained host layers and cleavage planes acted as conduits for the vein forming material. As layer parallel extension continued, fracturing events where localized along the necks in areas where strength contrast between newly precipitated material and host rock where highest (Figure 14D). Host slivers are predominant at this stage separating different veinlets. Stage B: Host grains acted as seeds for fibers. Progressive fracturing events cut across grains in the host, particularly along coarse-grain host. This process generated clean surfaces where a supersaturated fluid precipitated quartz using the host grain as template for growth, maintaining its crystallographic orientation. Repetition of this process allowed fibers to grow (Figure 14E). As fracturing becomes localized, the volume of host inclusions to vein material is reduced. Stage C: Recrystallization of early precipitated quartz into stable crystallographic orientation of the fibers. This process changed the composition of the newly precipitated quartz as evidenced by

differences in luminescence colors. This process caused vein fibers to grow laterally in width (Figure 14F). Quartz grains in the host inclusions is dissolved and recrystallized as well, reducing the size of the host inclusions.

2.8 Conclusions

Veinlets and fibers constitute the most characteristic textural features in the vein. Veinlets are thin (5-25 mm) veins parallel or at low angle to the host-vein interface. Fibers are elongated strips of quartz and calcite that grow perpendicular to the vein-host interface. Fibers contain fluid inclusion bands parallel to the vein host interface. Thick fibers (>150 mm) contain fluid inclusion trails parallel to the fiber long axis.

The vein textures vary along its length. Textural variations are evident when observed under polychromatic SEM-CL because quartz luminescence in fibers, veinlets and detrital host grains is different. Quartz fibers have pink luminescence, veinlets blue and detrital host grains show several luminescence colors (green, yellow, light blue, etc.). At the central region of the vein the body of the vein is predominantly formed by fibers whereas the tip region is formed by veinlets.

Veinlets represent cracks filled by quartz precipitating from a liquid. Coalescence of veinlets allows veins to lengthen and widen. Fibers are formed after recrystallization (dissolution-reprecipitation) of the quartz forming the veinlets.

The differences in texture along the vein represent an evolution through time. Early events of vein formation are characterized by the formation of veinlets. Fibers form

later from dissolution of the earlier precipitated quartz and reprecipitation into more stable phases.

The stress localization required for the formation and growth of these veins is controlled by local structures. In the Ouachitas, layer-parallel extension in recumbent fold limbs formed boudins. The boudin-necks are the areas where veining took place.

3. ENVIRONMENT OF FORMATION OF FIBROUS SYNTECTONIC VEINS. A CASE FROM THE OUACHITAS, ARKANSAS

3.1 Précis

Tectonic veins are evidence of the presence of fluids during deformation. We combined micro-textural observations, stable isotopes and fluid inclusions in a set of tectonic fibrous quartz-calcite veins from the Lower Ordovician Mazarn Formation, Arkansas' Ouachitas to understand the role of fluids in vein formation. Structurally, the veins are located at boudin necks and are synchronous with cleavage formation. Texturally, the veins are characterized by veinlets (thin veins between 5 and 25 μm thick) that parallel the vein-host interface and fibers (columns of quartz or calcite) perpendicular to the vein-host interface with widths between 30 and 350 μm. $\delta^{18}O$ values of vein quartz and host immediately adjacent to the vein are within 2‰ of each other suggesting that the fluid was local and rock-buffered. Nevertheless, $\delta^{18}O$ and $\delta^{13}C$ values in calcite define a 'J' shaped trend. Although it is not possible to date any portion of this curve, the simplest explanation is that the fluid evolved from rock-buffered and local into an open system. The change in fluid behavior is tracked by changes in texture. Fluid inclusions also track textures. High-T inclusions (between 200 and 250 ºC) formed in quartz precipitating in veinlets and Low-T inclusions (between 90 and 190 ºC) formed during recrystallization. P-T condition of vein formation determined from fluid inclusions and quartz-calcite oxygen isotopes thermometry is between 366 and 422 °C and 1500 and 3750 bars. The environmental conditions under

which the Ouachtia veins were formed are similar to those observed in other tectonic settings suggesting that greenschist facies metamorphic conditions are required for the formation of quartz fibrous veins.

3.2 Introduction

Veins or mineral filled extension cracks are common features in deformed rocks. The presence of veins indicate that fluids were both supersaturated with respect to the vein forming mineral and that the species were mobile during and/or after the deformation event (see review by Wiltschko et al., 1998). Despite the ubiquity of veins, the mechanisms of their growth are still poorly understood. At the center of the debate is the origin and amount of fluid required to precipitate the vein material. Two proposed mechanisms are, 1) force of crystallization (Taber, 1916, 1918 and 1920; Misik, 1971; Means and Li, 2001; Wiltschko and Morse, 2001) and, 2) repetitive fracturing or the "crack-seal" mechanism (Ramsay, 1980; Cox and Etheridge, 1983; Laubach et al., 2004). Force of crystallization requires diffusion as the transport mechanism of the vein forming material from the source to the vein. Veins need not to be part of a fracture network. The "crack-seal" mechanism as originally proposed (Ramsay, 1980) requires advection of fluid in and out of fractures to allow precipitation of the material in the veins. Fisher and Brantley (1992) and Fisher et al. (1995) show that the amount of fluid required to precipitate quartz veins by advection is far larger than the volume of a fracture and suggested instead that diffusion is the most likely mechanism of material transport. Their vein model is "crack-seal" but the material transport is by diffusion

where a fluid film of 10's of m length (depth) and μm's wide drive the fracturing process and allows for diffusion through the host to fill the fracture. For their model, fracture connectivity is required.

Some of the controversy over mechanisms of formation may be resolved by coupling stable isotope and textural observations. Specifically, stable isotopes provide an important constraint on the source of the vein forming fluids and inherently the mode of transport of the material. Veins whose components are precipitated from a fluid in equilibrium with the local host will be close in isotopic composition to that of the host rock (e.g., Cartwright et al., 1994; Al-Aasm et al., 1995; Kirschner et al., 1995; Henry et al, 1996; Kenis et al, 2002; Ghisetti et al., 2001; Richards et al., 2002; Hilgers et al., 2006). By contrast, veins with isotopic composition in disagreement with the host are interpreted to have precipitated from an allochthonous or introduced fluid, a fluid that may never have been in equilibrium with the local host (e.g., Dietrich et al., 1983; Shemesh et al, 1992; Kirschner et al., 1993; Nesbitt and Muehlenbachs, 1995; Templeton et al., 1998; Evans and Battles, 1999; Kirkwood et al., 2000; Suchy et al., 2000; Travé et al., 2000; Suchy et al., 2002).

External fluids require a network of conduits such as fractures and faults (e.g. Sibson, 1990). Local fluids may leave behind dissolution seams and chemical gradients around the features that allowed the transport of material (e.g. dissolution seams described by Rye and Bradbury, 1988; chemical gradients around veins described by Fisher et al., 1995). In the latter case, demonstrably connectedness among veins and fractures may be either lacking or bed-contained. For this reason, field descriptions of

structures around veins and microtextural descriptions of the veins combined with chemical analyses may yield important evidence for the mechanisms of vein formation and growth.

The environmental conditions under which fibrous veins are formed will influence the material transport mechanism involved in the process. We plotted the reported environmental conditions for different tectonic settings under which fibrous veins have been formed. Fibrous veins are found in both continent-continent collision settings (Appalachians, Variscan, Pyrennes, Appenines and Ouachitas) and in subduction zones, particularly in old accretionary prisms (Kodiak, Shimanto). Quartz fibrous veins are most commonly found in fine grain rocks (Table 1) whereas calcite veins are found where carbonates are present (Table 1). Calcite veins start to form under low metamorphic conditions, zeolite facies (fill squares in Figure 15) and can be found formed with quartz veins under medium metamorphic conditions, greenschist facies (Table 1). Quartz fibrous veins are mostly found in rocks subjected to greenschist metamorphic conditions (open squares in Figure 15). Most fibrous quartz veins formed between 200 and 350 °C and between 0.5 and 3 kbar (Figure 15). The narrow range of temperature and pressure and the low-porosity and low-permeability of the host rocks indicate that these conditions are required in the formation of fibrous veins and need to be incorporated into mechanism envisioned to explain their formation.

In this paper we combined structural data and microtextural descriptions of the veins with stable isotopes, fluid inclusions and mineralogical data to constrain the

Table 1. Pressure and Temperature conditions reported for areas where fibrous veins have been described.

Area	Rock Type	Age	Vein Type	T °C	P kbar	Methods
Southern Appalachians (a)	Shale interbedded with limestone	Upper Cambrian	Fibered calcite veins, blocky, crack-seal	80 - 110	0.5 - 0.9	Fluid inclusion Burial history
Ireland, Variscan (b)	Metaclastics overlying deformed sediments	Upper Paleozoic	Quartz veins	275 - 325	0.8 - 1.7	Fluid inclusion Burial history
Victoria Australia, Bendigo-Castelmaine (c)	Quartz-rich turbidite sandstones and siltstones	Ordovician-Early Devonian	Gold-quartz veins	180 - 310	0.8 - 1.4	Fluid inclusion
Queensland Australia (d)	Graphitic black slates	Middle Proterozoic	Quartz veins, Calcite veins?	325	1.2 - 2.8	Fluid inclusion
Central Pyrennees (e)	Black shales over limestones	Silurian shales	Quartz-chlorite and quartz-calcite veins	250 - 300	0.6 - 2.0	Fluid inclusion Chlorite thermometry
Central Pyrennees (f)	Contact between granodiorite and metasediments	Devonian sediments	Quartz veins with chlorite Crack-seal veins	310 - 360	2.0 - 5.0	Fluid inclusion Chlorite thermometry
Helvetic Nappes, Switzerland Alps (g)	Limestones, marls and shales	Mesozoic and Tertiary	Pressure shadow fibers (quartz)	200 - 270	1.2 - 1.7	Fluid inclusion Illite cryst. Coal rank
Helvetic Nappes, Switzerland Alps (h)	Metagraywacke, shales, slates and limestones	Oligocene	Quartz fibrous veins	210 - 250	2.1 - 2.9	Fluid inclusion Vitrinite refl. Stable isotope geothermometry
Kodiak Accretionary Prism, Alaska (i)	Slates, graywacke, and minor conglomerates	Maastrichtian	Quartz veins with chlorite Crack-seal veins	215 - 290	2.6 - 3.45	Fluid inclusion Burial history
Taconian Orogeny, Québec Canada (j)	Argillaceous or sandy limestone, calcareous shale	Cambro-Ordovician	Calcite veins	80 - 160	0.1 - 0.45	Multiphase fluid inclusions
Shimanto Complex, Japan (k)	Sandstones and mudstones	Cretaceous	Quartz and Calcite fibrous veins	200 - 270	1.5 - 3	Multiphase fluid inclusions
Shimanto Complex, Japan (l)	Sandstones and mudstones	Cretaceous	Quartz crack-seal veins	125 - 245	0.9 - 1.5	Multiphase fluid inclusions
Northern Appenines, Italy (m)	Sandstones interbedded with siltstones	Miocene	Quartz fibrous veins	220 - 280	0.7 - 2.15	Multiphase fluid inclusions

Fibrous veins have been named or described in all papers and veins were used in the determination of the conditions. From: a) Foreman and Dunne (1991), b) Fitzgerald et al. (1994), c) Gao and Kwak (1995), d) Xu (1997), e) Grant et al. (1990), f) Henderson and McCaig (1996), g) Frey et al. (1980), h) Schmidt et al. (1997), i) Vrolijk et al. (1988), j) Kirkwood et al. (2000), k) Hashimoto et al. (2002), l) Matsumara et al. (2003), m) Montomoli et al. (2001).

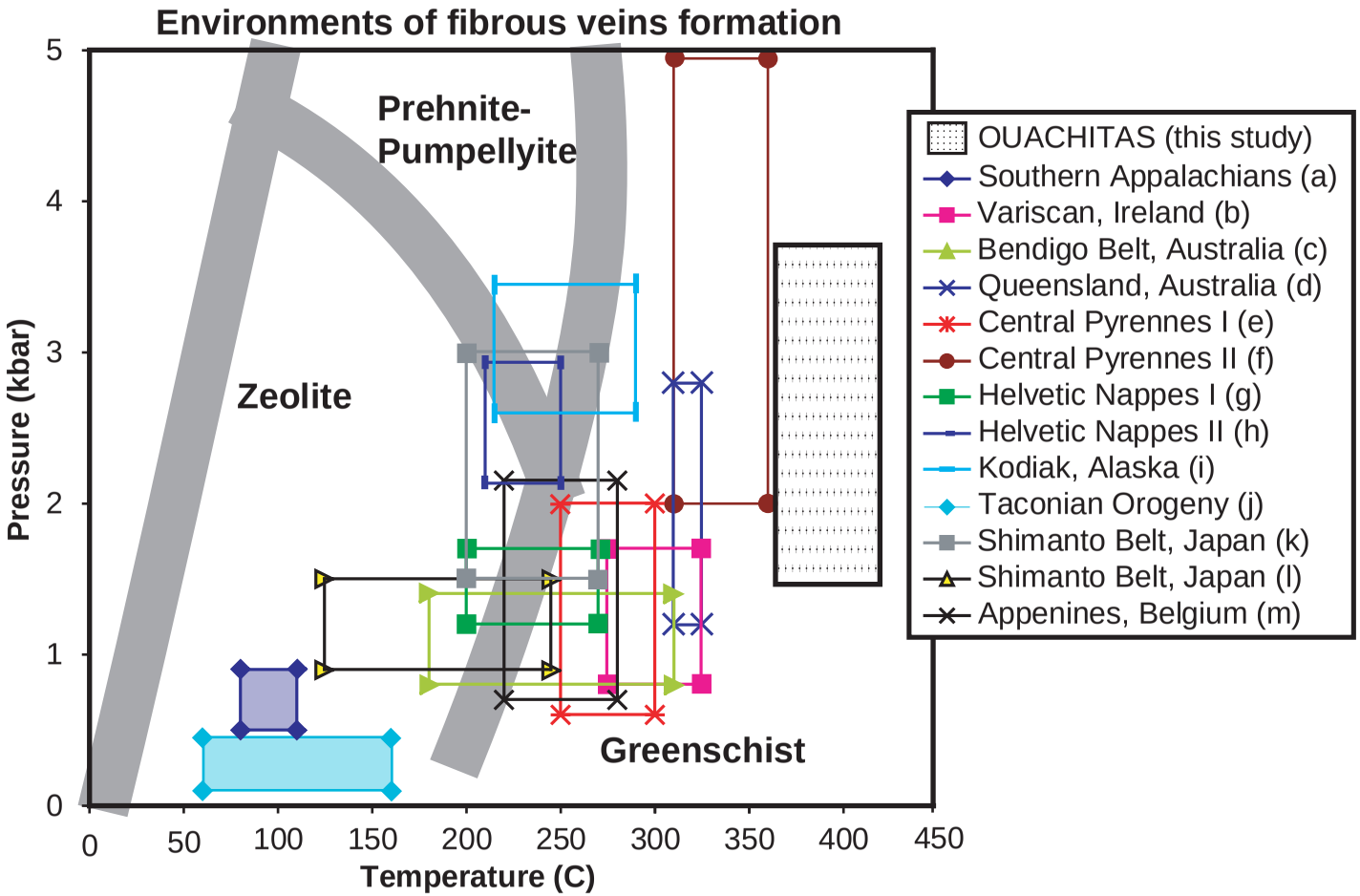

Fig. 15. Environment of formation of fibrous veins as reported for various tectonic settings. Ouachitas veins are represented by the hashed area and the information is discussed in the text. Filled rectangles represent information obtained from calcite veins. Unfilled rectangles represent information obtained from quartz veins. From: a) Foreman and Dunne (1991), b) Fitzgerald et al. (1994), c) Gao and Kwak (1995), d) Xu (1997), e) Grant et al. (1990), f) Henderson and McCaig (1996), g) Frey et al. (1980), h) Schmidt et al. (1997), i)Vrolijk et al. (1988), j) Kirkwood et al. (2000), k) Hashimoto et al. (2002), l) Matsumara et al. (2003), m) Montomoli et al. (2001). Metamorphic facies are drawn after Spear (1993). Quartz veins plot in greenschist facies whereas calcite veins plot in zeolite facies.

environment of formation of a particularly well-exposed set of fibrous, banded veins. These veins are important in that they both display features attributable to the ‘crack-seal’ mechanisms and features that yield new insight into the mode for formation of banded fibrous veins and that they are found in slates subjected greenschist metamorphic conditions (Figure 15).

3.3 Geological Setting

The veins of interest are found in the Benton uplift of the Ouachita fold and thrust belt. This orogenic belt trends east-west and extends from central Arkansas to southeastern Oklahoma (Figure 16). During the lower Paleozoic the area was a south facing passive continental margin followed in the Mississippian by collision with a southern, unknown continent (Viele, 1989; Lillie et al., 1983; Nelson et al., 1982). A Carboniferous marine shale facies at least 12 km thick was emplaced on coeval shelf carbonates (e.g., Houseknecht and Matthews, 1985). In the final stages of the orogeny reverse faults cut crystalline basement, resulting in the northward and vertical movement of a portion of the continental margin producing the Benton and Broken Bow uplifts. This deep-seated thrusting was a late event because sediments are continuous both north and south of the uplifts until late Pennsylvanian or earliest Permian. Shallower than expected paleo-thermal gradients on each thrusted sequence suggest that thrusting was synchronous with peak metamorphism (Underwood et al., 1985). Apatite fission track analysis results show that regional cooling of the Ouachitas

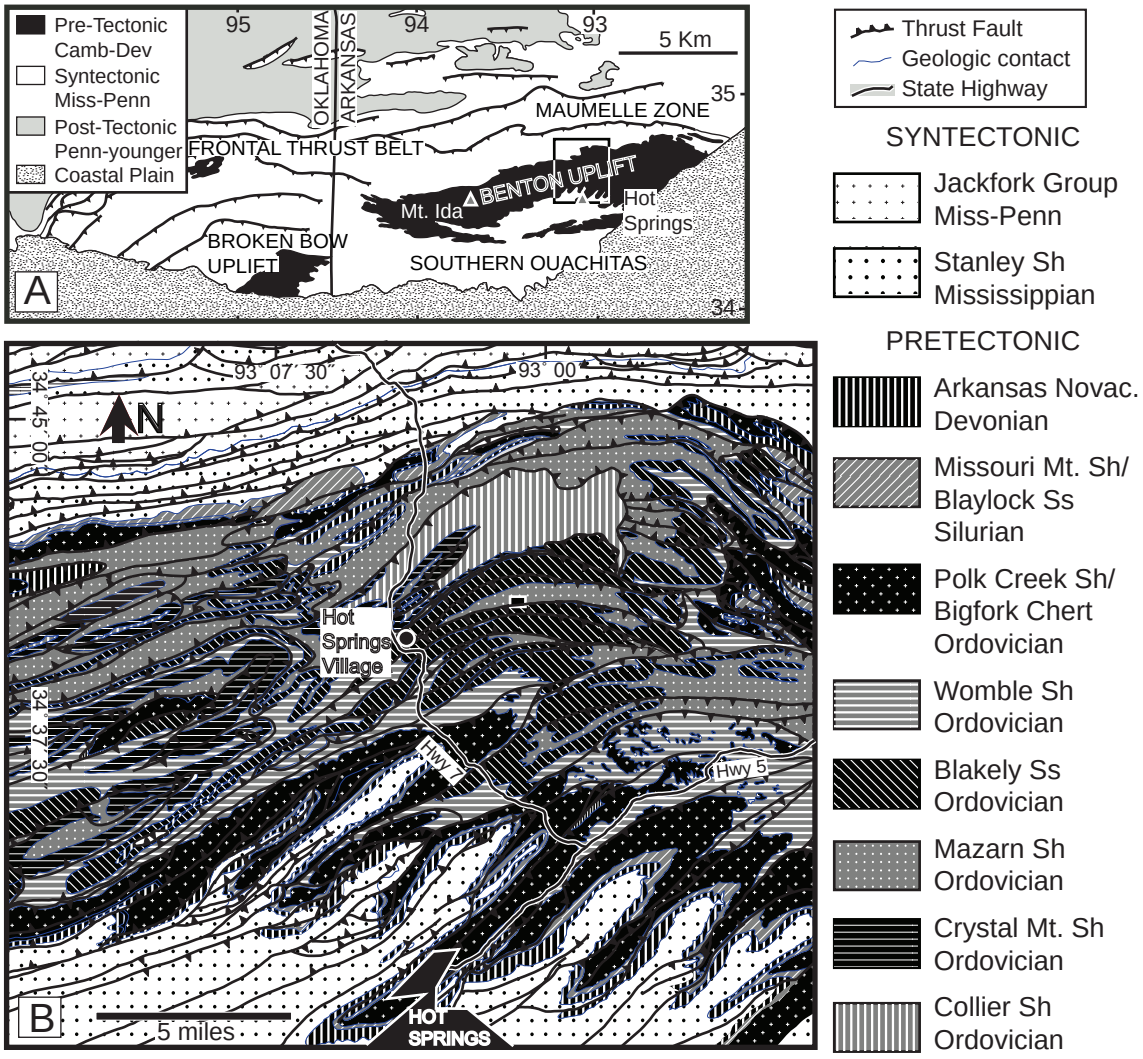

Fig. 16. Geologic map of the Ouachitas and the Hot Springs area, AR. A) Geologic map of the Ouachitas after Miser (1959). The white-black square shows the location of the Hot Springs area. B) Regional Geology of the Hot Springs, AR area with the location of the Lake Pineda Outcrop (solid black square) after Haley and Stone (1996)

took place in Late Paleozoic, before emplacement of postectonic Cretaceous plutons within the Mississippi Embayment (Arne, 1992).

Most of the rocks exposed in the Benton uplift are sedimentary. The pre-tectonic sequence consists of (<4 km thick) thinly bedded Cambrian to lower Mississippian deep-water shales, chert, submarine debris flow and turbidite sandstone represented by the Arkansas Novaculite and Arbuckle facies. The overlying tectonic sequence consists of thick (>13 km) Mississippian to Permian flysch represented by the Stanley shale through lower Atoka Formation (Houseknecht and Matthews, 1985, Blythe et al., 1988). Rock ages within the Benton Uplift range from Ordovician (Collier Shale) to Lower Mississippian (Arkansas Novaculite). The syntectonic Upper Mississippian Stanley Shale unconformably overlies the Arkansas Novaculite (Figure 16).

3.4 Outcrop Geology

All samples come from an outcrop located at Hot Spring Village, 13 miles north of Hot Springs, AK. The outcrop functions as the spillway of Lake Pineda Dam briefly described in Stone and others (1994). The rocks exposed at the outcrop are from the Lower Ordovician Mazarn Shale, an interbedded banded green and black slate, laminated fine-grained gray siltstone, and minor lenses of fine-grained brownish-gray quartzitic sandstone. In outcrop the host consists of interbedded sequences of fine-grained material (silt to clay size) and of coarse-grained material (medium sand to silt size). The thickness of each sequence varies from mm to m thick. This formation was deposited on the south-facing lower Paleozoic passive margin where siltstones and

sandstones layers were deposited as density and marine currents from sources in the north or northeast (Stone and McFarland, 1981; Lowe, 1989). These rocks were deformed as part of the Benton uplift and metamorphosed to greenschist facies. The outcrop is contained within one of the internally folded thrusts of an imbricate stack of Ordovician rocks typical of the east end of the Benton uplift (Figure 16).

The outcrop is crossed by two small thrust faults oriented N60E (Figure 17A). Folds are abundant with wavelengths ranging from cm to m. Small (cm to dm) folded sandstone layers are contained within shale beds whereas larger wavelength folds involve thicker (dm to m) sandstone beds. Poles to bedding (Figure 17B) are aligned NW-SE with a strong concentration of subhorizontal beds. The outcrop is characterized by pervasive cleavage in shales. Cleavage is subhorizontal and at a low angle to bedding (Figure 17C). Horizontal cleavage indicates vertical flattening of the outcrop. Boudinage is present at all scales within sanstone beds from mm to 0.5 m thick.

Veins in the outcrop are best exposed along slip surfaces and these slip surfaces correspond to thicker (dm to m thick) layers of sandstone. Veins are either subvertical or subhorizontal (Figure 17D) and are found within necks of boudinage structures in the sandstone beds. The veins described in this paper come from the vertical sets. It is convenient to group the veins in two categories based on vein length-to-width ratios in hand sample and outcrop. They are low and high aspect ratio which we also refer to as thin and lensatic, respectively. The low-aspect-ratio veins are between 0.1 and 1 m long and between 1 and 4 mm wide. The high aspect ratio veins range in length from 30 cm

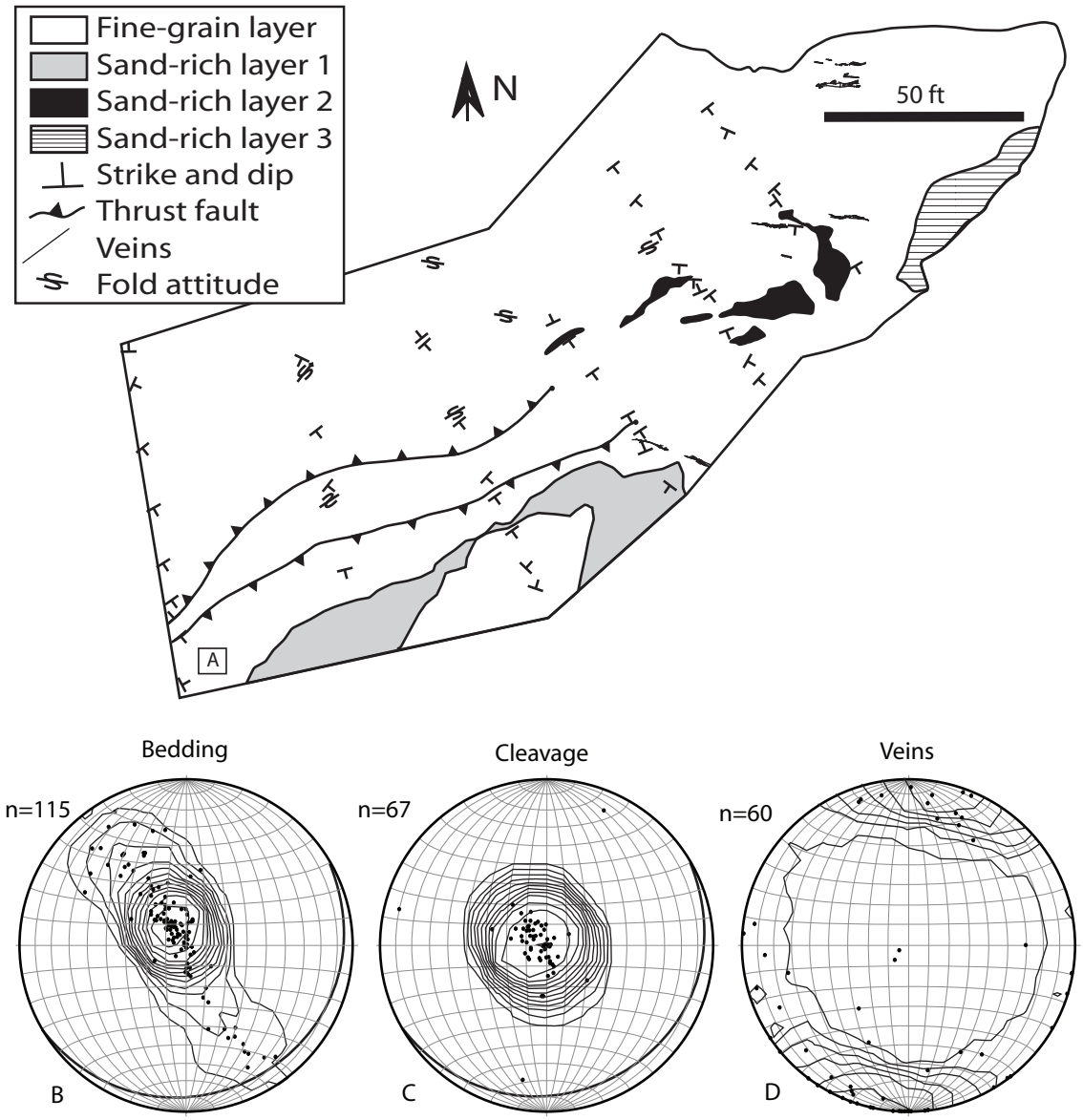

Fig. 17. Lake Pineda Dam outcrop geology and structural data. A) Geology of the Pineda Dam outcrop. B) Poles to bedding planes from the entire outcrop. The bold great circle represents the orientation of the main thrust fault in the outcrop. C) Poles to cleavage planes of the entire outcrop. Great circle represents the orientation of the main thrust fault. D) Poles to vein orientations. All figures are lower hemisphere, equal area projections. All contours are Kamb contours with σ=2.5.

to 5 m and in width from 5 to 40 cm. All veins are fibered with both quartz and calcite fibers. In hand sample, cross-cutting relationships show that veins are earlier than faults and synchronous with cleavage formation because cleavage and veins cross-cut each other.

Individual veins in the outcrop appear to be isolated from each other.

3.5 Vein Textures

3.5.1. Low Aspect Ratio Vein Textures

The vein we sampled is 62 cm long and up to 5 mm wide. Its midline is oriented N75W and the vein walls are vertical. The vein was cut into 15 blocks from tip to mid-section and thin sections were made (Figure 18A). *Veinlets* are ubiquitous throughout the length of the vein. Veinlets are defined as thin (5-25 μm) and elongated (mm's) veins parallel, or at a low angle, to the vein-host interface (Figure 19A, B, C and D). They have the same mineralogy as the larger vein and are defined in part by the 15 to 30 μm wide host segments separating them (Figure 19A, B, C and D). The mineralogy and texture of the host segments is the same as the host not affected by the vein. Fibers are elongated strips of quartz and calcite that are in optical continuity along their length and oriented perpendicular to the vein-host interface (Figure 19A, B, C and D). Quartz fibers are the most abundant in the vein (>85% of total number of fibers). Fibers contain fluid inclusions arrayed in both bands aligned parallel to the host-vein interface and trails aligned parallel to the long axis of the fibers. Inclusion bands are ubiquitous in quartz fibers whereas inclusion trails are found exclusively within thick fibers (>100

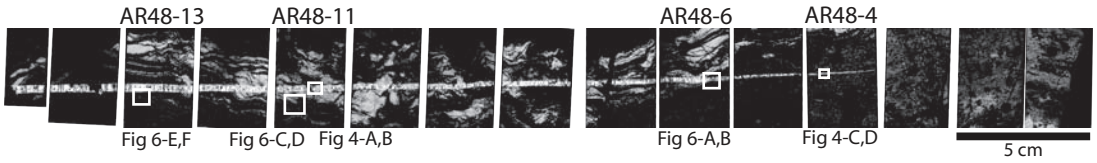

A)

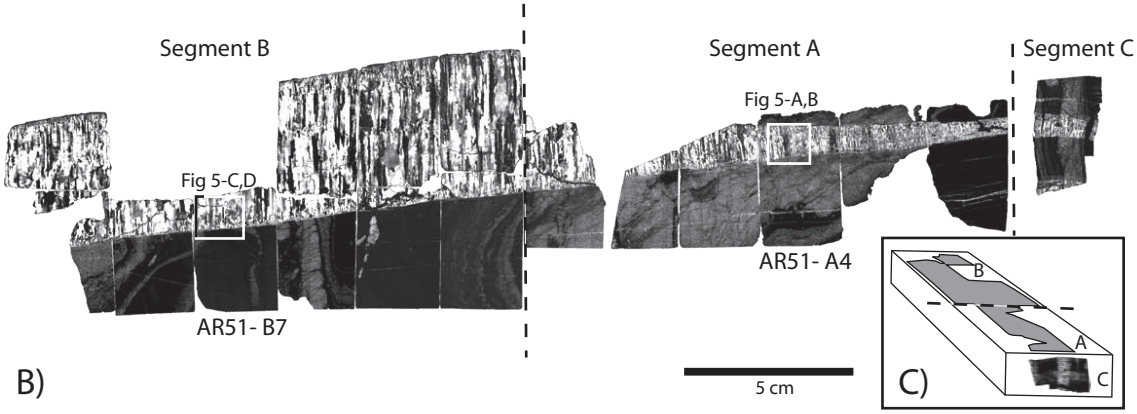

B)

C)

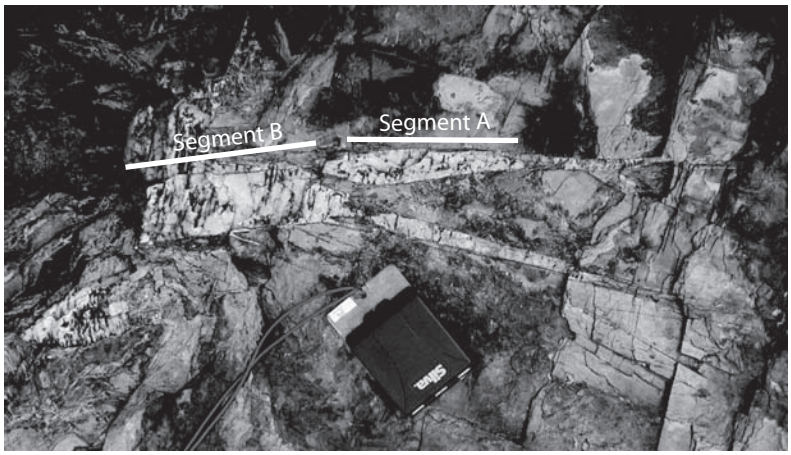

D)

Fig. 18. Types of veins at Pineda Lake outcrop. A) Thin and elongated. For reference, thin section AR-48-13, 11, 6 and 4 are marked. B) Lensatic vein. 3 Segments of the vein are shown, two parallel to bedding (A and B) and one perpendicular to bedding (C). C) Block diagram of the location of Segment C. White boxes on A) and B) represent the location of subsequent figures.D) Outcrop photograph of vein AR-51.

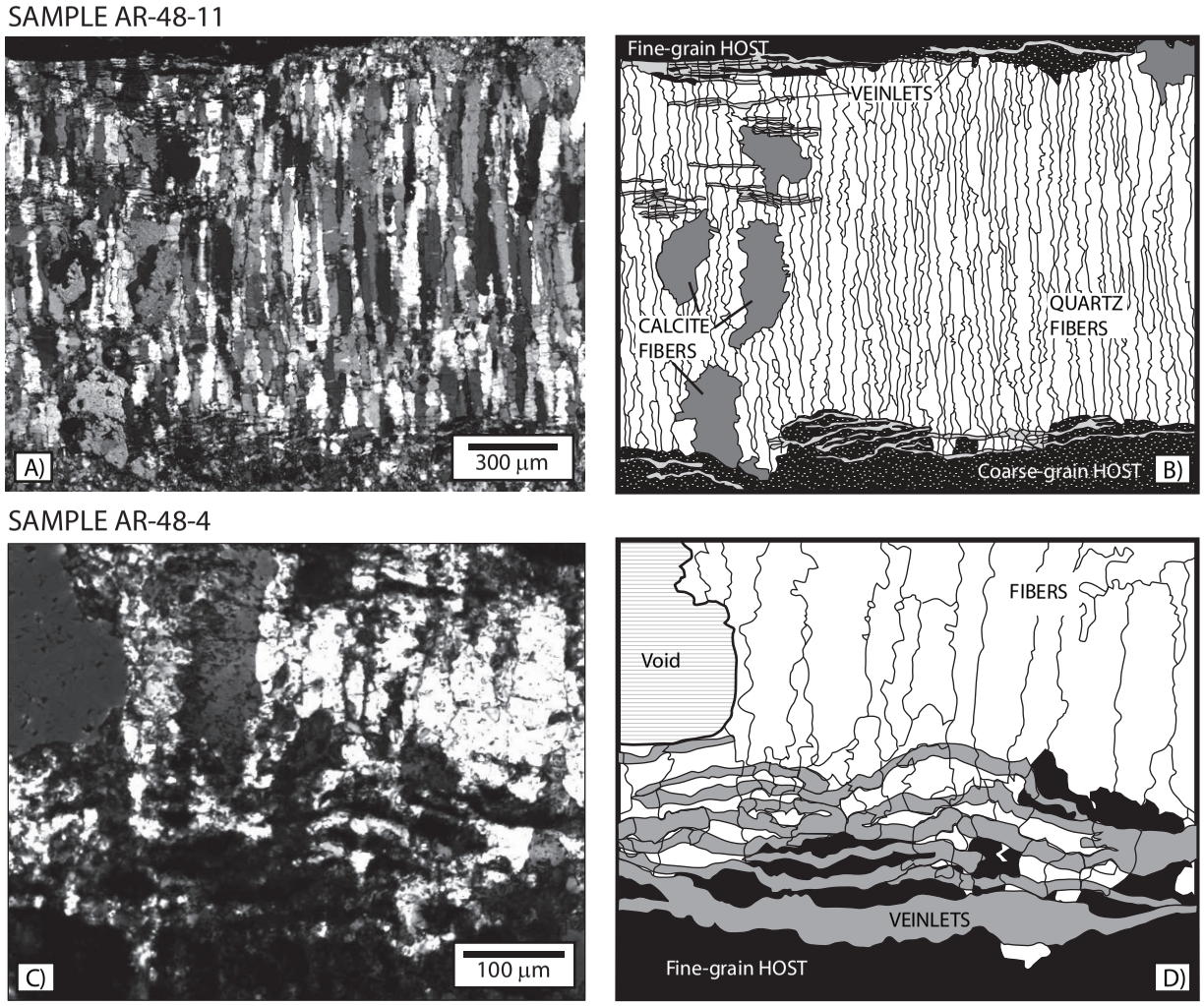

Fig. 19. Thin vein characteristics, see Figure 18 for location. A) Photomicrograph from section AR-48-11. B) Line trace of A showing fibers and veinlets. C) Photomicrograph from section AR-48-4. D) Line trace of C showing fibers and veinlets. The figure compares the textures in the mid-section of the vein (AR-48-11) and the textures close to the tip (AR-48-4).

μm). Thick fibers may show more than one trail spanning the length of the fiber. Contacts between adjacent fibers are jagged (compare Ramsay, 1980). The irregularities (steps) along fiber-to-fiber contacts are similar to the width of veinlets (Figure 19A, B, C and D).

3.5.2. High Aspect Ratio Vein Textures

Sample AR-51 represents one of several tips of an irregular vein (see Figure 18D). The sample was divided in 3 segments and cut into 16 blocks for thin sections. Segment A contains a series of thin veins (1-5 mm wide) that join to form the larger (5 cm wide) vein in segment B (Figure 18B and C). Segment A contains the area where the thin veins join to form the larger vein. The transition from thin veins to thick vein is very sharp (Figure 18B and C). Segment C is a perpendicular cut (cross-section) at the end of Segment B. All segments contain veinlets at the vein-host interface (Figure 20A, B, C and D). The width, length and composition of veinlets within the high aspect ratio vein are the same as those within the low aspect ratio vein.

Fibers differ within the three segments. Fibers in Segment A are thin, elongated, optically continuous and mostly quartz with minor calcite (Figure 20A). The fibers show inclusion bands, trails and jagged fiber-to-fiber contacts. Similar to the low aspect ratio vein, these irregularities along fiber contacts have dimensions comparable to veinlet dimensions, i.e., between 5 and 25 μm (Figure 20A and B). Fiber width in Segment A averages 70.5 μm.

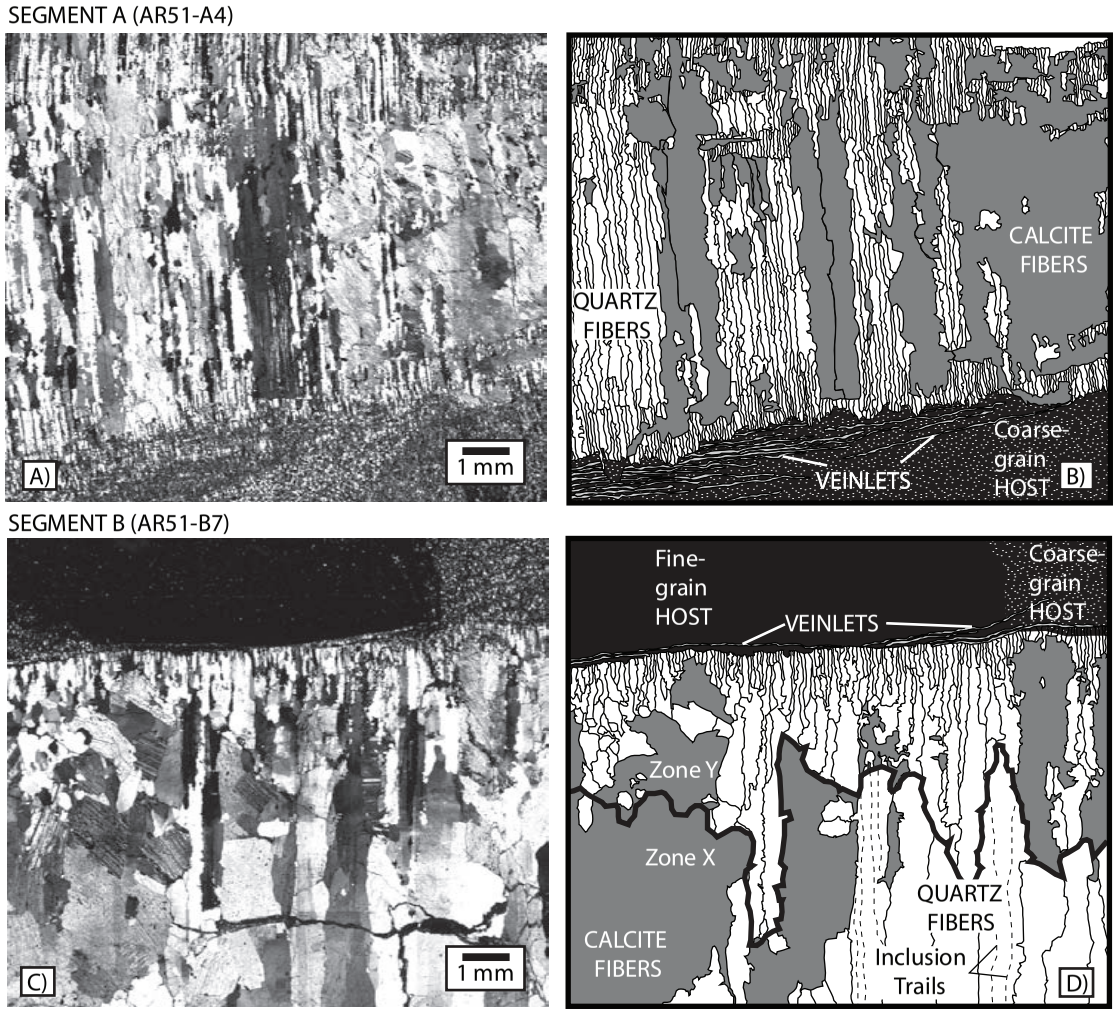

Fig. 20. Lensatic vein characteristics, see Figure 18 for location. Gray areas are calcite, solid black is host. A) Photomicrograph of Segment A inside section AR-51-A4. B) Line trace of A) showing the distribution of fibers and veinlets in the vein. C) Photomicrograph of Segment B from section AR-51-B7. D) Line trace of C) showing the textural differences between Zone X and Zone Y. Heavy black line in D) is the line of demarcation between Zones X and Y.

Fibers in Segment B show two distinct zones discernible by changes in fiber width and length. Zone X (Figure 20C, D) is represented by long (up to 2.5 cm) and wide fibers (average width 188 μm). The fibers show undulatory extinction. Wide fibers have several fluid inclusion trails that extend from over half to the entire fiber length (Figure 20C and D). The fiber sections divided by inclusion trails have an average width of 60.8 μm. Although fiber-to-fiber contacts are mostly jagged, there are cases where these contacts are smooth (Figure 20C and D). Zone Y is located next to the vein-host interface (upper interface in Figure 20C and D). Fibers in Zone Y are smaller with average width of 77 μm and shorter (up to 7 mm) than fibers in Zone X (Figure 20C and D).

Section C is perpendicular to the section at the end of Segment B (Figure 18B and C). Fibers are mostly quartz (99%) with sparse calcite fibers. As is true for Segment A and B, the sample shows no central parting. A small number of fibers span the entire width of the sample. Fiber width is similar to that of the fibers in the closest thin section from segment B indicating that in 3 dimensions fibers are prismatic or columnar in shape. Veinlets are also present in section C. Their characteristics (width, length and composition) are the same as those in Segments A and B.

3.5.3. Host

Electron-microprobe X-ray maps of thin sections and XRD analyses of both coarse-grained and fine-grained host-fractions were used to determine the mineralogy and abundances of the host material. Electron-microprobe maps were obtained with a

Cameca SX50 electron microprobe with 4 wavelength dispersive spectrometers (WSD) in the Department of Geology and Geophysics at Texas A&M University. The conditions selected for the analyses were an electron voltage of 15 kV, 25 μm beam diameter and 20 nA beam current. Each map included 3 stage scans of 4 elements each for a total of 12 element analyses. Scans resulted in a 512 by 512 pixels image. Pixel size was determined by the area analyzed.

The mineralogy of the coarse-grained host is mostly quartz representing around 40% to 55% by area on X-ray maps (Figure 21B and F) with variable amounts of aluminum-silicates like chlorite and clay minerals ranging between 35% and 45%. There are also traces of apatite, albite and iron oxides. The mineralogy of the fine-grained host contains less chlorite and clay minerals (<35%) and more quartz (>60%) by area on the X-ray maps (Figure 21B and D).

The distribution of calcite in the host is variable. Based on X-ray maps, calcite abundance ranges between 0% and 10% (Figure 21B, D and F). Calcite fibers in veins are typically adjacent to coarse-grained host that contains calcite (Figure 21B and F). Where the host is devoid of calcite, no calcite fibers are formed.

Host grain sizes in the two different host end members sampled along with the veins vary significantly. Measurements of the largest quartz grains in the host (grains large enough to be measured under a petrographic microscope) from several thin sections of both fine and coarse grained host show that although the grain sizes in both span a similar range of values (20 to 100 μm), the distribution of the grain sizes is

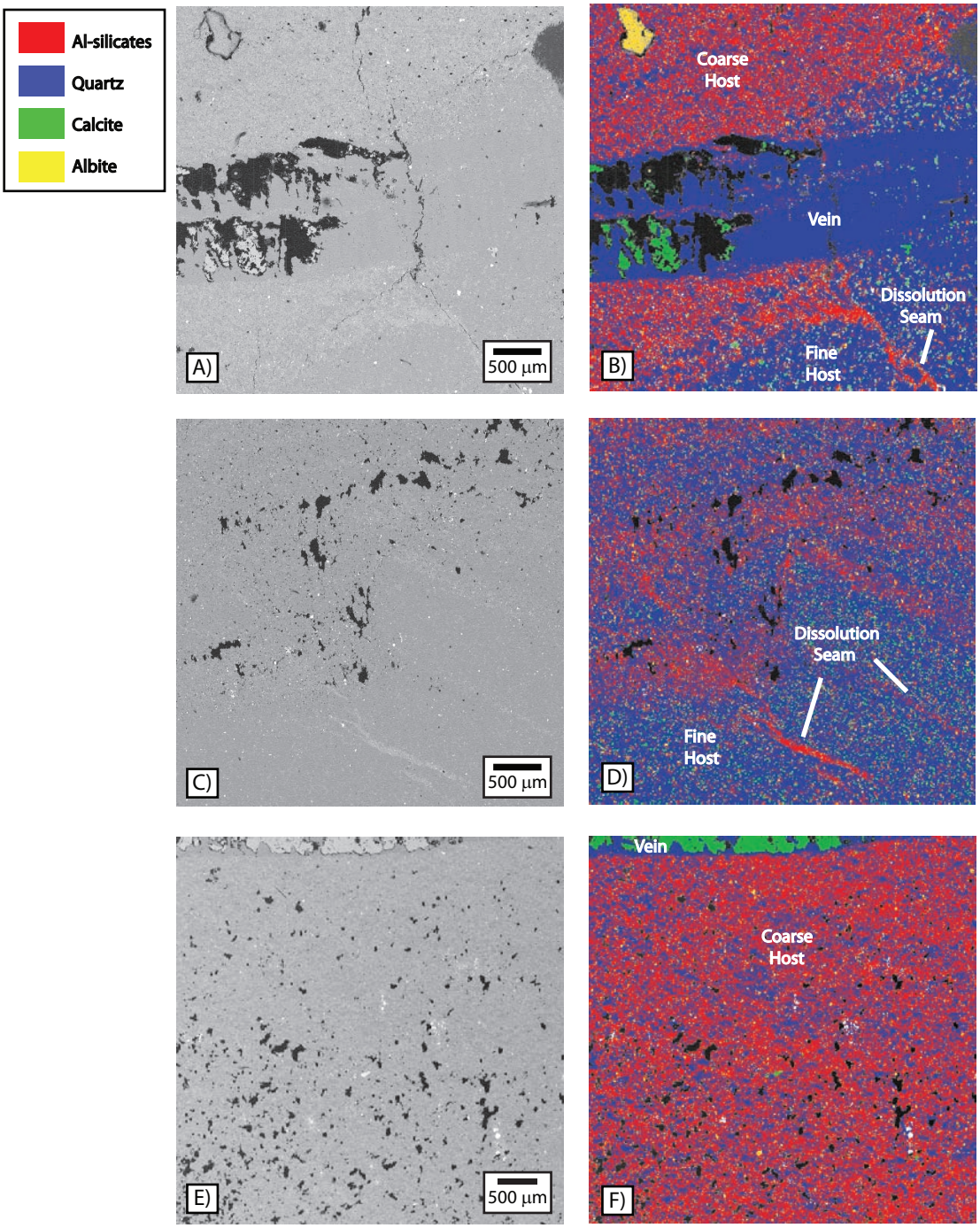

Fig.21. Secondary electron maps and X-ray microprobe maps from areas of thin sections from the thin and elongated vein. See Figure 18 for location. A) SE map of AR-48-6. Square sides are 4 mm long. B) X-ray map of AR-48-6. C) SE map of AR-48-11. Square sides are 6 mm long. D) X-ray map of AR-48-11. E) SE map of AR-48-13. Square sides are 5 mm long. Colors in the X-ray maps represent: blue-micas, red-quartz, green-calcite and yellow-albite. Black reprents areas were material plucking occurred. The figure shows the differences in abundance of quartz and aluminum-silicates between fine-grain host and coarse-grain host. Dissolution seams are shown as areas with high concentration of aluminum-silicates.

different. The fine-grained host size averages 19.4 μm whereas coarse-grained host sizes average 31.2 μm.

Cleavage planes are abundant throughout the host. Using the X-ray element maps, the cleavage planes contain aluminum-silicates (micas and clays) and are completely devoid of quartz and calcite (Figure 21B and D). The timing of cleavage and veins is synchronous because they crosscut each other (Figure 21A and B). Quartz is depleted towards the dissolution seam (Figure 22).

3.6 Stable Isotopes

The objectives of this part of the study were two: 1) to determine the origin of the material precipitated in the veins and 2) to identify changes in isotopic values across and along the vein that may represent stages in the evolution of the vein.

Samples were taken from the quartz and calcite fibers in both high- and low-aspect ratio veins. Since the host rock is characterized by an interbedded sequence of both fine-grained and coarse-grained laminations, samples of both were obtained along the host-vein contact around both veins.

3.6.1 Quartz Stable Isotopes

Analyses of the $\delta^{18}O$ in quartz were determined with the laser-extraction technique (Sharp 1992). All quartz samples were treated with dilute HCl to remove carbonate material. Samples weighing approximately 1 mg were heated with a 20 W CO_2 laser in a BrF_5 atmosphere. The liberated oxygen was cryogenically purified,

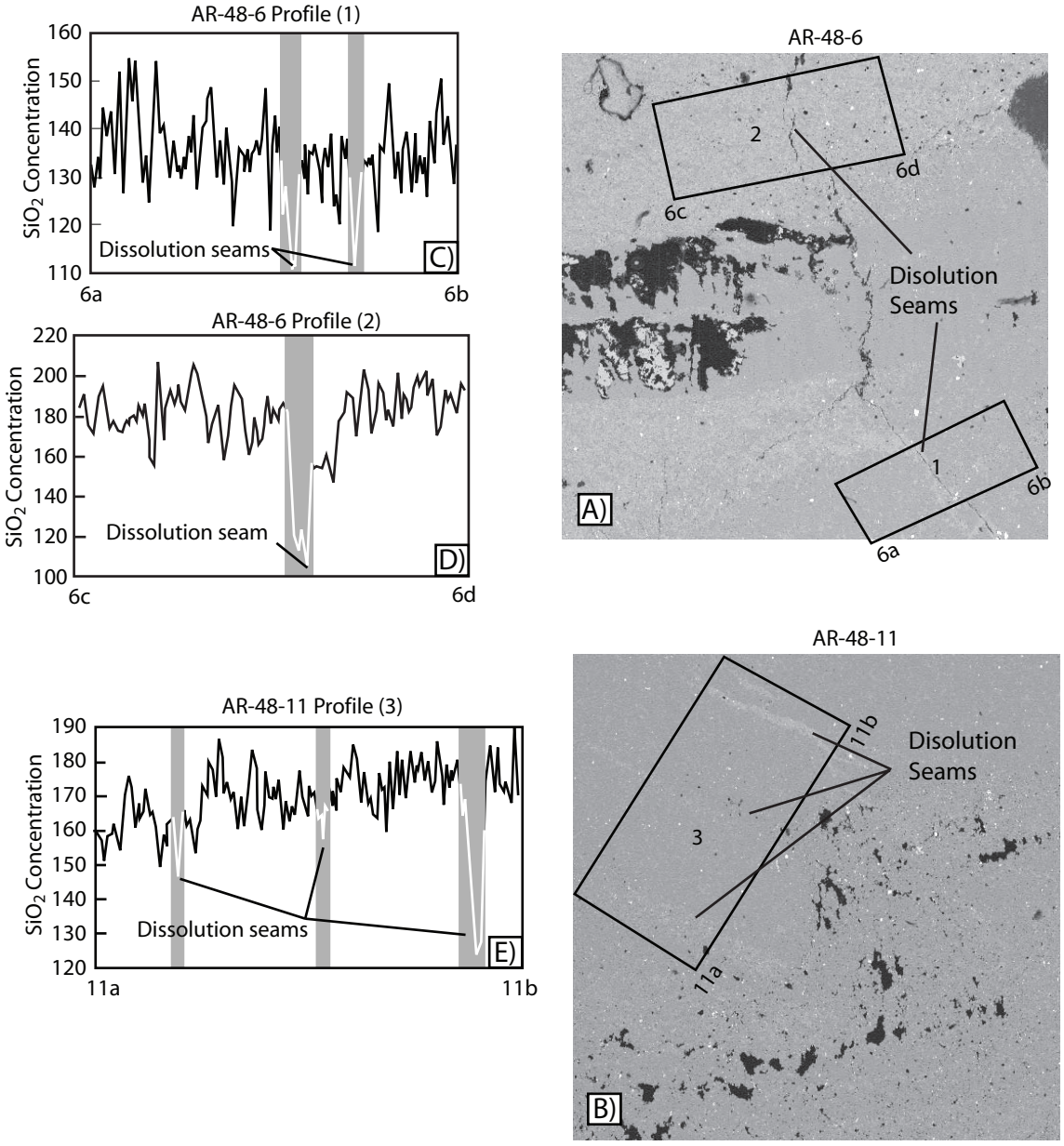

Fig. 22. Concentration profiles of silica obtained from X-ray maps. The profiles show the reduction of silica concentration as the dissolution seams are approached. See figure 18 for location of the MPSE maps. A) Secondary electron (MPSE) map from an area of section AR-48-6. B) MPSE map from an area of section AR-48-11. C) Concentration profile along the area represented by square 1 on sample AR-48-6. D) Concentration profile along the area represented by square 2 on sample AR-48-6. E) Concentration profile along the area represented by square 3 on sample AR-48-11. Concentration values are given relative to a pixel gray-scale value where 256 is the highest concentration possible and 0 the lowest. Profiles are obtained by adding columns of pixel values and dividing them by the number of pixels along the short dimension of each rectangle. Grey stripes on C), D) and E) represent the width of each dissolution seam measured from the MPSE image.

converted to CO_2 by combustion of a heated carbon rod using a platinum catalyst, and introduced directly on-line to the micro-inlet system of the mass spectrometer. Sharp (1992) estimate the reproducibility of the measurements as ±0.2‰ – 0.4 ‰.

Host whole rock oxygen isotopic values were similar from silicates in the host around both veins. $\delta^{18}O$ obtained from the fine-grained host rock around the thin and lensatic veins range between 16.1‰ and 17.1‰ (Figure 23) and 16.3‰ and 17.8‰ (Figure 24), respectively. Coarse-grained host rock $\delta^{18}O$ values are a few per mil heavier. Values fall between 18.2‰ and 19.2‰ and between 18.2‰ and 19.3‰ around the thin and lensatic veins respectively. All host rock values are within the range of values reported by Richards and others (2002) for samples from the Mazarn Formation in the Ouachitas.

Because the size of the fibers in the thin vein did not permit sampling of single fibers, our analyses represent an average value for several. $\delta^{18}O$ values fall between 19.2‰ and 19.5‰ (Figure 23), also within the range of values reported by Richards et al. (2002) for veins in the Mazarn Formation. The small variance in $\delta^{18}O$ observed in our quartz veins have been observed in other veins from the Mazarn Shale (Richards et al., 2002). $\delta^{18}O$ values along the vein are within 0.3‰ of each other.

The coarser texture of the high-aspect ratio vein fibers allowed for multiple samples per fiber. Samples across and along the vein were taken as well as multiple samples of individual fibers (Figure 24). $\delta^{18}O$ in quartz from the vein show a variability of over 1‰ with values between 18.2‰ and 19.4‰. $\delta^{18}O$ values from the thin veins in Segment A range between 18.2‰ and 18.7‰ (Figure 24), in fibers at the limit between

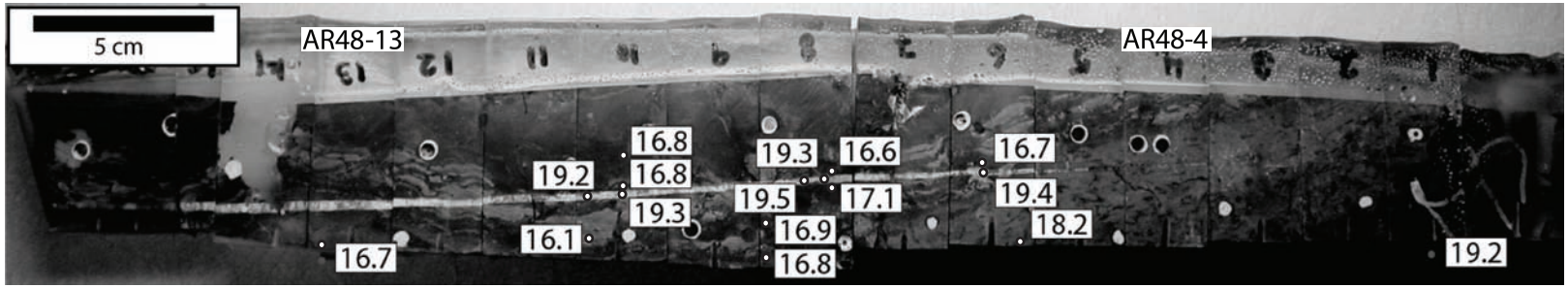

Fig. 23. Stable isotopes analyses on low-aspect ratio vein (sample AR-48). Numbers after the dots represent quartz $\delta^{18}O$ values reported with respect to SMOW. Isotopic analyses were done on the billets cut for thin sections. Billet numbers correspond to thin section numbers in Figure 18A.

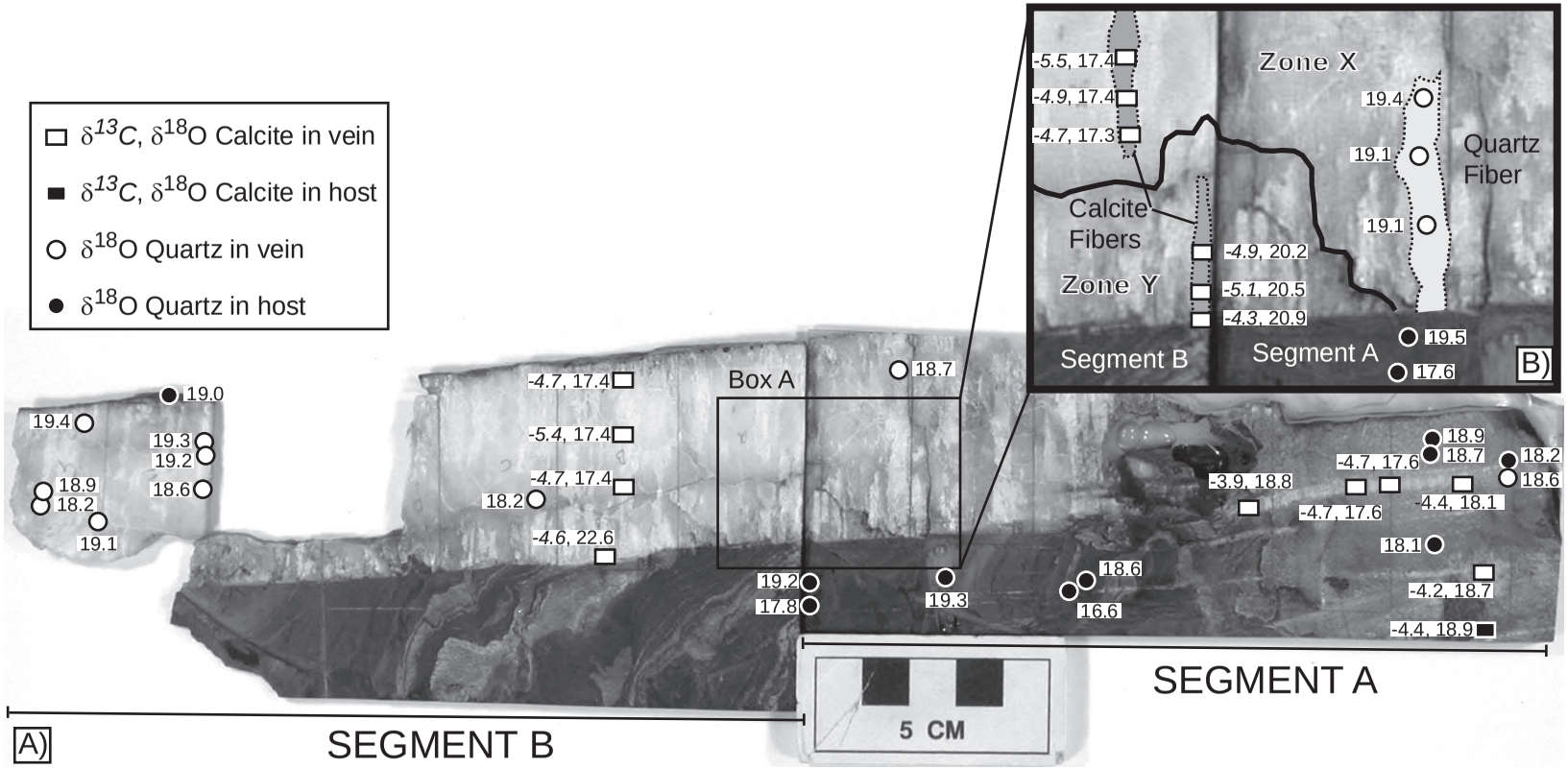

Fig. 24. Stable isotopes analyses on lensatic vein (sample AR-51). White symbols represent vein analyses. Black symbols represent host analyses. Squares represent calcite analyses where the first number indicate $\delta^{13}C$ values reported against PDB and the second number $\delta^{18}O$ values reported against SMOW. Circles represent quartz analyses where the $\delta^{18}O$ values are reported against SMOW. Gray rectangles behind a group of analyses indicate analyses done on a single fiber. Box A shows the change in texture between Zones X and Y and the selected quartz and calcite fibers where multiple analyses were done.

Segment A and B range between 18.2‰ and 19.4‰ and the values at the end of Segment B range between 18.2‰ and 19.4‰ (Figure 24). The inset in Figure (24) shows values of 3 samples along one fiber. $\delta^{18}O$ values in one fiber range between 19.1‰ and 19.4‰.

3.6.2 Calcite Stable Isotopes

Calcite from fibers in the high-aspect ratio vein was analyzed for carbon and oxygen stable isotopes. Samples of vein and host carbonate were removed with the aid of a microscope mounted drill in traverses perpendicular to the host/vein interface. The sampled carbonate was reacted with phosphoric acid at 75°C producing CO_2 gas. The resulting gas was analyzed for carbon and oxygen isotope ratios on a Finnigan MAT 251 mass spectrometer. Isotope ratios were measured relative to NBS-20 and are reported relative to PDB. Results are reproducible to ± 0.14‰ for $\delta^{13}C$ and ± 0.25‰ for $\delta^{18}O$.

The carbonate $\delta^{18}O$ and $\delta^{13}C$ values range between 17.3‰ and 22.6‰ and -3.92‰ and -7.1‰, respectively (Figure 24). These values are within the range of values reported by Richardson and others (2002) for vein calcite in the Mazarn formation. The carbonate $\delta^{18}O$ results fall into two groups. In the first group, $\delta^{18}O$ values range between 20‰ and 22‰ and in the second they are 3 to 4‰ lighter (17 to 19‰). Vein carbon and oxygen isotopic values are depleted in both ^{18}O and ^{13}C relative to the host (Figure 25).

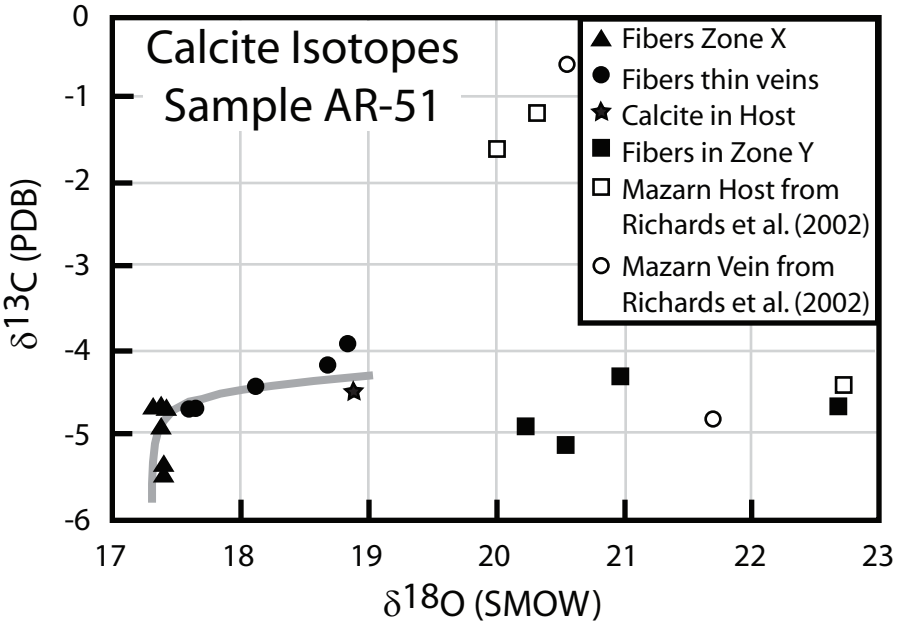

Fig. 25. Stable isotopes results for calcite, from high-aspect ratio vein (sample AR-51). $\delta^{13}C$ reported against PDB, $\delta^{18}O$ reported against SMOW. Curve represents a calculated isotopic path using Rye and Bradbury (1988) isotopic exchange equations. See text for details. Sampled fibers in Zone X and Y belong to Segment B and fibers in thin veins belong to Segment A.

3.6.3 Stable Isotope Thermometry

We used quartz-calcite oxygen stable isotopes thermometry to calculate the temperature of formation of the veins. We were able to use this technique because the veins studied are bi-mineralic with quartz and calcite fibers and the textures of the fibers (jagged contacts, optical continuity) suggest that both minerals precipitated at the same time. Consequently, the calcite and quartz fibers meet the requirement for the technique that both minerals were in equilibrium with the fluid when precipitation occurred. We used the empirical calibration equation developed by Kirschner et al. (1995) because it accounts for the observation that experimental calibrations underestimate the temperature of formation of veins formed during orogenic events. Kirschner et al. (1995) equation estates that:
$\Delta^{18}O_{quartz\text{-}calcite} = 0.87*(10^6/ T^2)$, where $\Delta^{18}O_{quartz\text{-}calcite}$ is the quartz calcite fractionation of the sample, and T is the temperature of formation in °K.

To calculate the fractionations we used the $\delta^{18}O$ of the two closest single fibers of quartz and calcite analyzed. The quartz fiber sampled is located in Segment B at the limit with segment A and the closest calcite fiber sampled is located in zone Y segment B (Figure 24 box A). $\delta^{18}O$ values for the quartz vein range from 19.1‰ to 19.4‰ whereas $\delta^{18}O$ values for the calcite fiber range from 17.3‰ to 17.5‰. The quartz-calcite fractionations obtained are between 1.8‰ and 2.2‰. The range of temperatures calculated using Kirschner et al. (1995) equation is between 366 °C and 422 °C, a 56 °C range.

Previous studies using fluid inclusion microthermometry have determined that the range in temperatures of the formation of veins in the Ouachita Mountains is between 100 to 315 °C (Engel, 1952; Koning and Stone, 1977; Pittenger and Koning, 1977; Kurrus, 1980; Keller et al., 1985; Shelton et al., 1986). Our temperature estimate is higher than the range of temperatures calculated in these studies but is similar to the range of temperature presented by Richards et al. (2002). The latter authors obtained a range in temperatures for the entire Ouachitas between 265 °C to 385 °C using the same technique and the same calibration.

3.7 Fluid Inclusions

Fluid inclusion analyses were performed in the low aspect ratio vein. The objectives were to determine the environment of formation of the veins and to identify patterns in the temperature of formation of fluid inclusions along the vein and relate these patterns to different episodes of vein growth. The thin section analyzed came from the central part of the vein (thin section AR-48-11, Figure 18A). The fluid inclusions analyzed span the entire width of the vein, specifically, from the center of the vein to the veinlets next to the vein-host interface. Fluid inclusion microthermometry was conducted using a Fluid Inc. modified U.S.G.S. gas flow heating/freezing stage at Texas A&M University. Calibration of the thermocouple with synthetic fluid inclusions shows that measurements of homogenization and melting temperatures are accurate within ±0.2 °C and reproducible to ±0.1 to 0.2 °C.

We focused on quartz veins both because the fluid inclusions are better preserved and the quartz vein fibers show no evidence of ductile deformation. From the latter observation we conclude that fluid inclusions were trapped at or after peak deformation conditions. However, SEM based cathodoluminescence shows evidence of recrystallization of some quartz fibers (Section 2). Fluid inclusions aligned parallel to fiber length and parallel to host-vein interface are always present in fibers that show recrystallization textures and we suggest that these fluid inclusions are formed during the recrystallization process (Figure 26). Fluid inclusions along inclusions trails are elongated with the orientation of the inclusion long axis parallel to fiber length (Figure 26). Based on their orientations and textures we assume these trails represent previous boundaries of early formed fibers. Fluid inclusions in inclusion bands are equant or elongated parallel to fiber length (Figure 26). Based on their orientations and textures we assume these bands represent previous veinlet boundaries. Inclusion trails and bands are not observed at the edge of the vein where veinlets are separated by host fragments from the main body of the vein. Isolated inclusions typically represent anticrystals or negative crystals (Figure 26) as defined by Roedder (1984). These inclusions are present throughout the entire body of the vein including veinlets.

All fluid inclusions are two-phase water-rich inclusions. The size of the water vapor bubble is varies between 5% and 40% by volume. Isolated inclusions have homogenization temperatures between 103.3 °C and 247 °C and melting temperatures between -5.4 °C and +2.7 °C. Fluid inclusions in trails show homogenization temperatures between 99.8 °C and 187.3 °C and melting temperatures between -4.8 °C

Fig. 26. Photomicrographs showing the 3 morphologies of observed fluid inclusions. A) Isolated inclusion with anti-crystal shape. B) Inclusion band. C) Inclusion trail. The figure shows the orientation of bands and trails with respect to fiber long axis.

and +0.6 °C. Fluid inclusions in bands show homogenization temperatures between 94.4 °C and 154.9 °C and melting temperatures between -5.2 °C and +4.9 °C (Figure 27). There are no systematic changes in melting temperature with homogenization temperature. The few measurements of initial melting temperature all yield temperatures close to -22 °C, indicating that NaCl is the most dominant dissolved salt in the fluid.

There are two families of fluid inclusions based on their homogenization temperatures, one high temperature (between 208.9 °C and 247.6 °C) and one low temperature (between 98.4 °C and 187.3 °C). All inclusions with the highest homogenization temperatures are isolated (Figure 27).

A small group of fluid inclusions (8 total) showed positive melting temperatures suggesting the presence of other phases.

3.7.1 Trapping Conditions

Isochores were calculated from the fluid inclusion data (Figure 24) using the program FLINCOR (Brown and Hagemann, 1995) and the equation of state of Brown and Lamb (1989) for the H_2O-NaCl system. Other equations of state (e.g. Zhang and Frantz, 1987) yield no significant differences.

Isochores calculated from fluid inclusions with high temperatures of homogenization show different trapping conditions than isochores calculated from fluid inclusions with low temperatures of homogenization (double and dashed lines, respectively, in Figure 28).

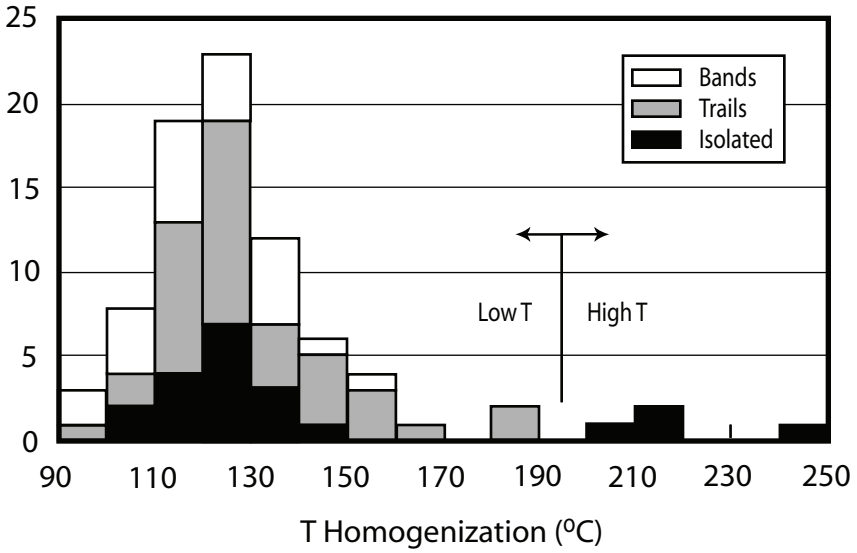

Fig. 27. Histogram of temperatures of homogenization from fluid inclusions. The diagram shows the cutoff between high and low temperatures of homogenization. White squares represent fluid inclusions in bands, gray squares fluid inclusions in trails and black squares isolated inclusions. High homogenization temperature inclusions are all isolated.

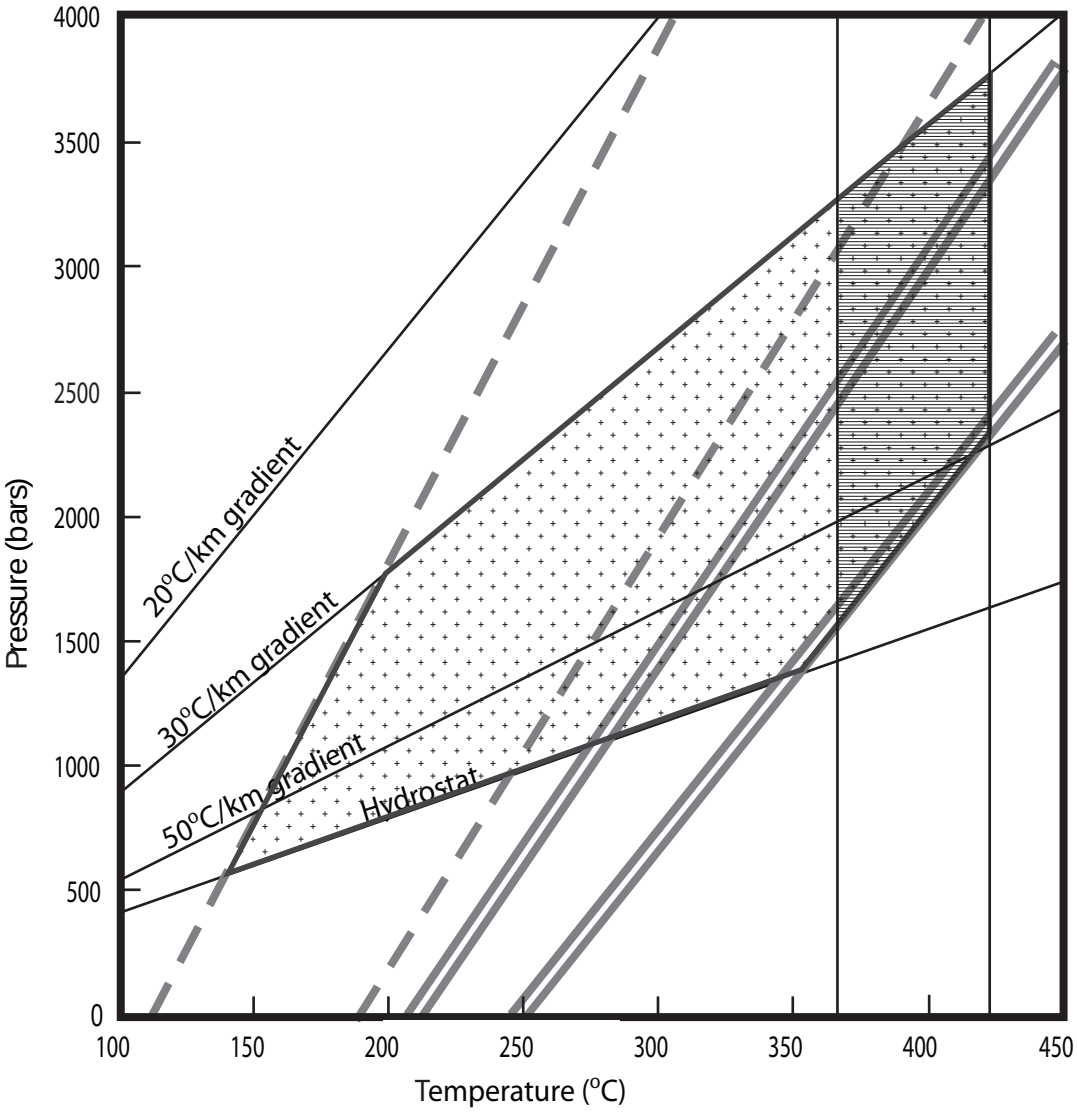

Fig. 28. Isochores calculated from fluid inclusions. The two gray double line isochores represent the range possible based on high homogenization temperature inclusions. The two gray single dashed lines isochores represent the same for the low homogenization temperature inclusions. Solid lines are hydrostat and three different lithostats from three different geothermal gradients are plotted. Region of small crosses represents the region where both types of inclusions can be formed in the same vein between hydrostatic and 30°C/km lithostatic geothermal gradient. Horizontal ruled region on the right represents the conditions for formation of the Ouachitas veins using the temperature constraints from stable isotope thermometry.

3.8 Discussion

Outcrop observations suggest that all veins in the outcrop are genetically and temporally related. For these reason we use the data on either vein or both of them to determine fluid characteristics and the environment of formation of all the veins in the outcrop.

3.8.1 Stable Isotopes

Isotopic variability between host and veins is an important indication of whether the vein-forming fluid was in equilibrium with the host or the vein-forming fluid was allochtonous and far-traveled.

Large isotopic variations between host and vein have been interpreted as evidence for vein material precipitated from advective or far-traveled fluids. For example, a 3.1‰ difference in calcite $\delta^{18}O$ between host and veins from a thrust fault zone in the Pyrenees suggested Rye and Bradbury (1989) that veins were formed from openly circulating fluids through faults. Similarly, Kirschner et al. (1993) observed that host quartz $\delta^{18}O$ was heavier by up to 7‰ than adjacent veins within the Morcles Nappe, Swiss Alps and concluded that faults acted as conduits for the vein forming fluid. Finally, Hilgers et al (2006) found differences in calcite $\delta^{18}O$ values between host and veins of up to 9‰ in late formed veins. They attributed this large isotopic difference to late fluid infiltration accompanying normal faulting.

In contrast, the closeness of isotopic values between vein and adjacent host has been interpreted by many workers to indicate that veins formed from fluids in equilibrium with the host rock. For example, Cartwright et al. (1994) found that fibrous quartz veins in quartzites and fibrous dolomite veins in dolomites from the Ormiston Gorge, central Australia have $\delta^{18}O$ values within 2‰ of the adjacent host. Similarly, Al-Aasm et al. (1995) found that calcite fibrous veins formed in marine mudrocks, near plutons from the Wrangellia Terrain, BC. have isotopic values ($\delta^{18}O$ and $\delta^{13}C$) within 2‰ of those of their host. Kirschner et al. (1995) in the Morcles nappe, Swiss Alps and Henry et al. (1996) in the Western Alps found that quartz and quartz-calcite veins formed under greenschist facies conditions have isotopic values ($\delta^{18}O$ and $\delta^{13}C$) within 3‰ or less of their adjacent host. The same was observed for calcite veins by Kenis et al. (2000) for veins from the Variscan front zone (France) and by Hilgers et al. (2006) for veins from the Jabal Akhdar dome, Oman Mountains. In both cases the isotopic composition ($\delta^{18}O$ and $\delta^{13}C$) of the calcite and dolomite veins and host rock lie close to each other (within 2‰). Finally, Ghisetti et al. (2001) found that slickenfibers and veins from the central Apennines, Italy formed in contractional features show isotopic values close to host values (within 4‰). The conclusion from all of these studies was that the vein-forming fluid was in equilibrium with the host.

For our veins, quartz $\delta^{18}O$ variations within both lensatic and elongated veins are largely a result of the isotopic variability of the host adjacent to the vein. This is better observed along the lensatic vein due to the ability to sample single fibers. $\delta^{18}O$ values from the thin veins in Segment A are similar to those of the adjacent coarse-grain host,

18.2‰ to 18.7‰ versus 18.2‰ to 18.9‰, respectively (Figure 24). Similarly, $\delta^{18}O$ values in fibers at the limit between Segment A and B have $\delta^{18}O$ values between 19.1‰ and 19.4‰ whereas the adjacent coarse-grain host has $\delta^{18}O$ values between 19.2‰ and 19.4‰ (Figure 24). The small differences in quartz isotopic values between vein and host and the control in isotopic composition of the host observed in our veins suggest that the vein-forming fluid was in equilibrium with the host.

Quartz $\delta^{18}O$ of the fine-grain host is consistently lighter than the coasrse-grained host. The fine-grain host contains larger amounts of aluminum-silicates and oxides that are hard to exclude while sampling. Oxygen isotopic fractionation in these minerals yields lighter $\delta^{18}O$ values than those in quartz, so the variable abundances of these minerals in the samples reduced the measured $\delta^{18}O$ values of the fine-grain host.

Calcite isotopic values show variations both along the width and across the length of the lensatic vein. Variations along the width of the vein follow the two zones previously defined on the basis of textures (Figure 20). Zone Y (Figure 20) $\delta^{18}O$ and $\delta^{13}C$ values range between 20.2‰ and 20.9‰ and -4.3‰ and -5.1‰, respectively, whereas Zone X $\delta^{18}O$ and $\delta^{13}C$ values range between 17.3‰ and 17.4‰ and -4.7‰ and -5.5‰, respectively (Figure 24 box A). The isotopic trend defined by the calcite $\delta^{18}O$ and $\delta^{13}C$ values from both zones (Figure 24) cannot be explained by changes in the temperature of the fluid. Rye and Bradbury (1988), using the calculations by Sverjensky (1980) and Shelton (1982), calculated the isotopic evolution of calcite from an initial host rock value to a value in equilibrium with an initial fluid composition (their figure 7). The molar fluid-rock ratio for oxygen, M_o, is

$$M_o = n_0 \left[\frac{\delta^{18}O^f_{CC} - \delta^{18}O^i_{CC}}{\delta^{18}O^i_{\Delta-\delta} - \delta^{18}O^i_{CC}} \right] \quad (1)$$

where n_0 is the number of moles of oxygen per mole of calcite, $\delta^{18}O^f_{CC}$ and $\delta^{18}O^i_{CC}$ are the final and initial oxygen isotopic compositions of the calcite in the rock, $\delta^{18}O^i_{\Delta-\delta}$ is the $\delta^{18}O$ value of the calcite in equilibrium with the initial fluid before exchange. The molar fluid-rock ration for carbon, M_c, is:

$$M_c = \frac{n_C}{X_{\Sigma C}} \left[\frac{\delta^{13}C^f_{CC} - \delta^{13}C^i_{CC}}{\delta^{13}C^i_{\Delta-\delta} - \delta^{13}C^i_{CC}} \right] \quad (2)$$

where n_C is the number of moles of carbon per mole of calcite, $X_{\Sigma C}$ is the number of moles of carbon in solution per mole of fluid, $\delta^{13}C^f_{CC}$ and $\delta^{13}C^i_{CC}$ are the final and initial carbon isotopic compositions of the calcite in the rock, respectively, and $\delta^{13}C^i_{\Delta-\delta}$ is the $\delta^{13}C$ value of the calcite in equilibrium with the initial fluid before exchange.

The curve in Figure 25 was calculated assuming closed system conditions. For the calculations $\delta^{18}O^i_{CC}$ and $\delta^{13}C^i_{CC}$ are the $\delta^{18}O$ and $\delta^{13}C$ values of the analyzed host, respectively, $\delta^{18}O^i_{\Delta-\delta}$ is the $\delta^{18}O$ value at the bend along the isotopic trend in Figure 25 (17.3‰), and $\delta^{13}C^i_{\Delta-\delta}$ is the lowest $\delta^{13}C$ value from the trend (-5.5‰). We used a molar water-rock ratio of 1 for both Carbon and Oxygen. The shape of the curve matches the isotopic trend observed only if the carbon in solution per mole of fluid ($X_{\Sigma C}$) is very small (<0.005). We conclude that the volume of fluid required for this trend is small and local considering the W/R ratio used. In addition, thin veins on Segment A show

closer values to the host whereas thick fibers in Segment B show lighter values that reflect a larger fluid influence. In Section 2 I proposed a model of vein formation in which veins start from a single veinlet and grow in width and length by addition of veinlets. Fracture localization required for the continuous addition of veinlets is possible because the process takes place at boudin necks. Fibers grow as a result of multiple fractures of pre-existing host grains where the material precipitating in each of the fractures takes the crystallographic orientation of the host grain. The final stage of vein evolution results in the obliteration of the original texture by recrystallization resulting in the widening of fibers and assimilation of host inclusions. The calcite isotopes trend is consistent with this model. The calcite in the thin veins was precipitated from the fluid contained in the rock whereas the calcite in the fibers shows evidence of carbon depletion that can be explain by a progressively larger fluid flux (Rye and Bradbury, 1988).

Overall, the quartz and calcite isotopic trends from both types of veins indicate that the vein material precipitated from a local source with relatively slow fluid flux in equilibrium with the host. There is no suggestion from the isotopes that the system was open for large advection of far-traveled fluids as suggested for other vein systems.

Richards et al. (2002) observed that $\delta^{18}O$ from quartz and adjacent host sampled across the Ouachitas differed by less than 2‰. They argue that the isotopic composition of the adjacent host dictates the composition of the vein. The data of Richards and others (2002) from just the Mazarn formation are plotted with the analyses from calcite in the lensatic vein in Figure 25. One of their host samples lies close to the calcite

analyses from the vein in zone Y. The calcite host sample analyzed for this study lie close to the calcite analyses from the vein in zone X. We suggest that the differences in calcite isotopic values between the two zones can be explained as representing two periods of vein formation where the material forming the vein came from two different host sources.

3.8.2 Fluid Inclusions

Isochores calculated from the two families of inclusions (high-temperature double line and low-temperature dashed line in Figure 28) define different pressure and temperature conditions for the formation of this set of veins. In contrast, vein textures suggest that both high- and low-temperature inclusions were formed contemporaneously. For this reason, the environment of formation of the Ouachita veins is going to be defined by the region where these two families of isochores overlap in temperature and pressure. This region is shown with the cross-hatched pattern in Figure 28. The pressure range defined by this region is between 550 and 3750 bars. This pressure range is reduced when considering our independent temperature determination from isotope thermometry (between 366 and 422 °C) to be between 1500 and 3750 bars.

All of the measured fluid inclusions were located inside fibers across the vein. Inclusions located in isolated veinlets were not possible to measure. Nevertheless, the textural differences between the inclusions of each of the populations suggest that they were formed by different processes. For instance, all high-temperature inclusions are

isolated whereas inclusions with low homogenization temperatures are elongated and most of them belong to either inclusion trails or bands. For these reasons we suggest that the high-temperature inclusions were formed as quartz precipitated in fractures forming veinlets and the low-temperature inclusions were formed during the process of recrystallization that obliterated the original textures resulting in wider fibers and assimilating host inclusions forming inclusion trails and bands.

The particular timing of formation of each fluid inclusion family is ambiguous and at least two different scenarios can explained them. In one, the two populations of fluid inclusions were formed under two different environmental conditions and represent two different times in the evolution of the veins. In another, the two populations of fluid inclusions were formed as a result of two quasi-contemporaneous processes under variable fluid conditions. In the first case an early population of inclusions formed at low pressure-high temperature conditions followed by a second population of inclusions formed at low temperature-high pressures. This would require that the veins were formed early in the deformation history, possibly during diagenesis under the influence of external high-temperature fluids and later evolved as pressure increased and temperature was reduced with tectonic burial.

Several observations argue against this possibility. First, cross-cutting relationships in outcrop and thin section show that cleavage and veins occur late in the deformation history of the Ouachitas. Second, stable isotopes show that the vein-forming fluid was local. Third, vein textures indicate that both veinlets and fibers are contemporaneous (Section 2).

In the second case, contemporaneous processes can occur under constant pressure or constant temperature. Constant pressure will require cyclic variation in temperature. Temperature variation can only be accomplished by the influence of an external source (hydrothermal fluids, magma intrusions, etc.). There is no evidence of an external influence that could have affected fluid temperature in this area of the Ouachitas (Viele and Thomas, 1989). Then, constant temperature would require variations in pressure. Pressure variation can be explained by changes of the fluid pressure during vein formation. We suggest that the changes in fluid pressure resulted in the formation of two different textures. This way, high temperature inclusions formed in open fractures as quartz precipitated to form veinlets. Fracturing caused a decrease in pressure bringing it close to hydrostatic. As quartz precipitated in the veinlets and sealed the fractures, fluid pressure was increased approaching lithostatic. High fluid pressures acted as the driving force for dissolution-reprecipitation allowing for the growth of fibers. Experiments by Jones and Pytokowicz (1973) and Willey (1974) of solubility of silica in seawater under constant temperatures show that the solubility of silica increases with increasing pressure. Willey (1974) found that silica solubility increases linearly with pressure in the pressure range between 270 and 1220 bars. The linear relationship is described by the following equation:

$$S = (9.7 * 10^{-3} P) + 31.9 \quad (3)$$

where: S is the solubility expressed as ppm Si and P is pressure in bars. From this relationship the concentration of silica on seawater at 500 bars is 36.75 ppm whereas the concentration at 1000 bars is 41.6 ppm, a 12% increase. Extrapolating this behavior

at higher temperatures, a fluid subjected to higher pressures would result in the dissolution of quartz to reach equilibrium.

3.8.3 Tectonic Implications

Quartz stable isotopes provide evidence that the fluid from which the veins were formed was local and that the material forming the vein came from the surrounding host. Both calcite and quartz stable isotopes suggest that vein precipitation started from a fluid in equilibrium with the adjacent host and as the vein grew a larger volume of fluid was accessible resulting in the depletion of carbon and oxygen (curve a in Figure 25). The influx of this later fluid explains the change in composition between Zones X and Y in Figures 20 and 24. This later fluid probably came from the same formation since no temperature change is required to explain the isotopic trend and the isotopic variations in the vein is less than 2‰.

Structures in outcrop support the assertion from stable isotopes that large scale advection did not play a part in the formation of these veins based on two observations: 1) although thrust faults are present in the outcrop, cross-cutting relationships and the absent of mineralization in the fault plane unequivocally lead us to suggest that faulting occurred after vein formation. Ruling faults out, there are no features that could have acted as conduits for large volume of fluids and 2) the veins appear to be isolated. Since large scale advection is ruled out for these veins, the mode of transport of the vein forming material was diffusion and/or small scale advection. Based on the observation that quartz is depleted around the few dissolution seams studied and that both veins and

dissolution seams are synchronous we suggest that cleavage planes acted as the pathways for diffusion. Rye and Bradbury (1988) showed that veins from a Pyrenean thrust sheet initially formed from local fluids in a closed system and evolved through time to an open system where the late fluid was not in equilibrium with the vein host. They suggested that dissolution seams served as conduits for the diffusing material for two reasons. The first is that the dissolution seams are contemporaneous with the veins and that the orientations of the dissolution seams (perpendicular to veins and most of them found at vein tips) are consistent with the strain history recorded by vein fibers. The second is that up to 40% of the material deposited in veins can be accounted for from the material loss at dissolution seams close to the veins.

Our field observations show that cleavage and veins are contemporaneous and were formed late in the evolution of folds. This observation is consistent with the thermal history of the Ouachitas calculated by Houseknecht and Matthews (1985). Using thermal maturity data they modeled the thermal history of the Stanley Shale (for stratigraphic position see Figure 16) using a simple path for rapid burial and later exhumation. They calculated the peak temperature for the Stanley Shale to be 240 °C at a burial depth of 10 km. Since the burial history of the Stanley Shale and the Mazarn Shale track each other (Viele and Thomas, 1989) our calculations of temperature and pressure of vein formation are consistent with the veins being syndeformational and formed at or near peak metamorphic conditions.

3.9 Conclusions

Veins from the Benton Uplift, Ouachitas, are dominated by the presence of veinlets and fibers. Veinlets are narrow, between 5 and 25 μm thick, typically one crystal wide and parallel to the larger vein orientation. Fibers are perpendicular to the vein wall, span 50-100% of the total vein width and are made of multiple veinlets.

Quartz $\delta^{18}O$ values of vein and adjacent coarse-grain host are within 2‰ of each other. The closeness of values indicates that the fluid from which the vein material precipitated was in equilibrium with the host rock. Calcite $\delta^{18}O$ and $\delta^{13}C$ values across the wide vein studied define a trend that represents the evolution of the fluid from local and rock-buffered to a short-traveled fluid. These observations suggest that the Ouachita veins were first formed from a small volume of fluid in equilibrium with the host and as the veins evolved the volume of fluid available for vein formation increased allowing for small scale advection.

The textural differences observed in the larger veins (variations in fiber width and length) are tracked by variations in calcite $\delta^{18}O$ and $\delta^{13}C$ values. The difference in isotopic values can not be explained by changes in temperature of the same vein-forming fluid suggesting that the isotopic difference represents two episodes of growth of the vein where the vein source material was different.

The two families of fluid inclusions analyzed are directly tied to the two processes that generate the textures in the Ouachita veins. High-homogenization temperature inclusions were trapped in quartz precipitating in veinlets whereas low-homogenization

inclusions were trapped during quartz recrystallization when fibers were widened forming inclusion trails and inclusion bands.

Quartz-calcite oxygen isotope thermometry and fluid inclusions determined the environment of formation of the Ouachita veins to be between 366 and 422 °C of temperature and between 1500 and 3750 bars of pressure. The environment of formation of the Ouachita veins (within greenschist facies) is consistent with the environment of formation of quartz fibrous veins in other tectonic settings.

The presence of low pressure-low temperature fluid inclusions suggests that veins textures were continuously changed throughout the history of the veins.

4. VEINLETS, THE INITIAL STAGE OF FIBROUS VEIN GROWTH

4.1 Précis

Despite observations on syntectonic veins spanning two centuries, fundamental questions remain unanswered. Although their origin as fractures is largely established, it is not know why these fractures initiate where they do and how the vein evolves once started. Here we present SEM-based cathodoluminescence and electron back-scattered diffraction (EBSD) observations on the initial stage of formation of a fibrous vein from the Ouachitas, Arkansas. We show that the crystallographic orientation of the newly precipitated material is inherited from the host grains at the micron scale and replicated as the fibers grown to centimetres in length. The fluid from which the vein precipitated was cyclically supersaturated yet never very far from saturation.

4.2 Results and Discussion

Veins are commonly thought to form by precipitation of materials in rock openings such as fractures, pore or other cavities. In the case of hydrothermal veins deposited around plutons, this can be demonstrated conclusively. However, in the case of syntectonic veins, or veins formed during deformation, the facts are less clear. This has led to two end-member views of vein formation. In the “crack-seal” model precipitation takes place in an initial microcrack and the orientation of the precipitating material will reflect that of a host grain in the fracture walls serving as seed. A preferred orientation will be present only if the host grains show a pre-existing preferred orientation

(Ramsay, 1980; Cox and Etheridge, 1983; Fisher and Brantley, 1992; Fisher et. al, 1995; Bons, 2000). Alternatively, the force of crystallization model should present a crystallographic preferred orientation favouring precipitation sites with the fastest direction of growth because grains grow under compressive stress (Kamb, 1959; Wiltschko and Morse, 2001; Means and Li, 2001). These studies have focused in the observation and analyses of the final stage of vein formation from samples taken at the centre of veins. Lacking from these studies is a description and understanding of the initial stage of vein formation.

The vein we studied is typical of those attributed to the crack-seal mechanism. It comes from an outcrop briefly described in Stone and others (1994) located at Hot Spring Village, 13 miles north of Hot Springs, AK. The rocks exposed are from the Lower Ordovician Mazarn Shale, a interbedded banded green and black slate, laminated fine-grained grey siltstone, and minor lenses of fine-grained brownish-grey quartzitic sandstone (Figure 29). These rocks were deformed as part of the Benton uplift and metamorphosed to greenschist facies (Viele and Thomas, 1989). Structurally, the outcrop is characterized by the presence of two thrust faults oriented N60E, folds with wavelengths ranging from cm to m and by pervasive cleavage in shales. Vertical flattening of the exposed rocks is indicated by subhorizontal cleavage and boudinage formation in sandier beds at all scales. Veins are found at necks of boudinage structures in the sandstone beds and they are best exposed along slip surfaces of the two thrust faults cutting across the entire outcrop. Individual veins in the outcrop are apparently isolated. In hand sample, cross-cutting relationships show that veins are earlier than

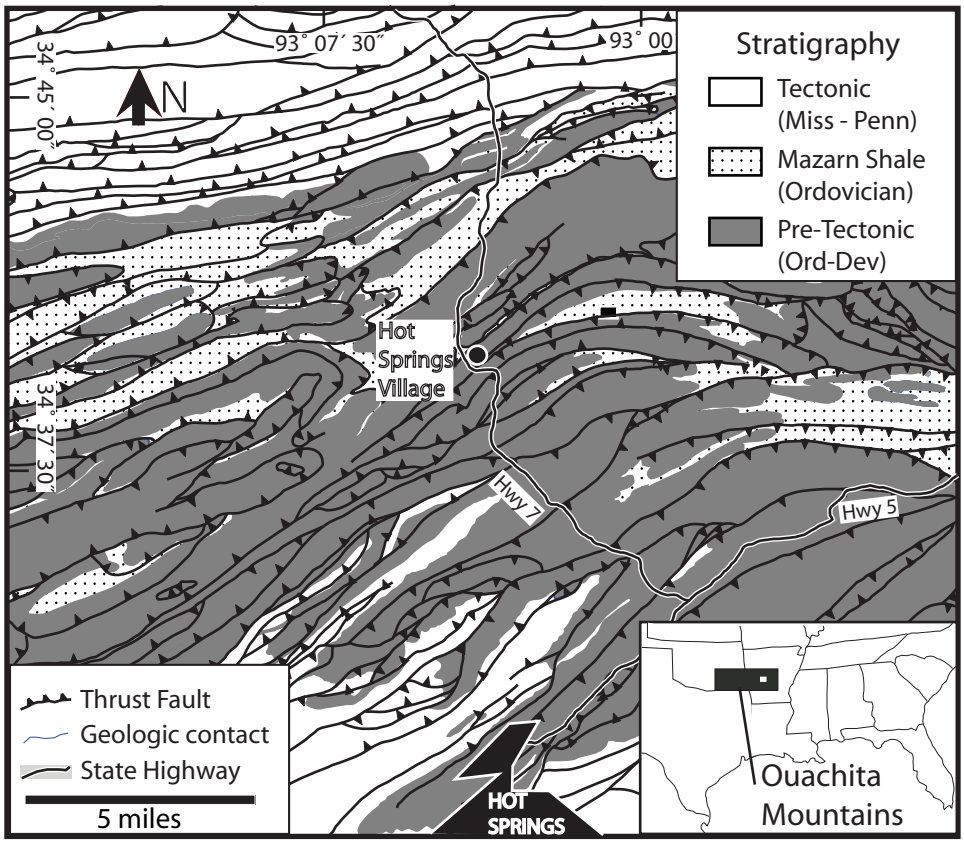

Fig. 29. Regional Geology of the Hot Springs, AR area with the location of the Lake Pineda Outcrop (solid black square) after Haley and Stone (1996). The black square in the inset shows the location of the Ouachita Mountains. Also show is the stratigraphic column of the area.

faults and synchronous with cleavage formation because cleavage and veins cross-cut each other.

In thin section the vein consists of fibres or elongate strips of calcite or quartz that are made up of multiple wall-parallel veinlets or lamellae. Fibers and veinlets are normal and parallel to the host-vein wall, respectively. There is no evidence of shear or offset within either the fibres or veinlets. Fibres are in optical continuity along their length, as first observed by Ramsay (1980) for this type of vein. Quartz fibres are the most abundant in the vein but calcite fibres are also present adjacent to host that contains calcite. Fibres contain fluid inclusion bands and trails that are normal and parallel to the long axis of the fibres, respectively. Contacts between fibres are jagged or stepped. These steps along fibre-to-fibre contacts are between 5 to 25 μm long or about the same size as veinlet thickness. The veinlets are defined, in part by the 15 to 30 μm wide host segments separating them (Figure 30B).

Both fibres and veinlets change character from the middle to the tip of the vein. Fibre width decreases towards the tip. While the thinnest fibres in all sections have similar values ranging between 50 and 100 μm, the thickest fibres are only found in the centre of the vein (150 to 350 μm thick). Wide fibres (>150 μm) show fluid inclusion trails parallel to fibre long axes. Veinlets are less recognizable in the centre of the vein than in the tip. Only 5% and 20% of the total volume of the vein can be recognized as originally veinlet in the central region whereas at the tip they represent between 40% and 100%, the rest being host fragments. At the very extremity of the vein only one veinlet constitutes the entire vein. In the centre, the vein is nearly pure calcite and

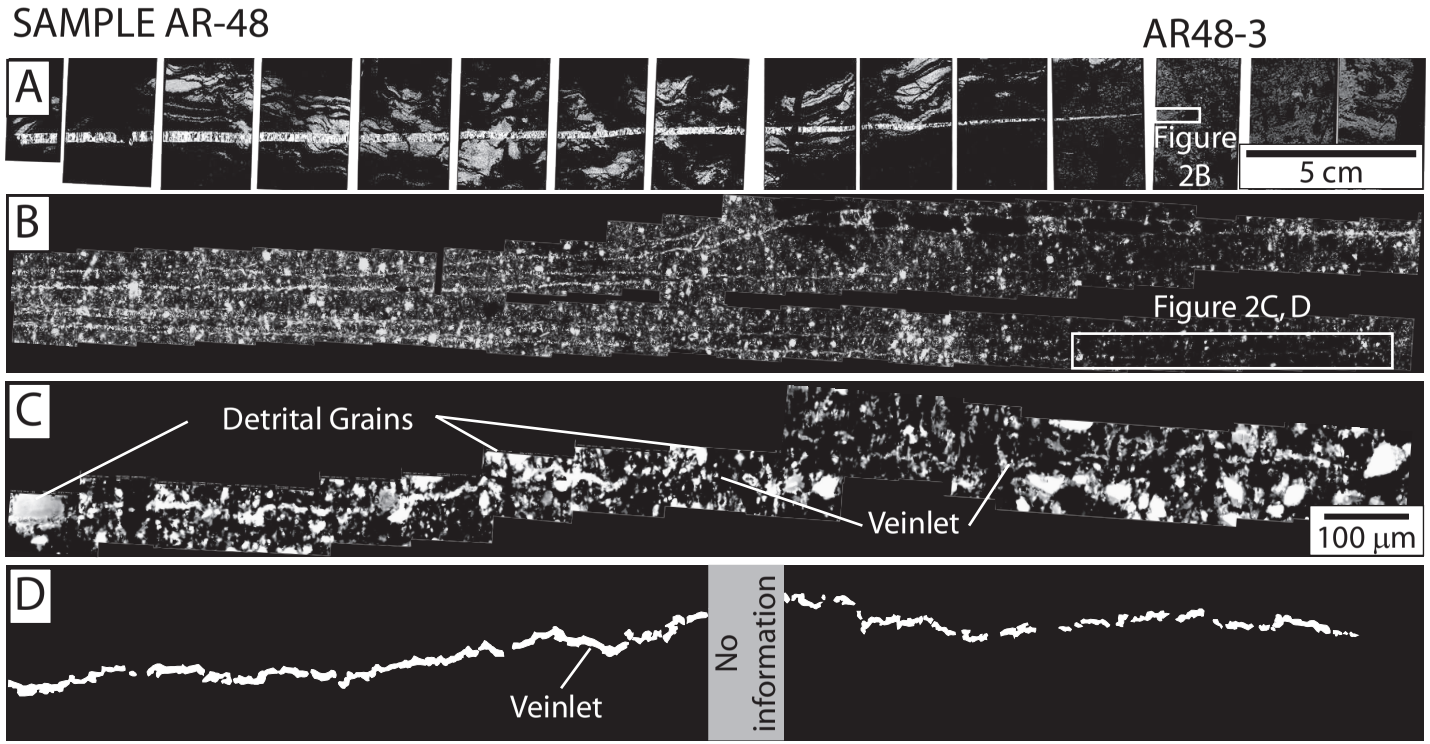

Fig. 30. Photomicrographs of vein AR-48 with location of the veinlet studied. A.- Shows the 15 thin sections cut from the sample vein with thin section AR-48-3 indicated. B.- Photomosaic under cross-polarized light of the vein across thin section AR-48-3. White square indicates the location of the veinlet studied. C.- SEM-CL polychromatic photomosaic of the veinlet studied. In the figure, detrital grains and veinlet are indicated. D.- Trace line of the veinlet in (C). The figure shows the irregular shape of the veinlet and its segmentation.

quartz whereas toward the tip, host fragments can make up as much as 60% of the vein width.

To understand the origin of the veinlets and therefore the vein as a whole, we have isolated a single veinlet at the tip of a larger vein. The veinlet shape is irregular throughout its length (Figure 30C and D). The veinlet appears to be formed by a series of small segments, defined by areas with precipitated quartz, closely aligned into one longer linear feature (Figure 30C and D). Areas between vein segments are devoid of secondary quartz or calcite (Figure 30C, D). The veinlet's width varies along its length but never exceeds 13 μm (Figure 31C). Close to the tip (less than 500 μm) a plot of thickness with distance of the veinlet forms a parabola; the tip is blunt (Figure 31C). Precipitating in the veinlet occur as individual crystals. The widths of these crystals range between 1 to 25 μm (Figure 31A, B). Where the veinlet cuts across detrital grains quartz precipitation covers the entire fracture as one single grain (Figure 32A, B, D and E). Most of the individual crystals in the veinlet do not appear to grow from seeds in the host, at least not seeds in the plane of the thin section (Figure 30C and D).

Veinlets have been described in the literature as: 1) thin filled fractures with no clear localization of the growth surface (Durney and Ramsay, 1973), 2) fracture and precipitation sites responsible for the formation of stretched-crystals (Passchier and Trouw, 1996) and 3) planar segments separated by short wall segments, inclined or at moderate angles to the vein margin (Cox, 1987). In our samples, the veinlets appear to represent single fracturing and precipitation events because they cut across host grains

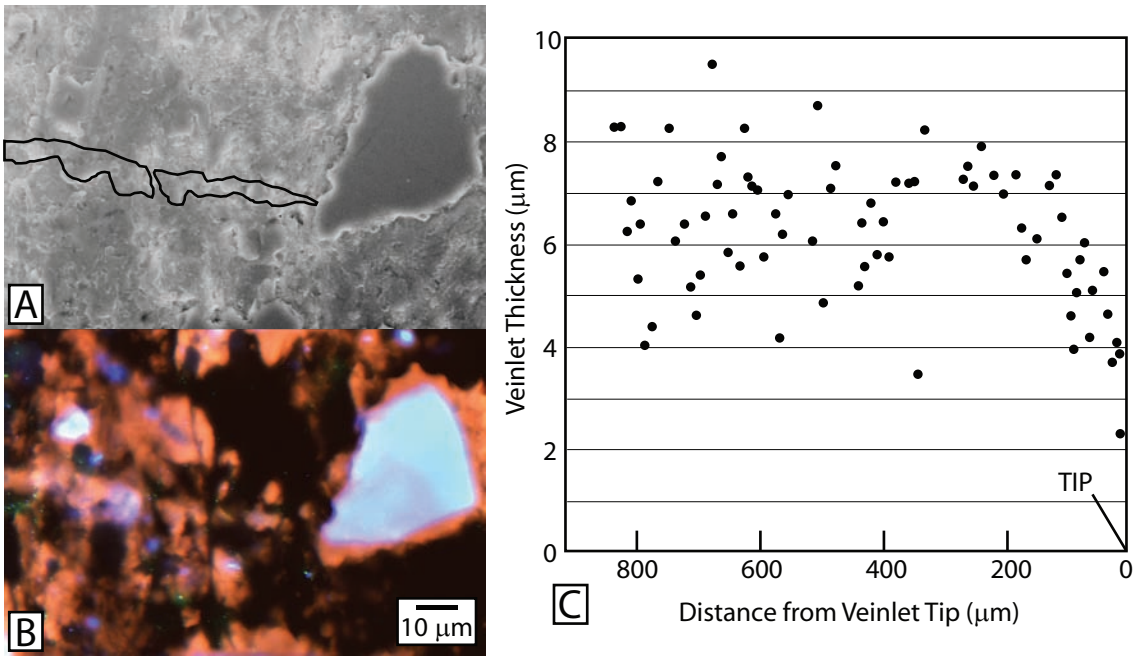

Fig. 31. Veinlet tip. A.- BSE image of the veinlet tip. Indicated is the veinlet shape based on its luminescence. B.- SEM-CL false color image of the veinlet tip. C.- Veinlet width measurements from the tip towards the center. Veinlet mineralization was used as proxy for veinlet width.

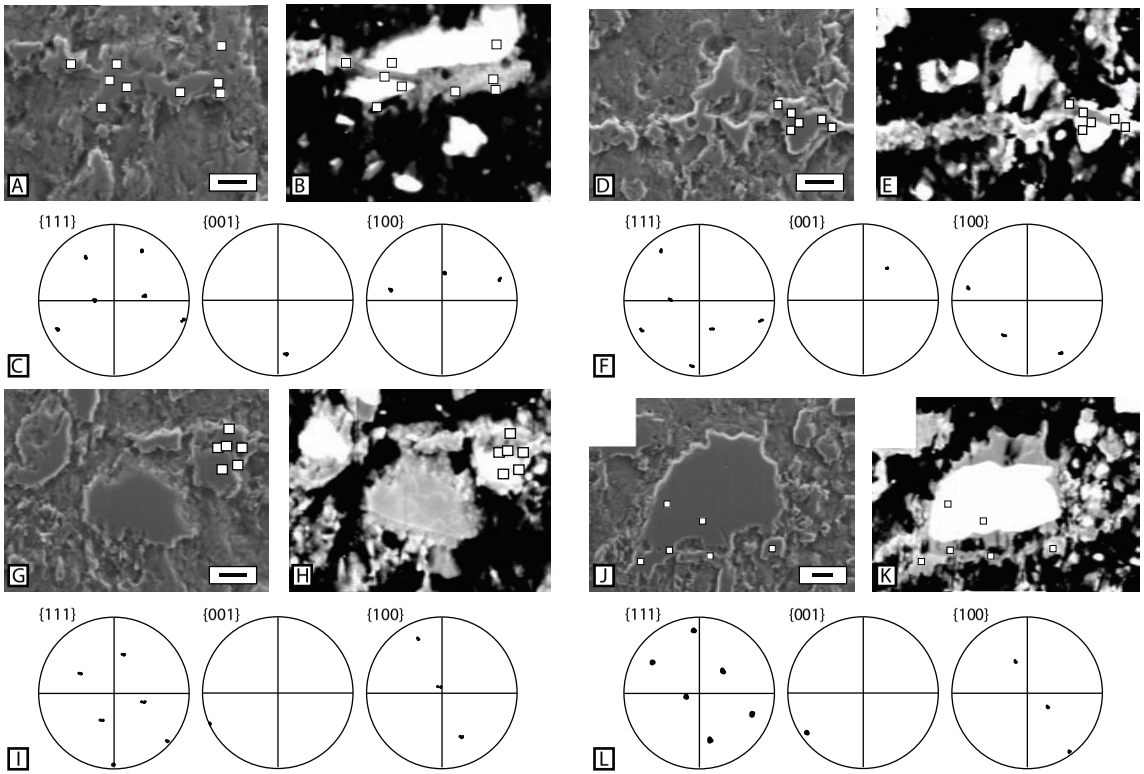

Fig. 32. Crystallographic orientation of individual grains in the host an in the veinlet. All plots are pole figures, equal area projections in an upper hemisphere. Crystallographic axes plotted are indicated in the parenthesis. All scale bars represent 10 ?m. A.- Back-scattered electron image of the grain with the location of EBSD measurements. B.- Cathodoluminescence polychromatic image of the grain in A with the location of EBSD measurements. C.- Plot of crystallographic axes {111}, {001}, and {100} for the measurements shown in A and B. D.- Back-scattered electron image of the grain with the location of the measurements. E) Cathodoluminescence polychromatic image of the grain in D with the location of EBSD measurements. F.- Plot of crystallographic axes {111}, {001}, and {100} for EBSD measurements shown in D and E. G.- Back-scattered electron image of the grain with the location of EBSD measurements. H.- Cathodoluminescence polychromatic image of the grain in G with the location of EBSD measurements. I.- Plot of crystallographic axes {111}, {001}, and {100} for EBSD measurements shown in G and H. J.- Back-scattered electron image of the grain with the location of EBSD measurements. K.- Cathodoluminescence polychromatic image of the grain in J with the location of EBSD measurements. L.- Plot of crystallographic axes {111}, {001}, and {100} for EBSD measurements shown in J and K. In all cases the orientations of the host and veinlet are the same.

and the resulting host fragments are displaced by mineralization (Figure 32A, B, D and E).

The veinlet width limit (never larger than 15 μm) and the bluntness of the veinlet tip are not the shapes predicted by the aspect ratio equation (width/length) of LEFM (e.g. Pollard and Segal, 1987). The equation predicts that the fracture wall displacement increases away from the tip, producing a parabolic fracture shape. The constant thickness of inclusion bands and veinlets has been observed in other fibrous veins (Ramsay, 1980, Cox and Etheridge, 1983; Cox, 1987; Fisher and Brantley, 1992; Fisher et al., 1995; Bons, 2000; Hilgers and Urai, 2002). An explanation of the veinlet width limit within the framework of LEFM is that fractures propagate across a sedimentary layer as bed-contained blade-like fractures (e.g., Olson, 1993). The fracture lengthens before propagating towards the boundaries of the layer. The lengthening process can be attained by coalescence of en-echelon micro-cracks growing on a similar plane (Figure 33). This process can explain the irregular shape of the veinlets and the segmentation. (Figure 30C, D). Olson (1993) show that original en-echelon arrays of small fractures result in fewer macroscopic fractures after propagation if the subcritical fracture growth index (n) is large (>6). Large n's are attributed to fractures propagating at subcritical velocities. The bluntness of the tip is a result of non-linear behaviour due to inelastic deformation in the grain scale. Ingraffea (1987) points out that LEFM is only applicable after a macroscopic fracture has initiated. Assumming each segment in the veinlet was a single crack in an en-echelon array with lengths of the order of 2 or 3 grains, then the shape of the tip would result from inelastic deformation and would not be predicted by

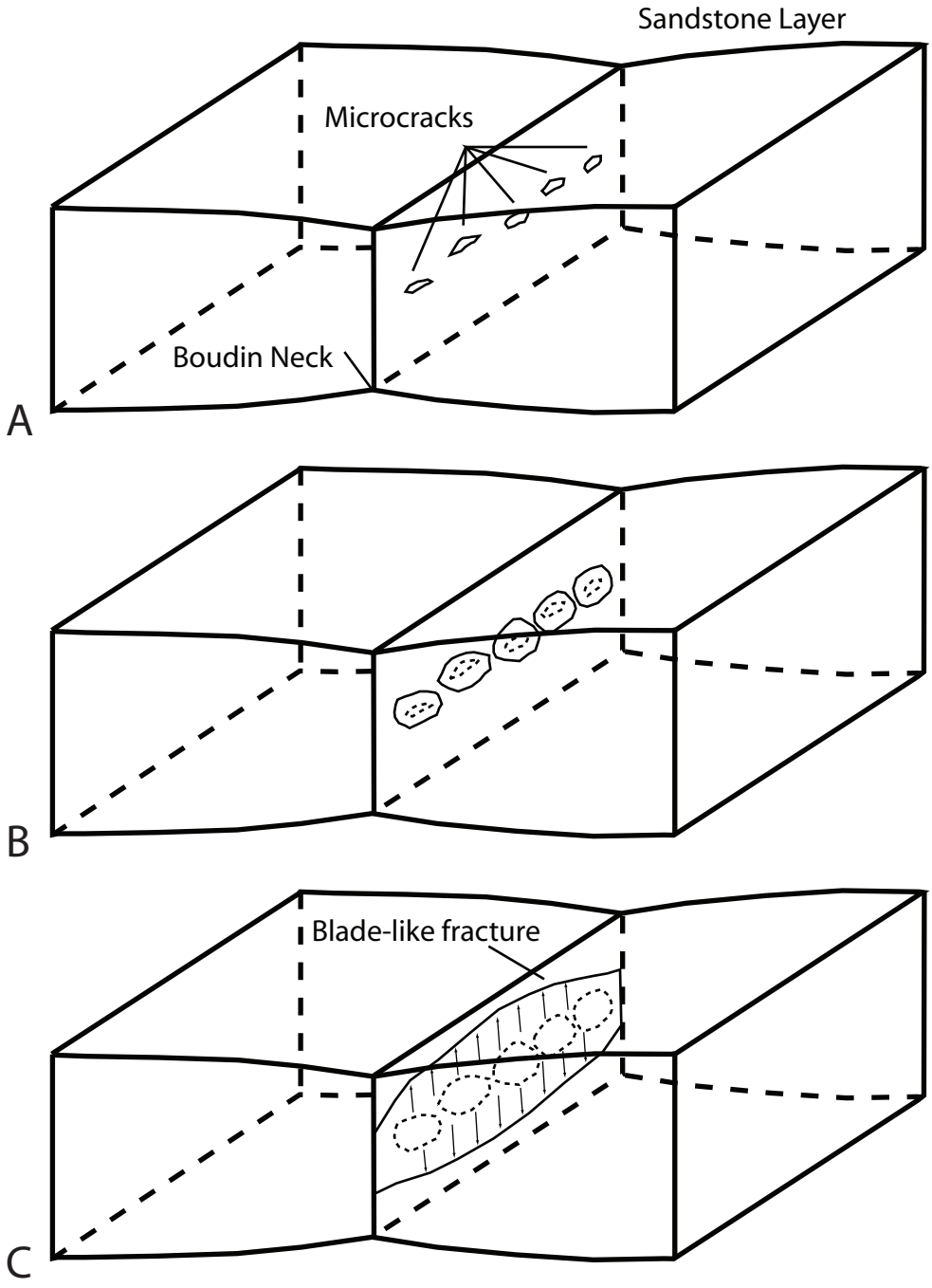

Fig. 33 Model of veinlet growth. A.- Microcrack en-echelon array (block diagram). B.- Microcrack initial propagation (block diagram). C.- Microcrack en-echelon array propagates as a blade-like fracture (block diagram).

LEFM (Figure 30D). The progression from one veinlet at the tip to fibers composed of multiple veinlets in the center of the vein suggests that the evolution of this vein was the successive addition of veinlets to the exclusion of host and, at least for this vein, late or subsequent obliteration of the veinlet fabric in the middle of the vein.

Crystal orientations of host grains and veinlet grains were measured using SEM based electron backscatter diffraction (EBSD); see Methods. Crystal orientations in the host indicate no preferred orientation (Figure 34A). Crystal orientations within the veinlet are as random as that of the host (Figure 34B). The lack of preferred orientation in the veinlets provides insight into the vein forming process. Where observations are possible the veinlet shows the same crystallographic orientation as that of the adjacent host when the host is cut by or attached to the veinltet (Figure 32A, B, C, D, E and F and Figure 32G, H, I, J, K and L, respectively). We suggest that this is evidence that precipitation in the veinlets start from a seed grain in the host. The strong crystallographic control of the substrate suggests that the fluid was never highly supersaturated with respect to quartz (e.g., Lasaga, 1998). If supersaturation were high, nucleation of new crystallites would be easy and evidence of crystal growth competition would be observed. This observation also suggests that force of crystallization as mechanism for crack propagation (Taber, 1916, 1918 and 1920; Misik, 1971; Li, 2000; Means and Li, 2001; Wiltschko and Morse, 2001) was not active during the formation of this vein. The reason for this is that grains growing under compression will orient themselves in such way that their stronger axis would be aligned against the principal compressive stress (Kamb, 1959). This process would

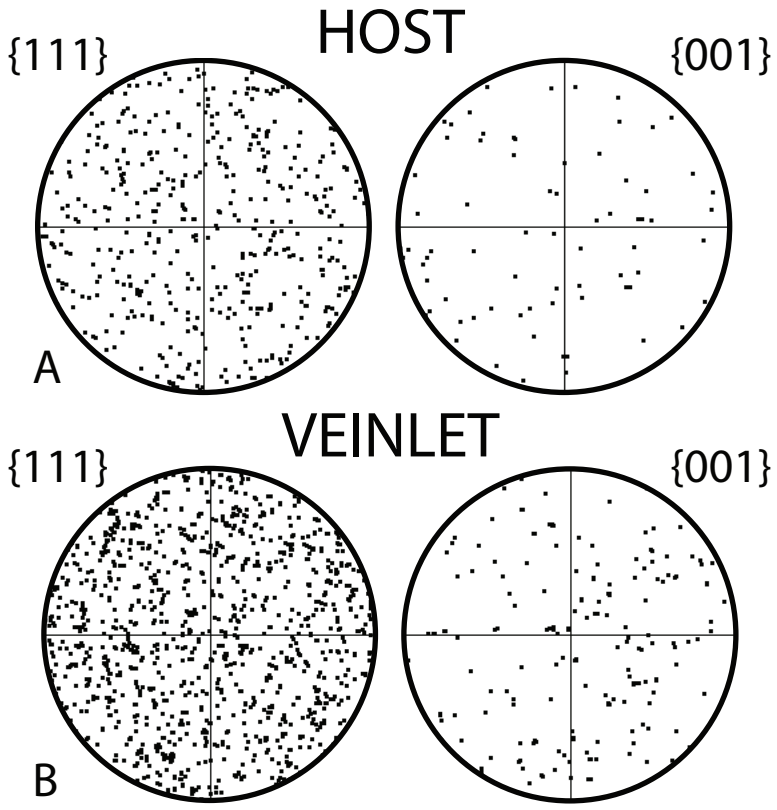

Fig. 34. Crystallographic orientations of host grains and veinlet grains determined using EBSD. A.- Host grains crystallographic orientations. B.- Veinlet grains orientations. In both cases the orientations are random.

establish a crystallographic preferred orientation in the growing crystals and our data shows no preferred orientation.

Boudinage of the sandstone localized fracturing and dilation in the boudin neck. This growth model (Figure 33) differs from previous models where fibrous veins were explained by continuous growth of a single crack (Ramsay, 1980; Etheridge and Cox, 1983; Hilgers and Urai, 2002; Laubach et al., 2004) or models where the new growth increment was always added right at the host-vein interface (Fisher and Brantley., 1993; Fisher et al., 1995). In our model veinlets form at boudin necks but not necessarily at the edge of previously formed veinlets. Although it is not possible at this time to date individual veinlets, the simplest explanation is that veinlets are added at or close to the vein-host interface, particularly once fibers are clearly developed.

4.3 Methods

Electron BackScattered Diffraction (EBSD) patterns and Cathodoluminescence (CL) images were obtained using a LEO-1530VP FESEM (field-emission SEM) at Texas A&M University equipped with and HKL EBSD detector and Gatan UKPANACL system for panchromatic cathodoluminescence imaging in wavelength region between 185 nm to 850 nm. Conditions for both EBSD and CL imaging were 20-kV acceleration voltage and 120 μm beam aperture. EBSD patterns were indexed using the software package Channel5 from HKL Software Company. More than five bands were detected allowing for unambiguous indexing. Uncertainty is given by mean angular deviation (MAD) between detected bands and simulated patterns. Indexing was

not accepted if MAD value was larger than 1°. Samples consisted of standard polished thin section subjected to additional chemical polishing for 90 minutes using a Syton suspension. The veinlet selected is located in thin section AR-48-3 (see Figure 30A, B and C), close to the tip.

5. CONCLUSIONS

Veinlets and fibers constitute the most characteristic textural features in the vein. Veinlets are thin (5-25 mm) veins parallel or at low angle to the host-vein interface. Fibers are elongated strips of quartz and calcite that grow perpendicular to the vein-host interface. Fibers contain fluid inclusion bands parallel to the vein host interface. Thick fibers (>150 mm) contain fluid inclusion trails parallel to the fiber long axis.

The vein textures vary along its length. Textural variations are evident when observed under polychromatic SEM-CL because quartz luminescence in fibers, veinlets and detrital host grains is different. Quartz fibers have pink luminescence, veinlets blue and detrital host grains show several luminescence colors (green, yellow, light blue, etc.). At the central region of the vein the body of the vein is predominantly formed by fibers whereas the tip region is formed by veinlets.

Veinlets represent cracks filled by quartz precipitating from a liquid. Coalescence of veinlets allows veins to lengthen and widen. Fibers are formed after recrystallization (dissolution-reprecipitation) of the quartz forming the veinlets.

The differences in texture along the vein represent an evolution through time. Early events of vein formation are characterized by the formation of veinlets. Fibers form later from dissolution of the earlier precipitated quartz and reprecipitation into more stable phases.

The stress localization required for the formation and growth of these veins is controlled by local structures. In the Ouachitas, layer-parallel extension in recumbent fold limbs formed boudins. The boudin-necks are the areas where veining took place.

Veins from the Benton Uplift, Ouachitas, are dominated by the presence of veinlets and fibers. Veinlets are narrow, between 5 and 25 μm thick, typically one crystal wide and parallel to the larger vein orientation. Fibers are perpendicular to the vein wall, span 50-100% of the total vein width and are made of multiple veinlets.

Quartz $\delta^{18}O$ values of vein and adjacent coarse-grain host are within 2‰ of each other. The closeness of values indicates that the fluid from which the vein material precipitated was in equilibrium with the host rock. Calcite $\delta^{18}O$ and $\delta^{13}C$ values across the wide vein studied define a trend that represents the evolution of the fluid from local and rock-buffered to a short-traveled fluid. These observations suggest that the Ouachita veins were first formed from a small volume of fluid in equilibrium with the host and as the veins evolved the volume of fluid available for vein formation increased allowing for small scale advection.

The textural differences observed in the larger veins (variations in fiber width and length) are tracked by variations in calcite $\delta^{18}O$ and $\delta^{13}C$ values. The difference in isotopic values can not be explained by changes in temperature of the same vein-forming fluid suggesting that the isotopic difference represents two episodes of growth of the vein where the vein source material was different.

The two families of fluid inclusions analyzed are directly tied to the two processes that generate the textures in the Ouachita veins. High-homogenization temperature inclusions were trapped in quartz precipitating in veinlets whereas low-homogenization inclusions were trapped during quartz recrystallization when fibers were widened forming inclusion trails and inclusion bands.

Quartz-calcite oxygen isotope thermometry and fluid inclusions determined the environment of formation of the Ouachita veins to be between 275 and 385 °C of temperature and between 1100 and 3400 bars of pressure. The environment of formation of the Ouachita veins (within greenschist facies) is consistent with the environment of formation of quartz fibrous veins in other tectonic settings.

Veinlets are formed by a series of small segments, defined by areas with precipitated quartz, closely aligned into one longer linear feature. Areas between vein segments are devoid of secondary quartz or calcite. This suggests that veinlets start as microcracks aligned in en-echelon arrays.

Veinlets show a constant width throughout its length. An explanation of the veinlet width limit within the framework of LEFM is that fractures propagate across a sedimentary layer as bed-contained blade-like fractures.

The lack of preferred crystallographic orientation in the host and within the veinlet and the observation that the crystallographic orientation of the veinlets and adjacent host is the same when the host is cut by or attached to the veinlet suggest that precipitation in veinlets start from a seed grain in the host.

The strong crystallographic control of the substrate suggests that fluid fluidsupersaturation was cyclical but never far from equilibrium.

REFERENCES

Al-Aasm, I. S., Coniglio, M. & Desrochers, A. 1995. Formation of complex fibrous calcite veins in Upper Triassic strata of Wrangellia Terrain, British Columbia, Canada. *Sedimentary Geology* **100**, 83-95.

Arbenz, J. K. 1989. The Ouachita system. In: *The geology of North America - an overview* (edited by Bally, A. W. & Palmer, A. R.) **A**. Geological Society of North America, Boulder, CO, 371-396.

Arne, D. C. 1992. Evidence from apatite fission-track analysis from regional Cretaceous cooling in the Ouachita Mountain fold belt and Arkoma basin of Arkansas. *American Association of Petroleum Geologist Bulletin* **76**, 392-402.

Bass, M. & Ferrara, G. 1969. Age of adularia and metamorphism, Ouachita mountains, Arkansas. *American Journal of Science* **267**(4), 491-498.

Bignall, G., Sekine, K. & Tsuchiya, N. 2004. Fluid-rock interaction processes in the Te Kopia geothermal field (New Zealand) revealed by SEM-CL imaging. *Geothermics* **33**, 615-635.

Blythe, A. E., Sugar, A. & Phipps, S. P. 1988. Structural Profiles of the Ouachita Mountains, Western Arkansas. *American Association of Petroleum Geologist Bulletin* **72**, 810-819.

Bojar, H. P., Bojar, A. V., Mogessie, A., Fritz, H. & Thalhammer, O. A. R. 2001. Evolution of veins and sub-economic ore at Strassegg, Paleozoic of Graz, Eastern Alps, Austria: Evidence for local fluid transport during metamorphism. *Chemical Geology* **175**, 757-777.

Bons, P. D. 2000. The formation of veins and their microstructures. *Journal of the Virtual Explorer* **2**, 12.

Brown, P. E. & Hagemann, S. G. 1995. MacFlinCor and its application to fluids in Archaean lode-gold deposits. *Geochimica et Cosmochimica Acta* **59**, 3943-3952.

Brown, P. E. & Lamb, W. M. 1989. P-V-T properties of fluids in the system H_2O-CO_2-NaCl: New graphical presentations and implications for fluid inclsuion studies. *Geochimica et Cosmochimica Acta* **45**, 1209-1221.

Cartwright, I., Power, W. L., Oliver, H. S., Valenta, R. K. & Mclatchie, G. S. 1994. Fluid migration and vein formation during deformation and greenschist facies

metamorphism at Ormiston Gorge, central Australia. *Journal of Metamorphic Geology* **12**, 373-386.

Cox, S. F. 1987. Antitaxial crack-seal vein microstructures and their relationship with displacement paths. *Journal of Structural Geology* **9**, 779-787.

Cox, S. F. & Etheridge, M. A. 1983. Crack-seal fibre growth mechanisms and their significance in the development of oriented layer silicate microstructures. *Tectonophysics* **92**, 147-170.

De Paor, D. G., Simpson, C., Bailey, C. M., McCaffrey, K. J. W., Beam, E., Gower, R. J. W. & Aziz, G. 1991. The role of solution in the formation of boudinage and tranverse veins in carbonate rocks at Rheems, Pennsylvania. *Geological Society of America Bulletin* **103**, 1552-1563.

Denison, R. E., Burke, W. H., Otto, J. B. & Heatherington, E. A. 1977. Age of igneous and metamorphic activity affecting the Ouachita foldbelt. In: *Symposium on the geology of the Ouachita Mountains* (edited by Stone, C. G.) **Volume I,** Arkansas Geological Commission, Little Rock, Arkansas, 25-40.

Dietrich, D., McKenzie, J. A. & Song, H. 1983. Origin of calcite in syntectonic veins as determined from carbon-isotope ratios. *Geology* **11**, 544-551.

Dove, P. 1999. The dissolution kinetics of quartz in aqueous mixed cation solutions. *Geochimica et Cosmochimica Acta* **63**(22), 3715-3727.

Dove, P., Han, N. & De Yoreo, J. J. 2005. Mechanisms of classical crystal growth theory explain quartz and silicate dissolution behavior. *Proceedings of the National Academy of Sciences* **102**(43), 15357-15362.

Durney, D. W. & Ramsay, J. G. 1973. Incremental strains measured by syntectonic crystal growths. In: *Gravity and Tectonics* (edited by De Jong, K. A. & Scholten, R.). Wiley, New York, 67-96.

Engel, A. E. J. 1952. Quartz crystal deposits of western Arkansas. In: *U.S. Geological Survey Bulletin*, 173-260.

Evans, M. A. & Battles, D. A. 1999. Fluid inclusion and stable isotope analyses of veins from the central Appalachian Valley and Ridge province: Implications for regional synorogenic hydrologic structure and fluid migration. *Geological Society of America Bulletin* **111**(12), 1841-1860.

Fisher, D. M. & Brantley, S. 1992. Models of quartz overgrowth and vein formation: Deformation and episodic fluid flow in an ancient subduction zone. *Journal of Geophysical Research* **97**, 20043-20061.

Fisher, D. M., Brantley, S. L., Everett, M. & Dzvonik, J. 1995. Cyclic fluid flow through a regionally extensive fracture network within the Kodiak accretionary prism. *Journal of Geophysical Research* **100**(B7), 12881-12894.

Fitzgerald, E., Feely, M., Johnston, J. D., Clayton, G., Fitzgerald, L. J. & Sevastopulo, G. D. 1994. The Variscan thermal history of west Clare, Ireland. *Geological Magazine* **131**, 545-558.

Foreman, J. L. & Dunne, W. M. 1991. Conditions of vein formation in the southern Appalachian foreland: Constraints from vein geometries and fluid inclusions. *Journal of Structural Geology* **13**, 1173-1183.

Frey, M., Teichmüller, M., Teichmüller, R., Mullis, J., Künzi, B., Breithschmid, A., Gruner, U. & Schwizer, B. 1980. Very low grade metamorphism in external parts of the Central Alps: Illite crystallinity, coal rank and fluid inclusion data. *Eclogae geol. Helv.* **73**, 173-203.

Gao, Z. L. & Kwak, T. A. P. 1995. Turbidite-hosted gold deposits in the Bendigo-Ballart and Melbourne Zones, Australia. II. Nature of the ore fluid. *International Geology Review* **37**, 1007-1038.

Ghisetti, F., Kirschner, D. L., Vezzani, L. & Agosta, F. 2001. Stable isotope evidence for contrasting paleofluid circulation in thrust faults and normal faults of the Central Appennines, Italy. *Journal of Geophysical Research* **106**(5), 8811-8825.

Goldstein, R. H. & Rossi, C. 2002. Recrystallization in quartz overgrowths. *Journal of Sedimentary Research* **72**(3), 432-440.

Grant, N. T., Banks, D. A., McCaig, A. M. & Yardley, B. W. D. 1990. Chemistry, source, and behavior of fluids involved in alpine thrusting of the Central Pyrenees. *Journal of Geophysical Research* **95**(B6), 9123-9131.

Haley, B. R. & Stone, C. G. 1996. CoGeo Map of Arkansas (edited by Survey, U. S. G. & Commission, A. G.), Little Rock, Arkansas.

Hasimoto, Y., Enjoji, M., Sakaguchi, A. & Kimura, G. 2002. P-T conditions of cataclastic deformation associated with underplating: An example from the Cretaceous Shimanto complex, Kii Peninsula, SW Japan. *Earth Planets Space* **54**, 1133-1138.

Henderson, I. H. C. & McCaig, A. M. 1996. Fluid pressure and salinity variations in shear zone-related veins, central Pyrenees, France: Implications for the fault-valve model. *Tectonophysics* **262**, 321-348.

Henry, C., Burkhard, M. & Goffe, B. 1996. Evolution of synmetamorphic veins and their wallrocks through a Western Alps transect: No evidence for large-scale fluid flow. Stable isotope, major- and trace-element systematics. *Chemical Geology* **127**, 81-109.

Hervig, R. L. & Peacock, S. M. 1989. Implications of trace element zoning in deformed quartz from the Santa Catalina mylonite zone. *Journal of Geology* **89**, 343-350.

Hilgers, C., Kirschner, D. L., Breton, J. P. & Urai, J. L. 2006. Fracture sealing and fluid overpressures in limestones of the Jabal Akhdar dome, Oman mountains. *Geofluids* **6**, 168-184.

Hilgers, C. & Urai, J. L. 2002. Microstructural observations of natural syntectonic fibrous veins: Implications for the growth porcess. *Tectonophysics* **352**, 257-264.

Houseknecht, D. W. & Matthews, S. M. 1985. Thermal maturity of Carboniferous strata, Ouachita Mountains. *American Association of Petroleum Geologist Bulletin* **69**, 335-345.

Ihinger, P. D. & Zink, S. I. 2000. Determination of relative growth rates of natural quartz crystals. *Nature* **404**, 865-869.

Ingraffea, A. R. 1987. Theory of crack initiation and propagation in rock. In: *Fracture Mechanics of Rock* (edited by Atkinson, B. K.). Academic, San Diego, California, 71-110.

Iwasaki, H., Iwasaki, F., Balitsky, V. S., Balitskaya, L. V. & Makhina, I. B. 1998. Growth rates anisotropy of synthetic quartz crystals grown on Z-cut hexagonal seeds and computer simulations of growth processes. *Journal of Crystal Growth* **187**, 481-489.

Jones, M. M. & Pytokowicz, R. M. 1973. Solubility of silica in seawater at high pressures. *Bulletin of the Society of Royal Sciences of Liege* **42**, 118-120.

Kamb, B. W. 1959. Theory of preferred crystal orientation developed by crystallization under stress. *Journal of Geology* **67**, 153-170.

Kawasaki, M. 2003. Growth-induced inhomogeneities in synthetic quartz crystals revealed by the cathodoluminescence method. *Journal of Crystal Growth* **247**, 185-191.

Keller, W. D., Stone, C. G. & Hoersch, A. L. 1985. Textures of Paleozoic chert and novaculite in the Ouachita Mountains of Arkansas and Oklahoma and their geological significance. *Geological Society of America Bulletin* **96**, 1353-1363.

Kenis, I., Muchez, P., Sintubin, M., Mansy, J. L. & Lacquement, F. 2000. The use of a combined structural, stable isotope and fluid inclusion study to constrain the kinematic history at the Variscan front zone (Bettrechies, north France). *Journal of Structural Geology* **22**, 589-602.

Kirkwood, D., Ayt-Ougougdal, M., Gayot, T., Beaudoin, G. & Pironon, J. 2000. Paleofluid-flow in a foreland basin, Northern Appalachians: From syntectonic flexural extension to Taconian overthrusting. *Journal of Geochemical Exploration* **69-70**, 269-273.

Kirschner, D. L., Sharp, Z. D. & Masson, H. 1995. Oxygen isotope thermometry of quartz-calcite veins: Unraveling the thermal-tectonic history of the subgreenschist facies Morcles nappe (Swiss Alps). *GSA Bulletin* **107**(10), 1145-1156.

Kirschner, D. L., Sharp, Z. D. & Teyssier, C. 1993. Vein growth mechanisms and fluid sources revealed by oxygen isotope laser microprobe. *Geology* **21**, 85-88.

Koning, R. H. & Stone, C. G. 1977. Geology of abandoned Kellog lead-zinc-silver-copper mines, Pulaski County, Arkansas. In: *Symposium on the Ouachita Mountains* (edited by Stone, C. G.) **Miscellaneous Publication 14**. Arkansas Geological Commission, Little Rock, Arkansas.

Kurrus, A. W. 1980. Geochemistry, geothermometry and mineralogy of quartz and base metal vein deposits, Montgomery County, Arkansas. Unpublished M.S. thesis, University of Arkansas.

Lander, R. H., Gale, J. F. W., Laubach, S. E. & Bonnell, L. M. 2002. Interaction between quartz cementation and fracturing in sandstones. In: *AAPG annual convention with SEPM* **Annual Meeting Expanded Abstracts**, Tulsa, OK, 98-99.

Lasaga, A. C. 1998. *Kinetics Theory in the Earth Sciences*. Princeton University Press, Princeton, New Jersey.

Laubach, S. E., Reed, R. M., Olson, J. E., Lander, R. H. & Bonnell, L. M. 2004. Coevolution of crack-seal texture and fracture porosity in sedimentary rocks: Cathodoluminescence observations of regional fractures. *Journal of Structural Geology* **26**, 967-982.

Li, T. 2000. Experimental Growth of Fibers and Fibrous Veins. Unpublished Doctor of Philosophy dissertation, University at Albany, State University of New York.

Lillie, R. J., Nelson, K. D., de Voogd, B., Brewer, J. A., Oliver, J. E., Brown, L. D., Kaufman, S. & Viele, G. W. 1983. Crustal structure of Ouachita Mountains, Arkansas: A model based on integration of COCORP reflection profiles and regional geophysical data. *American Association of Petroleum Geologist Bulletin* **67**, 907-931.

Lowe, D. R. 1989. Stratigraphy, sedimentology, and depositional setting of pre-orogenic rocks of the Ouachita Mountains, Arkansas and Oklahoma. In: *The Appalachian-Ouachita Orogen in the United States* (edited by Hatcher, R. D., Thomas, W. A. & Viele, G. W.). *DNAG, The Geology of North America* **F-2**. Geological Society of America, Boulder, Colorado, 575-590.

Mandal, N., Chakraborty, C. & Kumar Samanta, S. 2000. Boudinage in multilayered rocks under layer-normal compression: A theoretical analysis. *Journal of Structural Geology* **22**, 373-382.

Matsumura, M., Hashimoto, Y., Kimura, G., Ohmori-Ikehara, K., Enjohji, M. & Ikesawa, E. 2003. Depth of oceanic-crust underplating in a subduction zone: Inferences from fluid-inclusion analyses of crack-seal veins. *Geology* **31**(11), 1005-1008.

Means, W. D. & Li, T. 2001. A laboratory simulation of fibrous veins: Some first observations. *Journal of Structural Geology* **23**, 857-863.

Miser, H. D. 1959. Structure and vein quartz of the Ouachita Mountains of Arkansas and Oklahoma. In: *Ouachita Symposium* (edited by Cline, L. M., Hilsewick, W. J. & Feray, D. E.). Dallas and Ardmore Geological Societies, Dallas, Texas, 30-43.

Misik, M. 1971. Observations concerning calcite veinlets in carbonate rocks. *Journal of Sedimentary Petrology* **41**, 450-460.

Monecke, T., Kempe, U. & Götze, J. 2002. Genetic significance of the trace element content in metamorphic and hydrothermal quartz: A reconnaissance study. *Earth and Planetary Science Letters* **202**, 709-724.

Montomoli, C., Ruggieri, G., Boiron, M. C. & Cathelineau, M. 2001. Pressure fluctuation during uplift of the Northern Appenines (Italy): A fluid inclusion study. *Tectonophysics* **341**, 121-139.

Morris, R. C. 1989. Stratigraphy and sedimentary history of post-Arkansas Novaculite Carboniferous rocks of the Ouachita Mountains. In: *The Appalachian-Ouachita orogen in the United States* (edited by Hatcher, R. D. J., Thomas, W. A. & Viele, G. W.). *Geology of North America* **F-2**. Geological Society of America, Boulder, Colorado, 591-602.

Nelson, K. D., Lillie, R. J., de Voogd, B., Brewer, J. A., Oliver, J. E., Kaufman, S., Brown, L. D. & Viele, G. W. 1982. COCORP seismic reflection profiling in the Ouachita Mountains of western Arkansas: Geometry and geologic interpretation. *Tectonics* **1**, 413-430.

Nesbitt, B. E. & Muehlenbachs, K. 1995. Geochemical studies of the origins and effects of synorogenic curstal fluids in the southern Omineca Belt of British Columbia, Canada. *Geological Society of America Bulletin* **107**, 1033-1050.

Nielsen, K. C., Viele, G. W. & Zimmerman, J. 1989. Structureal setting of the Benton-Broken Bow uplifts. In: *The Appalachian-Ouachita orogen in the United States* (edited by Hatcher, R. D., Thomas, W. A. & Viele, G. W.). *Geology of North America* **F-2**. Geological Society of North America, Boulder, Colorado, 635-660.

Olson, J. E. 1993. Joint Pattern Development: Effects of Subcritical Crack Growth and Mechanical Crack Interaction. *Journal of Geophysical Research* **98**(B7), 12251-12265.

Paquette, J. & Reeder, R. 1995. Relationship between surface structure, growth mechanism, and trace element incorporation in calcite. *Geochimica et Cosmochimica Acta* **59**, 735-749.

Passchier, C. W. & Trouw, R. A. J. 1996. *Microtectonics*. Springer, Berlin.

Perny, B., Eberhardt, P., Ramseyer, K., Mullis, J. & Pankrath, R. 1992. Midrodistribution of aluminum, lithium, and sodium in α quartz: Possible causes and correlation with short lived cathodoluminescence. *American Mineralogist* **77**, 791-800.

Pittenger, G. C. & Koning, R. H. 1977. Geochemistry, geothermometry and mineralogy of copper, lead, zinc, and antimony deposits of Sevier County, Arkansas. In: *Symposium on the Ouachita Mountains* (edited by Stone, C. G.) **Miscellaneous Publication 14**. Arkansas Geological Commission, Little Rock, Arkansas.

Pollard, D. D. & Fletcher, R. C. 2005. *Fundamentals of Structural Geology*. Cambridge University Press, Cambridge.

Pollard, D. D. & Seagall, P. 1987. Theoretical displacements and stresses near fractures in rock: With applications to faults, joints, veins, dikes and solution surfaces. In: *Fracture Mechanics of Rocks* (edited by Atkinson, B. K.). Academic Press, London, 277-350.

Ramsay, J. G. 1980. The crack-seal mechanism of rock deformation. *Nature* **284**, 135-139.

Richards, I. J., Connelly, J. B., Gregory, R. T. & Gray, D. R. 2002. The importance of diffusion, advection, and host-rock lithology on vein formation: A stable isotope study from the Paleozoic Ouachita orogenic belt, Arkansas and Oklahoma. *GSA Bulletin* **114**(11), 1343-1355.

Roedder, E. 1984. *Fluid inclusions*. Mineralogical Society of America., Troy, NY.

Rye, D. M. & Bradbury, H. J. 1988. Fluid flow in the crust; and example from a Pyrenean thrust ramp. *American Journal of Science* **288**, 197-235.

Schmidt D., Schmidt, S. T., Mullis, J., Ferreiro Mahlmann, R. & Frey, M. 1997. Very low grade metamorphism of the Taveyanne formation of western Switzerland. *Contributions to Mineralogy and Petrology* **129**, 385-403.

Sharp, Z. D. 1992. In situ laser microprobe techniques for stable isotope analysis. *Chemical Geology* **101**, 3-19.

Shelton, K. L. 1982. Evolution of the porphyry copper and skarn deposits at Murdochville, Gaspe Peninsula, Quebec: A geochemical, stable isotopic and fluid inclusion study. Unpublished Ph.D. dissertation, Yale University.

Shelton, K. L., Reader, J. M., Ross, L. M., Viele, G. W. & Seidemann, D. E. 1986. Ba-rich adularia from the Ouachita Mountains, Arkansas: Implications for a post collisional hydrothermal system. *American Mineralogist* **71**, 916-923.

Shemesh, A., Ron, H., Erel, Y., Kolodony, Y. & Nur, A. 1992. Isotopic composition of vein calcite and its fluid inclusions: Implication to paleohydrological systems, tectonic events and vein formation processes. *Chemical Geology* **94**, 307-314.

Sibson, R. H. 1990. Conditions for fault-valve behaviors: Deformation Mechanisms Rheology and Tectonics. *Geological Society Special Publications* **54**, 15-28.

Sintubin, M., Kenis, I., Schroyen, K., Muchez, P. & Burke, E. A. J. 2000. "Boudinage" in the High-Ardenne slate belt (Belgium), reconsidered from the perspective of the "interboudin" veins. *Journal of Geochemical Exploration*(69-70), 511-516.

Smith, R. B. 1977. Formation of folds, boudinage, and mullions in non-Newtonian materials. *Geological Society of America Bulletin* **88**, 312-320.

Spear, F. S. 1993. *Metamorphic Phase Equilibria and Pressure-Temperature-Time Paths*. Mineralogical Society of America, Troy, NY.

Stone, C. G., Boyd, R. H. & Davis, M. H. 1994. Guidebook to Paleozoic Rocks in the Eastern Ouachita Mountains Arkansas (edited by Williams, N. F.). State of Arkansas, Arkansas Geological Commission, Little Rock, Arkansas, 1-46.

Stone, C. G. & McFarland, J. D. 1981. Field guide to the Paleozoic rocks of the Ouachita Mountain and Arkansas Valley Provinces, Arkansas. In: *Arkansas Geological Commision Guidebook.* Arkansas Geological Commision, Little Rock, Arkansas, 140.

Suchy, V., Dobes, P., Filip, J., Stejskal, M. & Zeman, A. 2002. Conditions of veining in the Barradian Basin (Lower Palaeozoic), Czech Republic: Evidence from fluid inclusion and apatite fission track analysis. *Tectonophysics* **348**, 25-50.

Suchy, V., Heijlen, W., Sykorova, I., Muchez, P., Dobes, P., Hladikova, J., Jackova, I., Safanda, J. & Zeman, A. 2000. Geochemical study of calcite veins in the Silurian and Devonian of the Barradian Basin (Czech Republic): Evidence for widespread post-Variscan fluid flow in the central part of the Bohemian Massif. *Sedimentary Geology* **131**, 201-219.

Sverjensky, D. A. 1980. The origin of Mississippi Valley-type deposits in the Viburnum Trend, Southeast Missouri. Unpublished Ph.D. dissertation, Yale University.

Swanson, M. T. 1992. Late Acadian-Alleghenian transpresssional deformation: Evidence from asymmetric boudinage in the Casco Bay area, coastal Maine. *Journal of Structural Geology* **14**(3), 323-341.

Taber, S. 1916. The growth of crystals under external pressure. *American Journal of Science* **41**, 532-556.

Taber, S. 1918. The genesis of asbestos and asbestiform minerals. *American Institute of Mining Engineers Transactions* **57**, 62-98.

Taber, S. 1920. The mechanics of vein formation (with discussion). *American Institute of Mining and Metallurgical Engineers Transactions* **61**, 3-41.

Templeton, A. S., Chamberlain, C. P., Koons, P. O. & Craw, D. 1998. Stable isotopic evidence of mixing between metamorphic fluids and surface-derived waters during recent uplift of the Southern Alps, New Zealand. *Earth and Planetary Science Letters* **154**, 73-92.

Trave, A., Calvet, F., Sans, M., Verges, J. & Thirlwall, M. 2000. Fluid history related to the Alpine compression at the margin of the south-Pyrenean Foreland basin: The El Guix anticline. *Tectonophysics* **321**, 73-102.

Underwood, M. B. & Viele, G. W. 1985. Early Pennsylvanian tectonic transition within the frontal Ouachitas of Arkansas. *Geological Society of America Abstracts with Programs* **17**, 195.

Urai, J. L., Spaeth, G., Van der Zee, W. & Hilgers, C. 2001. Evolution of Mullion (Boudin) structures in the Variscan of the Ardennes and Eifel. *Journal of the Virtual Explorer* **3**, 1-6.

Viele, G. W. 1989. The Ouachita orogenic belt. In: *The Appalachian-Ouachita orogen in the United States* (edited by Hatcher, R. D., Thomas, W. A. & Viele, G. W.). *Geology of North America* **F-2**. Geological Society of North America, Boulder, Colorado, 555-561.

Viele, G. W. & Thomas, W. A. 1989. Tectonic synthesis of the Ouachita orogenic belt. In: *The Appalachian-Ouachita orogen in the United States* (edited by Hatcher, R. D., Thomas, W. A. & Viele, G. W.). *Geology of North America* **F-2**. Geological Society of North America, Boulder, Colorado, 695-728.

Vrolijk, P., Myers, G. & Moore, J. C. 1988. Warm fluid migration along tectonic mélanges in the Kodiak accretionary complex, Alaska. *Journal of Geophysical Research* **93**(B9), 10313-10324.

Watson, E. B. & Liang, Y. A. 1995. A simple model for sector zoning in slowly grown crystals: Implications for growth rate and lattice diffusion, with emphasis on accesory minerals in crustal rocks. *American Mineralogist* **80**, 1179-1187.

Watt, G. R., Wright, P., Galloway, S. & McLean, C. 1997. Cathodoluminescence and trace element zoning in quartz phenocrysts and xenocrysts. *Geochimica et Cosmochimica Acta* **61**(20), 4337-4348.

Willey, J. D. 1974. The effect of pressure on the solubility of amorphous silica in seawater at 0^{o}C. *Marine Chemistry* **2**, 239-250.

Wiltschko, D. V. & Morse, J. W. 2001. Crystallization pressure versus "crack-seal" as the mechanism for banded veins. *Geology* **29**(1), 79-82.

Wiltschko, D. V., Morse, J. W., Sharp, Z. D. & Lamb, W. M. 1998. *Analysis of Veins in Low Temperature Environments - Introduction for Structural Geologists*. Geological Society of America, Toronto, Canada.

Xu, G. 1997. Fluid inclusions in crack-seal veins at Dugald River, Mount Isa Inlier: implications for palaeostress states and deformation conditions during orogenesis. *Journal of Structural Geology* **19**(11), 1359-1368.

Zhang, Y. & Frantz, J. D. 1987. Determination of the homogenization temperatures and densities of supercritical fluids in the system NaCl-KCl-$CaCl_2$-H_2O using synthetic fluid inclusions. *Chemical Geology* **64**, 335-350.

VITA

Name:	Pablo Cervantes
Address:	BP America Inc., 501 Westlake Blvd., Houston, TX 77079
Email Address:	pcervantes@tamu.edu
Education:	B.S., Engineering Geology, UNAM, Mexico, 1995
	M.S., Geology, Texas A&M University, 1999
Work Experience:	Compañía Minera Nukay, Geologist, 1996
	Ocean Drilling Program, Research Assistant 1997-1999
	Texas A&M University, R. A and T. A., 2000-2005
	Blinn College, Instructor, 2005-2006
	BP America Inc., Geologist, 2006-present

Abstracts:

P. Cervantes and Wiltschko, D.V., 2004, Growth of syntectonic fibrous veins in shale, Ouachitas Orogen, Arkansas; EOS, Transactions AGU, vol. 85-47, p.T51A-0433

P. Cervantes, Wiltschko, D.V. and Sharp Z., 2004, Kinematics of vein growth and evolution in the Ouachitas, Arkansas; Geological Society of America Abstract with Programs, vol. 36-1, p. 27

P. Cervantes, Wiltschko, D.V. and Sharp Z., 2003, Influence of faults in vein formation. A case from the Ouachitas, Arkansas; Geological Society of America Abstract with Programs, vol. 35-6, p. 178

P. Cervantes and Wallace P., 2000, Water in subduction zone magmatism: New insights from melt inclusions in high-Mg basalts from central Mexico; EOS, Transactions AGU, vol. 81-48, p. F1371

P. Cervantes and Wallace P., 1999, Water in primitive subduction-related basaltic magmas from central Mexico: implications for mantel enrichment processes above subduction zones; EOS, Transactions AGU, vol. 80-46, p. F1203

P. Wallace and **Cervantes P**., 1999, Magma degassing and basaltic eruption styles: A case study of the 2000 yr B.P. eruption of Xitle volcano, central Mexico; EOS, Transactions AGU, vol. 80-46, p. F1089

Publications

P. Cervantes and Wallace P., 2003, The role of H2O in subduction zone magmatism: New insights from melt inclusions in high-Mg basalts from central Mexico; Geology, v. 31, no. 3, p. 235-238

P. Cervantes and Wallace P., 2003, Magma degassing and basaltic eruption styles: a case study of ~2000 year BP Xitle volcano in central Mexico; Journal of Volcanology and Geothermal Research, v. 120, p. 249-270

D. J. Miller and **Cervantes P**., 2001, Platinum group element mineralization and sulfide mineral chemistry and petrography in gabbroic rocks from the southwest Indian Ridge; In: Natland, J., Dick, H., Miller, J., and Von Herzen, R., (Eds.) Proc. ODP Sci. Results, 176: College Station, TX (Ocean Drilling Program)